

UC Davis

UC Davis Previously Published Works

Title

α -Actinin-1 promotes activity of the L-type Ca^{2+} channel $\text{Ca}_v 1.2$.

Permalink

<https://escholarship.org/uc/item/9397z2t5>

Journal

The EMBO journal, 39(5)

ISSN

0261-4189

Authors

Turner, Matthew
Anderson, David E
Bartels, Peter
et al.

Publication Date










2020-03-01

DOI

10.15252/emj.2019102622

Peer reviewed

α -Actinin-1 promotes activity of the L-type Ca^{2+} channel $\text{Ca}_v1.2$

Matthew Turner^{1,†}, David E Anderson^{1,†}, Peter Bartels^{2,†} , Madeline Nieves-Cintron^{2,†} ,
Andrea M Coleman^{1,2} , Peter B Henderson², Kwun Nok Mimi Man² , Pang-Yen Tseng²,
Vladimir Yarov-Yarovoy³ , Donald M Bers², Manuel F Navedo² , Mary C Horne^{2,*} ,
James B Ames^{1,**}  & Johannes W Hell^{2,***} 

Abstract

The L-type Ca^{2+} channel $\text{Ca}_v1.2$ governs gene expression, cardiac contraction, and neuronal activity. Binding of α -actinin to the IQ motif of $\text{Ca}_v1.2$ supports its surface localization and postsynaptic targeting in neurons. We report a bi-functional mechanism that restricts $\text{Ca}_v1.2$ activity to its target sites. We solved separate NMR structures of the IQ motif (residues 1,646–1,664) bound to α -actinin-1 and to apo-calmodulin (apoCaM). The $\text{Ca}_v1.2$ K1647A and Y1649A mutations, which impair α -actinin-1 but not apoCaM binding, but not the F1658A and K1662E mutations, which impair apoCaM but not α -actinin-1 binding, decreased single-channel open probability, gating charge movement, and its coupling to channel opening. Thus, α -actinin recruits $\text{Ca}_v1.2$ to defined surface regions and simultaneously boosts its open probability so that $\text{Ca}_v1.2$ is mostly active when appropriately localized.

Keywords calmodulin; gating charge; IQ motif structure; open probability; surface expression

Subject Categories Membranes & Trafficking; Neuroscience

DOI 10.15252/emj.2019102622 | Received 5 June 2019 | Revised 4 December 2019 | Accepted 6 December 2019 | Published online 27 January 2020

The EMBO Journal (2020) 39: e102622

Introduction

Ca^{2+} influx through $\text{Ca}_v1.2$ is critical for the functions of many organs as strikingly illustrated by Timothy syndrome (Splawski *et al*, 2004). In this disease, a point mutation in $\text{Ca}_v1.2$ causes, among other symptoms, lethal arrhythmias, autistic-like behaviors, immune deficiency, and webbing of fingers (Splawski *et al*, 2004). $\text{Ca}_v1.2$ is the main L-type channel in heart (Seisenberger *et al*, 2000), vascular smooth muscle cells (Ghosh *et al*, 2017), and brain

(Hell *et al*, 1993; Sinnegger-Brauns *et al*, 2004). Ca^{2+} influx through $\text{Ca}_v1.2$ triggers cardiac contraction, regulates arterial tone (Ghosh *et al*, 2017), mediates different forms of synaptic long-term potentiation (Grover & Teyler, 1990; Patriarchi *et al*, 2016; Qian *et al*, 2017), and controls neuronal excitability (Marrion & Tavalin, 1998; Berkefeld *et al*, 2006). Furthermore, L-type channels are much more strongly coupled to gene expression than other Ca^{2+} channels (Dolmetsch *et al*, 2001; Li *et al*, 2012; Ma *et al*, 2014; Cohen *et al*, 2018). Finally, $\text{Ca}_v1.2$ forms a physical and functional complex with the β_2 adrenergic receptor (Davare *et al*, 2001) making it a prime target for signaling by norepinephrine (Patriarchi *et al*, 2016; Qian *et al*, 2017; Man *et al*, 2020), which is important for wakefulness, attention, and various forms of learning (Cahill *et al*, 1994; Berman & Dudai, 2001; Hu *et al*, 2007; Minzenberg *et al*, 2008; Carter *et al*, 2010).

$\text{Ca}_v1.2$ consists of the pore-forming $\alpha_11.2$ subunit and auxiliary $\alpha_2\delta$ and β subunits, which facilitate release from the endoplasmic reticulum and the controlled trafficking of $\text{Ca}_v1.2$ to the cell surface (Dai *et al*, 2009; Dolphin, 2012, 2016; Zamponi *et al*, 2015; Ghosh *et al*, 2018). However, $\alpha_2\delta$ and β subunits do not target $\text{Ca}_v1.2$ to specific sites in the plasma membrane. Rather, $\text{Ca}_v1.2$ anchoring at defined regions at the cell surface is mediated by α -actinin, which binds to the IQ motif in the C-terminus of $\alpha_11.2$ (Hall *et al*, 2013; Tseng *et al*, 2017).

A systematic yeast two-hybrid screen defined three residues in the IQ motif of $\alpha_11.2$, whose mutations to alanine residues affect α -actinin binding: K1647A, Y1649A, and I1654A. All three mutations reduced surface expression of $\text{Ca}_v1.2$ by ~35% but current density by 70–80% (Tseng *et al*, 2017). These results suggest that α -actinin binding to the IQ motif promotes not only surface localization but also channel activity. Such a multifunctional role would ensure that $\text{Ca}_v1.2$ is mostly active at its ultimate destinations and much less so when in transit and outside its target areas.

1 Department of Chemistry, University of California, Davis, CA, USA

2 Department of Pharmacology, University of California, Davis, CA, USA

3 Department of Physiology and Membrane Biology, University of California, Davis, CA, USA

*Corresponding author. Tel: +1 530 752 7723; E-mail: mhorne@ucdavis.edu

**Corresponding author. Tel: +1 530 752 6358; E-mail: jbames@ucdavis.edu

***Corresponding author. Tel: +1 530 752 6540; E-mail: jwhell@ucdavis.edu

†These authors contributed equally to this work

The closely related α_1 1.3 subunit of the L-type channel Ca_v 1.3 shares nearly 100% sequence identity with α_1 1.2 in its membrane-proximal 165 residues of its C-terminus in which the IQ motif is embedded (the eponymous Ile is I1654 of α_1 1.2 and I1609 of α_1 1.3; Appendix Fig S1). Ca^{2+} -free calmodulin (apoCaM) binds to this IQ motif, and mutation of I1609 in α_1 1.3 impairs both, apoCaM binding and open probability P_o of Ca_v 1.3 (Ben Johny *et al*, 2013; Adams *et al*, 2014; Ben-Johny *et al*, 2014). We solved the NMR structures of the third and fourth EF hands of α -actinin-1 (EF3 and EF4, residues 822–892; Fig 1A) and of full-length apoCaM bound to the α -helical IQ motif of Ca_v 1.2 (residues 1,646–1,664). This work provided new insight into the structure of Ca_v 1.2 especially as relevant for these two critical binding partners and informed experiments that dissected the exact functions of α -actinin versus apoCaM binding. Refined analysis of Ca_v 1.2 activity by cell-attached single-channel recording revealed that point mutations that affected α -actinin-1 but not those that affected apoCaM binding dramatically decreased the channel P_o by impairing gating charge movement as well as its coupling to channel opening. We conclude that α -actinin plays a dual role by anchoring Ca_v 1.2 at specific subcellular domains such as the postsynaptic sites and at the same time boosting its open probability. This mechanism ensures that the activity of Ca_v 1.2 is minimal when in transit during secretory trafficking and outside its intended location at the cell surface, where its Ca^{2+} conductance could adversely affect cell functions, but maximal at its final destination.

Results

Binding of α -actinin-1 EF3/EF4 to the Ca_v 1.2 IQ motif

α -actinin is encoded by four homologous genes with α -actinin-1 and α -actinin-2 being most prominent in neurons (Wyszynski *et al*, 1997; Hall *et al*, 2013; Hell, 2014; Matt *et al*, 2018). α -actinins consist of two N-terminal calponin homology domains (CH1, CH2; residues 19–192), four central spectrin repeats (SR1–4), which form a rod-like coiled-coil structure (Ribeiro Ede *et al*, 2014), and four EF hands at their C-termini (residues 750–892; Fig 1A). We first performed NMR spectroscopy with the CH1/CH2 region (residues 19–192). Two-dimensional NMR spectra of ^{15}N -labeled CH1/CH2 recorded in the presence and absence of unlabeled IQ peptide appeared to be virtually identical, consistent with a lack of IQ binding to CH1/CH2 under NMR conditions (Fig EV1A). The lack of IQ binding to the CH1/CH2 domain is supported by the absence of detectable binding measured by fluorescence polarization (see below Fig 1F). In stark contrast, the NMR spectrum of ^{15}N -labeled EF-hand domain of α -actinin-1 (residues 750–892) showed clearly detectable spectral changes upon adding a saturating amount of unlabeled IQ peptide, demonstrating a binding interaction (Fig EV1B). The NMR peaks of α -actinin-1 most affected by the binding of IQ (see labeled peaks in Fig EV1B) were assigned to residues in EF3 and EF4 (the C-lobe of the EF-hand region; residues 822–892). Consistently, the NMR spectrum of ^{15}N -labeled α -actinin-1 EF3/4 (residues 822–892) exhibited large spectral changes upon the addition of the IQ peptide (Fig EV1C), which are similar to those seen with the construct that contains all four EF hands (Fig EV1B). We conclude that the IQ peptide binds to the α -actinin-1 C-lobe.

NMR structure of α -actinin-1 EF3/4 bound to the IQ motif of Ca_v 1.2

We had previously reported NMR spectral assignments for α -actinin-1 EF3/4 (BMRB accession number 25902) (Turner *et al*, 2016). We used these assignments to obtain NMR-derived structural restraints for high-resolution structural analysis of α -actinin-1 EF3/4 bound to the Ca_v 1.2 IQ motif (EF3/4-IQ). Atomic-level NMR structures were calculated on the basis of distance restraints derived from the analysis of NOESY spectra and long-range orientational restraints derived from residual dipolar coupling (RDC) data (Fig EV2A). EF34 in the complex was resolved for 69 residues, starting at T823 and ending at L892. The 10 lowest energy NMR structures are overlaid in Fig 1B and structural statistics summarized in Table 1. The overall precision of the ensemble was expressed by an RMSD of 0.3 Å calculated from the coordinates of the main chain atoms. The energy-minimized average structure of EF3/4-IQ (Fig 1C, calculated from the ensembles in Fig 1B) contained two EF-hand motifs (α 1: A826–A837; α 2: M845–E851; α 3: P854–R863; α 4: M880–Y887; β 1: Y842–T844; β 2: A876–D878) bound to an α -helical IQ motif (Ca_v 1.2 residues 1,646–1,664). The NMR structure of EF3/4-IQ (Fig 1C) was quite similar (1.8 Å RMSD) to the NMR structure of α -actinin-2 bound to the seventh Z-repeat of titin (Atkinson *et al*, 2001). It contained important intermolecular contacts that stabilize the EF3/4–IQ interaction (Fig 1C–E). Most striking were a salt bridge between IQ K1647 and EF3/4 E847/E851 (Fig 1C) and hydrophobic contacts involving IQ I1654 and EF3F833 (Fig 1D). The IQ residue F1658 was mostly solvent exposed in the EF3/4–IQ complex contributing minimally if at all to the EF3/4–IQ interaction (Fig 1E), in contrast to being buried inside apoCaM in the apoCaM/IQ complex (see below).

Validation of the α -actinin-1 EF3/4–IQ NMR structure by mutagenesis

Mutations in both α -actinin-1 EF3/4 and IQ peptide were designed to verify their predicted intermolecular contacts. A synthetic fluorescein-labeled IQ peptide (residues 1,644–1,666) was titrated with EF3/4 and fluorescence polarization (FP) monitored to determine their K_d values. The IQ peptide bound to α -actinin-1 EF3/4 with nearly the same affinity as to full-length α -actinin-1 (Fig 1F; Table 2). The IQ peptide did not bind to α -actinin-1 EF1/2 (Fig 1F). Accordingly, IQ interacts exclusively with the C-lobe but not N-lobe of the EF-hand domain in α -actinin-1.

The salt bridges formed between IQ residue K1647 and α -actinin-1 residues E847 and E851 (Fig 1C) provided an opportunity for charge inversion experiments. The single-residue alterations K1647A and K1647E in the IQ peptide increased the K_d by ~5-fold and mutating E847 and E851 in α -actinin-1 EF3/4 to lysine (K) by ~12-fold (Fig 1F; Table 2). Combining the E847K/E851K mutations in α -actinin-1 EF3/4 with the K1647E substitution in the IQ peptide mostly but not fully restored the binding affinity to the K1647E IQ peptide. This powerful charge inversion experiment unequivocally identified the importance of those salt bridges for the α -actinin-1–IQ interaction. Furthermore, I1654 of the IQ motif was predicted to form hydrophobic interactions with F833 in EF3 (Fig 1D). In fact, the α -actinin-1 EF3/4 mutant F833A showed an ~8-fold decrease in binding affinity, which is consistent with the decrease observed for

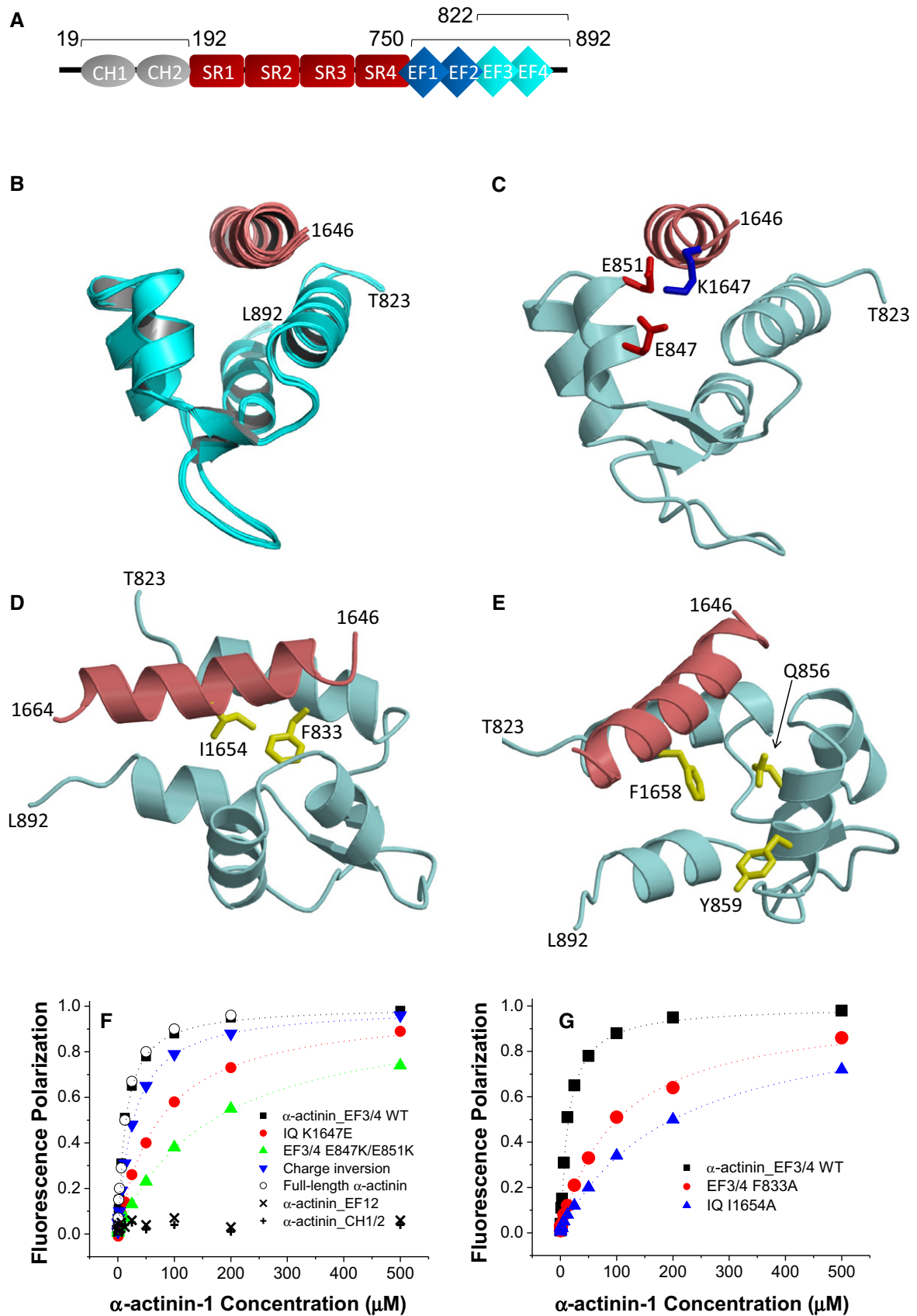


Figure 1.

Figure 1. α -Actinin-1 forms electrostatic and hydrophobic contacts with $\text{Ca}_v1.2$.

- A Linear model of α -actinin domains (CH: calponin homology domains; SR: spectrin repeats; EF: EF hands). Bars and numbers on top of the model depict the segments used in this work.
- B Ensemble of 10 lowest energy NMR-derived structures of α -actinin-1_EF34 (cyan) bound to IQ peptide (red). Structural statistics are given in Table 1.
- C Energy-minimized average structure of α -actinin-1_EF34 (cyan) bound to IQ (red), revealing intermolecular salt bridges between K1647 of IQ and E847/E851 of α -actinin-1. The K1647 side-chain amino nitrogen atom is 2.8 and 2.5 Å away from the side-chain carbonyl oxygen atoms of E847 and E851, respectively.
- D Intermolecular hydrophobic contacts between I1654 of IQ (red) and F833 of α -actinin-1 (cyan). The I1654 side-chain methyl carbon atom is 2.9 Å away from the closest aromatic ring atom of F833. Side-chain atoms are colored yellow.
- E Lack of direct contacts between F1658 of IQ (red) and α -actinin-1 (cyan). The aromatic side chain of F1658 is primarily solvent exposed and does not directly contact α -actinin-1. The aromatic ring of F1658 is closest to the aromatic ring of Y859 and β -methylene carbon of Q856 of α -actinin-1, which are 5.2 and 4.3 Å apart, respectively.
- F FP titrations show binding of WT α -actinin-1_EF34 to IQ peptides WT (black) and K1647E (red), of α -actinin-1_EF34 mutant E847K/E851K to IQ peptides WT (green) and K1647E (blue), of full-length α -actinin-1 to IQ WT (o), and lack of IQ binding to α -actinin-1_CH1-CH2 (+) and α -actinin-1_EF12 (x; see Table 2 for binding parameters and standard errors).
- G FP titrations showing binding of wild-type α -actinin-1_EF34 to IQ peptides WT (black) and I1654A (blue) and of ACTN1_EF34 mutant F833 to IQ WT (red; see Table 2 for binding parameters and standard errors).

the I1654A substitution in the IQ peptide (Fig 1G; Table 2). These results confirmed two important intermolecular interactions that had been seen in the NMR structure (Fig 1C): a salt bridge contact between K1647 ($\text{Ca}_v1.2$) and E847/E851 (α -actinin-1) and the linchpin hydrophobic contact between I1654 ($\text{Ca}_v1.2$) and F833 (α -actinin-1).

NMR structure of apoCaM bound to the IQ motif of $\text{Ca}_v1.2$

ApoCaM is predicted to bind to the IQ motif of $\text{Ca}_v1.3$ under basal conditions to augment Po (Adams *et al*, 2014) but no structure has so far been available to aid data interpretation. The ^1H - ^{15}N HSQC NMR spectrum of ^{15}N -labeled apoCaM showed detectable spectral changes upon adding a saturating amount of unlabeled IQ peptide, demonstrating binding (Fig EV1D). The NMR peaks of apoCaM most affected by the binding of IQ (see labeled peaks in Fig EV1D) were assigned to residues in its C-lobe (CaM EF3/4). Complete NMR

spectral assignments for apoCaM bound to the IQ peptide had been reported previously (Lian *et al*, 2007). We used these assignments to obtain NMR-derived structural restraints and determine the atomic-level NMR structure of apoCaM bound to the IQ peptide (called apoCaM-IQ). NMR-derived structures were calculated on the basis of NOESY distance restraints and long-range orientational restraints derived from NMR RDC data (Fig EV2B) (Tjandra & Bax, 1997). Our NMR chemical shift analysis indicated that the IQ peptide contacted residues in the C-lobe (residues 82–148) but not N-lobe of apoCaM (residues 1–78; Fig 2). The 10 lowest energy NMR structures are overlaid in Fig 2A and structural statistics summarized in Table 3. The overall precision of the ensemble was expressed by an RMSD of 0.6 Å calculated from the coordinates of the main chain atoms. The energy-minimized average structure of apoCaM/IQ (Fig 2B, calculated from the ensembles in Fig 2A) contained two EF-hand motifs (EF3 and EF4) in a semi-open conformation akin to that observed for apoCaM bound to the IQ motif in voltage-gated Na^+ channels (Chagot & Chazin, 2011; Feldkamp *et al*, 2011). This semi-open apoCaM C-lobe structure was bound to the α -helical IQ motif ($\alpha_11.2$ residues 1,646–1,665; Fig 2B) with an orientation that was opposite to that observed in the crystal structure of Ca^{2+} -CaM bound to IQ (Van Petegem *et al*, 2005).

The NMR-derived structure of apoCaM bound to $\alpha_11.2$ IQ peptide contained a number of important intermolecular contacts that

Table 1. NMR structural statistics for α -actinin-1 EF34/IQ.

NMR structural restraints	
Intermolecular NOEs	73
Hydrogen bonds	62
RDC Q-Factor	0.095
$^3\text{D}_{\text{HN}}\text{RDC}$	34
RDC correlation coefficient (R)	0.99
Root mean squared deviation from average structure	
α -actinin-1 backbone atoms	0.5 Å \pm 0.3 for 200 structures
α -actinin-1 backbone atoms (refined)	0.3 Å \pm 0.2 for 50 structures
Haddock scoring	
Cluster size	194
Van der Waals energy	-40.2 \pm 6.2
Electrostatic energy	-395.4 \pm 37.1
Restraints violation energy	278.0 \pm 6.23
Ramachandran plot	
Most favored regions	96.7%
Allowed regions	2.2%
Unfavored regions	1.1%

Table 2. K_d (in μM) for α -actinin-1 EF3/EF4 binding to IQ as determined by FP.

	α -actinin-1 EF3/4		
	WT	E847K/E851K	F833A
Ca _v 1.2 IQ			
WT	14 \pm 2	167 \pm 20	100 \pm 10
K1647E	73 \pm 10	27 \pm 2	/
K1647A	67 \pm 10	/	/
Y1649A	42 \pm 4	/	/
I1654A	200 \pm 20	/	/
F1658A	20 \pm 2	/	/
K1662E	20 \pm 2	150 \pm 20	/

Shown are mean \pm SD ($n = 3$ for all conditions).

stabilized this interaction (Fig 2B–D). The most striking intermolecular interactions were as follows: (i) a salt bridge between IQ residue K1662 and apoCaM residue E88 (Fig 2B); (ii) hydrophobic contacts involving the side-chain atoms of IQ residue I1654 and apoCaM residue F90 (Fig 2C); and (iii) hydrophobic contacts involving the side-chain atoms of IQ residue F1658 and apoCaM residues F90/M110 (Fig 2D).

Validation of the apoCaM–IQ NMR structure by mutagenesis

Mutations in both apoCaM and IQ peptide were introduced to verify their predicted intermolecular contacts. We titrated fluorescein-labeled IQ peptide (residues 1,644–1,666) with apoCaM and measured FP. The K_d for WT IQ peptide was 10 μ M (Fig 2E, Table 4), similar to the K_d of 13 μ M in earlier work (Evans *et al*, 2011). To understand why this K_d is ~20-fold higher than the K_d of 580 nM deducted previously from isothermal titration calorimetry (ITC) measurements (Findeisen *et al*, 2013), we performed ITC experiments by adding increments of apoCaM (100 μ M) to the IQ peptide (10 μ M) under near physiological salt concentration (100 mM KCl, Appendix Fig S2A). No heat signal other than that of dilution was detectable (Appendix Fig S2B). The prior ITC experiments were performed at 5 mM KCl (Findeisen *et al*, 2013) and may represent a non-physiological electrostatic attraction between oppositely charged apoCaM and IQ that is suppressed by more physiological salt levels (100 mM KCl). Indeed, apoCaM binds to the IQ peptide with nearly fourfold higher affinity in the absence of salt (Appendix Fig S2C; K_d is 2.6 μ M at 0 KCl and 10 μ M at 100 mM KCl).

According to our FP-binding assay, the K1662E mutation in the IQ peptide and the E88K mutation in apoCaM each decreased the binding affinity between IQ peptide and apoCaM by more than fivefold (Fig 2E; Table 4). Combining the apoCaM E88K mutation with the IQ peptide alteration K1662E restored the binding affinity to some degree although not completely (Fig 2E). The apoCaM mutant F90A showed a ~3.3-fold decrease in binding affinity for WT IQ peptide (Fig 2F; Table 4). Consistently, I1654A and F1658A substitutions in the IQ peptide resulted in a comparable reduction in their affinity for apoCaM (Fig 2F). These results confirmed three important intermolecular interactions that had been seen in the NMR structure: (i) a salt bridge between IQ residue K1662 and apoCaM residue E88; (ii) hydrophobic contact between IQ residue I1654 and apoCaM residue F90; and (iii) hydrophobic contact between IQ residue F1658 and apoCaM residues F90 and M110.

α -Actinin and apoCaM do not form a ternary complex with $Ca_v1.2$ IQ

The structures of α -actinin-1 (Fig 1) and apoCaM (Fig 2) each bound to the IQ peptide reveal that both binding sites are structurally overlapped and therefore should preclude formation of a ternary complex (α -actinin-1/IQ/apoCaM), in contrast to what was suggested previously (Hall *et al*, 2013). The possibility of ternary complex formation was further ruled out by NMR titrations (Fig EV3). The NMR spectrum of 15 N-labeled α -actinin-1 EF-hand domain (Fig EV3A, black peaks) exhibited spectral changes upon the addition of an equivalent amount of unlabeled IQ peptide (Fig EV3A, red peaks marked by arrows) that are reversed by the addition of fivefold excess of unlabeled apoCaM (Fig EV3A, green peaks marked by arrows). This result indicates that α -actinin-1 and apoCaM both compete for binding to the IQ peptide, which implies that α -actinin-1 and apoCaM do not simultaneously bind to $Ca_v1.2$ IQ and therefore rules out the possibility of a ternary complex. A similar result was observed for the NMR titration with 15 N-labeled apoCaM binding to unlabeled IQ (Fig EV3B). The IQ-induced spectral changes to apoCaM are reversed by the addition of fivefold excess of unlabeled α -actinin-1 (Fig EV3B, green peaks marked by arrows), demonstrating that α -actinin-1 and apoCaM do not bind simultaneously to the IQ peptide, which argues against a ternary complex.

α -Actinin binding to the $Ca_v1.2$ IQ motif augments open probability of individual channels

Point mutations that impaired α -actinin binding to the IQ motif of $\alpha_11.2$ reduced current density upon reconstitution of $Ca_v1.2$ in HEK293 cells by 70–80% but surface expression by only 35–40% as determined by two different methods (Tseng *et al*, 2017). We performed cell-attached recordings (Fig 3A) to precisely determine single-channel parameters of $Ca_v1.2$ as before (Davare *et al*, 2001; Patriarchi *et al*, 2016; Qian *et al*, 2017; Bartels *et al*, 2018). All three mutations in the IQ motif that impaired α -actinin binding (Table 2) (Tseng *et al*, 2017), i.e., K1647A, Y1649A, and I1654A, decreased functional availability by 79–93%, ensemble averages by 84–91%, and single-channel activity by ~85–92% without affecting unitary current amplitudes (i) (Figs 3B–G and EV4).

The single-channel activity is the product of the number (N) of channels in a patch, the open probability (P_o), and unitary current amplitudes (i) of each individual channel (i.e., $N \cdot P_o \cdot i$). Because i

Figure 2. ApoCaM forms electrostatic and hydrophobic contacts with $Ca_v1.2$.

- Ensemble of 10 lowest energy NMR-derived structures of apoCaM/IQ complex. Structural statistics are given in Table 3.
- Energy-minimized average structure of apoCaM (cyan) bound to IQ (red), showing an intermolecular salt bridge between IQ K1662 and apoCaM E88. The K1662 side-chain amino nitrogen atom is 2.7 Å away from the side-chain carbonyl oxygen of E88.
- Intermolecular hydrophobic contacts between IQ I1654 (red) and apoCaM F90 (cyan). Side-chain atoms colored yellow. The I1654 side-chain methyl carbon atom is 2.2 Å away from the closest aromatic ring atom of F90.
- Intermolecular hydrophobic contacts between F1658 of IQ and F90/M110 in apoCaM. The aromatic side-chain atoms of F1658 are 2.3 and 2.6 Å away from the closest side-chain atom of F90 and M110, respectively.
- FP titrations showing binding of apoCaM to IQ peptides WT (black) and K1662E (red) and of apoCaM mutant E88K to IQ WT (green) and IQ peptide K1662E (blue, “charge inversion”; see Table 4 for binding parameters and standard errors).
- FP titrations showing binding of apoCaM to IQ peptides WT (black), I1654A (red), and F1658A (green) and of apoCaM mutant F90A to IQ WT (blue; see Table 4 for binding parameters and standard errors).

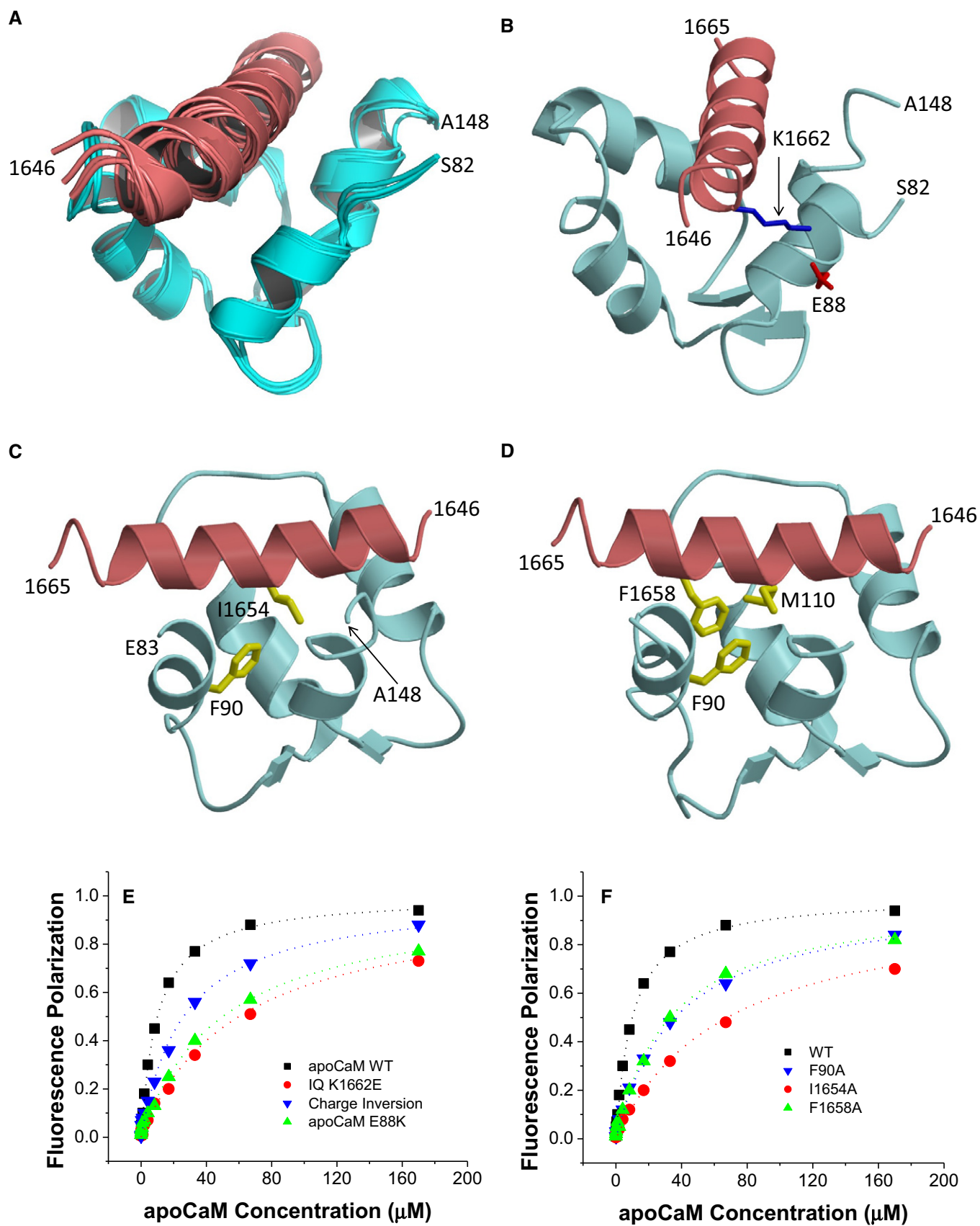


Figure 2.

Table 3. NMR structural statistics for apoCaM/IQ.

NMR structural restraints	
Hydrogen bonds	62
RDC Q-Factor	0.089
¹ D _{HN} RDC	36
RDC Correlation Coefficient (R)	0.99
Root mean squared deviation from average structure	
CaM backbone atoms	0.6 Å ± 0.3 for 200 structures
CaM backbone atoms (refined)	0.6 Å ± 0.2 for 92 structures
Haddock scoring	
Cluster size	200
Van der Waals energy	-56.8 ± 0.6
Electrostatic energy	-463.5 ± 20.7
Restraints violation energy	99.8 ± 36.2
Ramachandran plot	
Most favored regions	89.8%
Allowed regions	8.0%
Unfavored regions	2.3%

was unaffected (Fig 3F), the mutations must affect NPo. Given that surface expression of all three mutations decreased by only 35–40% versus WT α_1 1.2 under exactly the same conditions (Tseng *et al*, 2017), the ~90% reduction of NPo for all three mutants to ~10% of WT Ca_v1.2 suggests that Po of the remaining ~60% channels is only ~1/6 of the Po of WT Ca_v1.2. These observations suggest a remarkable ~6-fold decrease in Po upon loss of α -actinin binding. To corroborate this notion, we determined N for each recording and derived Po for individual channels. Accordingly, Po is reduced by ~90% for individual channels carrying a K1647A, Y1649A, or I1654A mutation (Fig 3E; Table 5a–e). At the same time, the F1658A and K1662E mutations, which diminish apoCaM binding, did not alter NPo (Table 5f,g).

To further scrutinize the role of α -actinin in Po of Ca_v1.2, Ca_v1.2 was co-expressed with WT α -actinin-1 or its binding-deficient E847K/E851K mutant (Fig 4A) and availability, NPo, Po, i, and assemble averages determined (Fig 4B–G). Overexpression of WT

Table 4. K_d (in μ M; means \pm SEM) for apoCaM binding to IQ as determined by FP.

	apoCaM		
	WT	E88K	F90A
Ca _v 1.2 IQ			
WT	10 ± 3	50 ± 10	33 ± 5
K1647E	12 ± 3	53 ± 1.0	/
K1647A	11 ± 3	/	/
Y1649A	16 ± 4	/	/
I1654A	68 ± 1.0	/	/
F1658A	33 ± 5	/	/
K1662E	60 ± 10	26 ± 5	/

Shown are mean \pm SD ($n = 3$ for all conditions).

but not E847K/E851K mutant α -actinin-1 increased Po of Ca_v1.2 WT by more than twofold from 3.4% seen with Ca_v1.2 alone to 7.9% (Fig 4E; Table 6a–c). Availability, NPo, and assemble averages but not unitary current amplitudes were also increased by WT but not E847K/E851K mutant α -actinin-1 (Fig 4B, C, D, F and G; Table 6a–c). Accordingly, in HEK293 cells functional occupancy of Ca_v1.2 by endogenous α -actinin appears to be far from complete.

To further test whether α -actinin needs to bind to the Ca_v1.2 IQ motif to augment Po, we used a charge inversion experiment by mutating K1647 to the negatively charged glutamyl rather than neutral alanyl residue and then attempted rescue of the expected reduction in Po by pairing expression of K1647E Ca_v1.2 with charge-inverted E847K/E851K α -actinin-1. Co-expression of K1647E mutant Ca_v1.2 with WT α -actinin-1 yielded a low availability, NPo, Po, and ensemble average (Fig 5C–E and G; Table 6d), which were well below the values observed upon expression of WT Ca_v1.2 alone or co-expression of WT Ca_v1.2 with E847K/E851K mutant α -actinin-1 (Fig 4C–E and G; Table 6a–c). The reduction in availability was statistically significantly, though not fully, rescued when K1647E mutant Ca_v1.2 was paired with E847K/E851K mutant rather than WT α -actinin-1 (Fig 5A; Table 6e). Po also appears to be partially rescued although the P value was 0.07 versus pairing of WT α -actinin-1 with K1647E mutant Ca_v1.2. This rescue of loss of availability and likely Po for K1647E mutant Ca_v1.2 by E847K/E851K mutant α -actinin-1 must be due to either enhanced opening of individual channels, a change in channel surface expression, or both. This rescue is difficult to explain by a mechanism other than that α -actinin-1 binding augments channel activity, including binding of endogenous apoCaM. Consistently, impairing apoCaM binding to the Ca_v1.2 IQ motif by mutating F1658 to Ala or K1662 to Glu had no effect on availability, NPo, and Po, and did not affect ensemble averages (Fig 3C–G; Table 5).

One possibility for a reduction in Po is that K1647A, Y1649A, and I1654A shift the voltage dependence of Ca_v1.2 to more positive potentials such that WT channels open upon depolarization to 0 mV more readily than mutant channels. However, neither the reversal potential nor the voltage dependence of activation was significantly affected by the K1647A and Y1649A mutations and only minimally by the I1654A mutation (Appendix Fig S3; Table 7a–d).

To test whether this charge inversion rescue for the K1647E mutant promoted surface expression of Ca_v1.2, we performed surface biotinylation experiments (Fig 6). As expected, co-expression of WT α -actinin-1 with WT Ca_v1.2 increased α_1 1.2 biotinylation by ~60% versus WT α_1 1.2 alone. Thus, WT Ca_v1.2 expression at the surface is enhanced by α -actinin-1 (Fig 6A). That the increase in surface expression of WT Ca_v1.2 by WT α -actinin-1 overexpression was smaller than the increase in Po is analogous to the smaller effects of the α_1 1.2 K1647A, Y1649A, and I1654A mutations on surface expression compared to charge density (Tseng *et al*, 2017) and the larger decrease in Po and NPo we report here (Fig 3). Importantly, this increase in Ca_v1.2 surface expression by α -actinin-1 was not seen when WT α_1 1.2 was co-expressed with E847K/E851K mutant α -actinin-1 or K1647E mutant α_1 1.2 with WT α -actinin-1 (Fig 6B). However, the charge inversion we performed by combining these mutants failed to increase surface expression of Ca_v1.2 to a degree that would be detectable (Fig 6B). This result is in contrast to our findings that K1647E α_1 1.2 availability and likely Po were partially rescued by the E847K/E851K α -actinin-1 charge

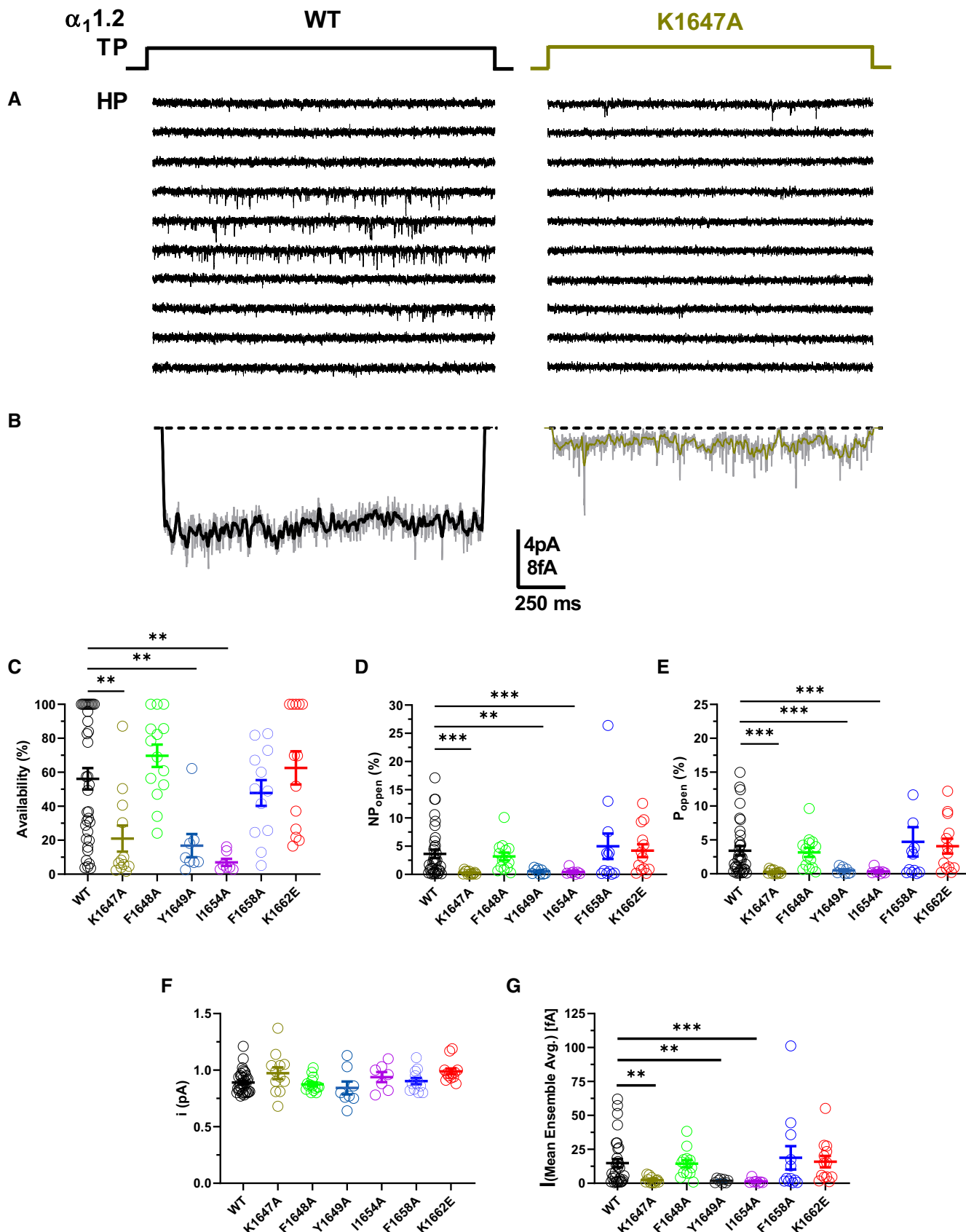


Figure 3.

Figure 3. Ca_v1.2 mutations that affect α -actinin-1 drastically decrease channel open probability.

HEK293 cells were transfected with α_1 1.2, $\alpha_2\delta$ -1, and β_{2A} and cultured for 22–24 h before cell-attached patch recording in 110 mM Ba²⁺.

- A Single Ca_v1.2 channel recordings of Ca_v1.2 WT and K1647A. Holding potential (HP) was –80 mV and test potential (TP) 0 mV. Shown are 10 consecutive sweeps from representative experiments (see Fig EV4 for more sweeps).
- B Mean assemble averages for all experiments with Ca_v1.2 WT and K1647A, which are based on a total of 2,744 and 868 sweeps, respectively (see Table 5).
- C–G Dot plots and means \pm SEM for availability (i.e., likelihood that a sweep had at least one event; C), NP_{open} (D), Po (E), unitary current amplitude i (F), and the mean of the current of a single channel at any point in time calculated from the ensemble averages of each experiment (G) (***P* < 0.01, ****P* < 0.001 compared to WT; one-way ANOVA with Bonferroni post hoc test (C) or Welch ANOVA with Tamhane T2 test (D–G); *n* = 7–35. see Table 5 for more details).

Table 5. Biophysical properties of Ca_v1.2 microscopic single-channel currents for WT versus IQ motif mutants.

Gating parameter	Availability (%)	NP _{open} (%)	P _{open} (%)	I (mean ensemble avg.) [fA]	Unitary current (pA)	Sweeps	<i>n</i>
WT (a)	56.2 \pm 6.3	3.6 \pm 0.75	3.4 \pm 0.7	14.8 \pm 3.1	0.89 \pm 0.02	2,744	32–35
K1647A (b)	21.0 \pm 7.6**	0.30 \pm 0.09***	0.27 \pm 0.08***	2.3 \pm 0.6**	0.97 \pm 0.05	868	12
F1648A (c)	69.7 \pm 6.6	3.2 \pm 0.7	3.2 \pm 0.7	14.4 \pm 2.6	0.87 \pm 0.02	1,221	13–14
Y1649A (d)	16.8 \pm 6.8**	0.53 \pm 0.17**	0.49 \pm 0.2***	1.9 \pm 0.5**	0.84 \pm 0.06	556	8
I1654A (e)	7.0 \pm 2.1**	0.44 \pm 0.2***	0.35 \pm 0.2***	1.4 \pm 0.6***	0.94 \pm 0.04	589	7
F1658A (f)	47.8 \pm 7.6	5.0 \pm 2.2	4.7 \pm 2.2	18.8 \pm 8.6	0.90 \pm 0.03	986	12
K1662E (g)	62.5 \pm 9.7	4.2 \pm 1.1	4.1 \pm 1.1	15.9 \pm 4.2	0.99 \pm 0.03	1,015	13
One-Way ANOVA	a-b [†]	a-b [‡]	a-b [‡]	a-b [‡]	NS		
	a-d [†]	a-d [‡]	a-d [‡]	a-d [‡]			
	a-e [†]	a-e [‡]	a-e [‡]	a-e [‡]			

HEK293 cells were transiently transfected with WT and IQ domain mutant Ca_v1.2 (α_1 1.2, $\alpha_2\delta$ -1, and β_{2A}) for recording of single-channel activity in 110 mM Ba²⁺ upon depolarized from a holding potential –80 mV to a test potential (TP) of 0 mV for 2 s at an interpulse rate of 0.14 Hz. Availability is quantified as the fraction of sweeps showing channel activity over the number of total sweeps. Statistical significance was determined by pairwise multiple testing WT (a) against K1647A (b), F1648A (c), Y1649A (d), I1654A (e), F1658A (f), and K1662E (g) by a one-way ANOVA with Bonferroni[†] post hoc test or Welch ANOVA with Tamhane[‡] T2 test. Given are mean values \pm SEM (**P* < 0.05, ***P* < 0.01, ****P* < 0.0001).

reversal (Fig 5). It is conceivable that a small rescue effect did occur but was indiscernible for statistical reasons as 95% confidence intervals (CIs) are larger than a potentially partial rescue of, e.g., 30% of the impairment of ~50% by the K1647E mismatch with WT α -actinin-1 (Appendix Table S1; a 30% rescue would translate into only an ~15% increase in surface expression).

 α -Actinin binding to the Ca_v1.2 IQ motif augments gating charge movement as well as its coupling to channel opening

To test the molecular mechanism underlying the α -actinin-induced increase in Po in more detail, we analyzed gating charge movement at the Ba²⁺ current reversal potential (Fig 7) by whole-cell patch-clamp recording. This approach measures all of the Ca²⁺ channels on the surface, thereby ruling out any potential limitation caused by the channel selection inherent in the cell-attached patch recordings in Figs 3–5. The K1647A, Y1649A, and I1654A mutations reduced gating currents (Q_{on}) by 66–77% (Fig 7A, B and D; Table 7) suggesting that α -actinin fosters gating charge movement. This reduction is stronger than the reduction in surface expression (Tseng *et al*, 2017) but not quite as strong as the 90% reduction in NPo for these mutants (Fig 5). Thus, we investigated whether α -actinin also augments coupling of gating charge movement to channel opening. We analyzed the relationship of tail currents (I_{tail}) to Q_{on} and determined the slopes of the regression curves as an established parameter for quantification of the coupling of Q_{on} to I_{tail} (Tuluc *et al*, 2009; Yang *et al*, 2010). Accordingly, the slopes for

K1647A, Y1649A, and I1654A mutant Ca_v1.2 were strongly reduced compared to WT (Fig 7C; Table 7a–d). Because large gating events were rare for these mutants, we combined all data from those three mutants for further analysis to better cover that range of the curve. This analysis confirmed that the slope of the resulting curve was substantially smaller than for WT Ca_v1.2 (Fig 7E). Collectively, these data indicate that binding of α -actinin to the Ca_v1.2 IQ motif augments not only surface expression but also gating charge movement and its coupling to channel opening. Neither gating charge movements nor their coupling to channel opening were significantly affected by the F1658A or K1662E mutations (Fig 7; Table 7e,f), once more arguing against a role in apoCaM binding to the IQ motif in defining NPo under basal conditions.

Discussion

The NMR structures of α -actinin-1 and apoCaM bound to the Ca_v1.2 IQ motif presented here revealed distinct intermolecular interactions that were verified by mutagenesis experiments involving charge inversion for both interactions. The EF hands in α -actinin-1 are not capable of binding to Ca²⁺ under physiological conditions because their EF-hand loops lack the proper residues for ligating Ca²⁺ with high affinity (Backman, 2015). Therefore, the α -actinin-1 EF-hand domain bound to Ca_v1.2 is in the Ca²⁺-free state under basal conditions ([Ca²⁺]_i of ~100 nM) and adopts a semi-open conformation of Ca²⁺-free EF hands like that

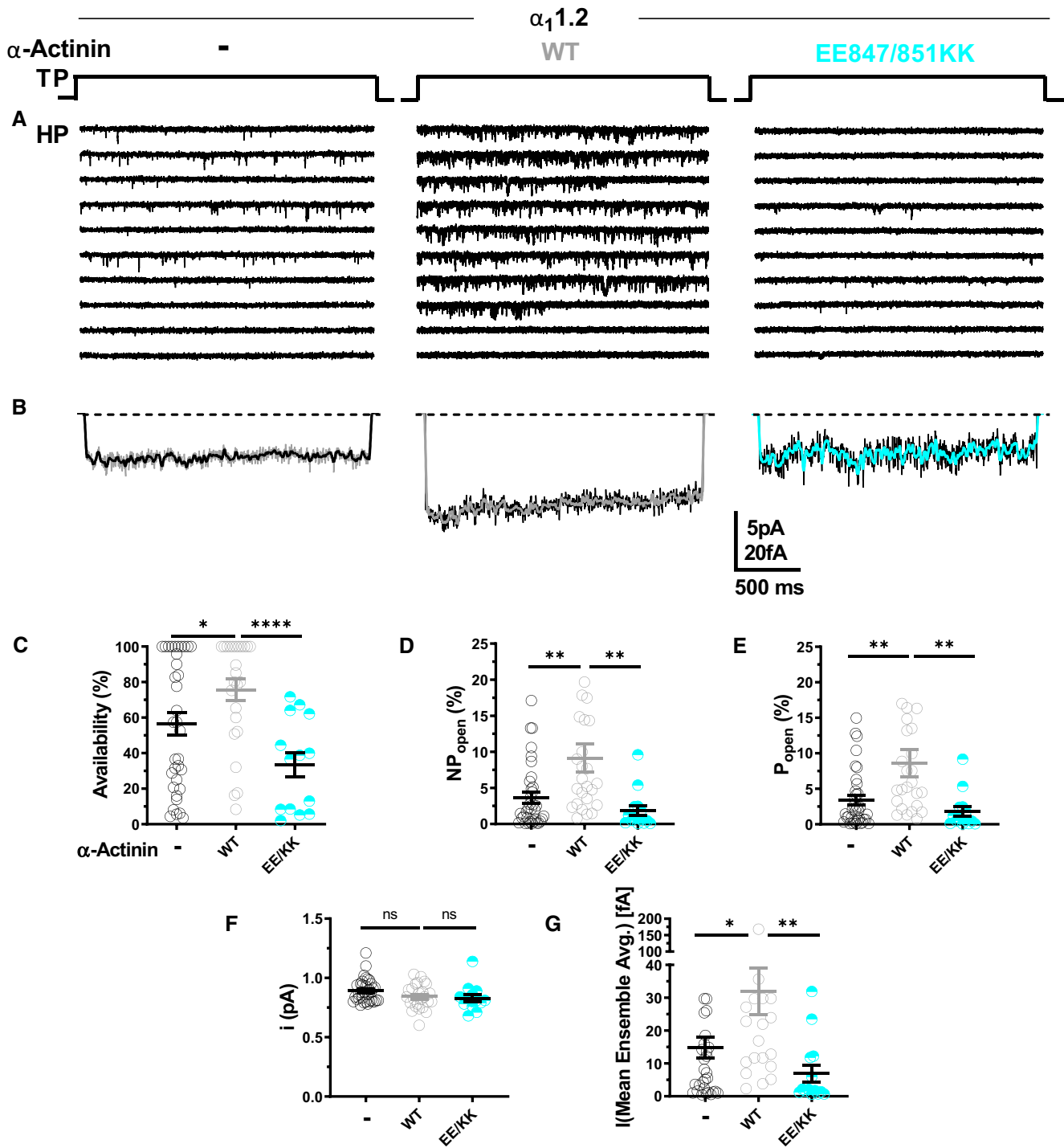


Figure 4. Ectopic α -actinin-1 expression increases $\text{Ca}_v1.2$ open probability.

HEK293 cells were transfected with $\alpha_11.2$, $\alpha_2\delta-1$, and β_{2A} plus, if indicated, α -actinin-1 before cell-attached patch recording.

A Representative single $\text{Ca}_v1.2$ channel recordings of WT $\text{Ca}_v1.2$ alone or with WT or E847K/E851K mutant α -actinin-1.

B Mean ensemble averages for all experiments for each combination.

C-G Dot plots and means \pm SEM for availability (C), NPo (D), Po (E), unitary current amplitude i (F), and the mean of the current of a single channel calculated from the ensemble averages of each experiment (G) (* $P < 0.05$, ** $P < 0.01$, **** $P < 0.001$; unpaired t-test; $n = 13-35$; see Table 6 for more details).

Table 6. Effect of α -actinin-1 ectopic expression on biophysical properties of Ca_v1.2 single-channel currents.

Gating parameter	Availability (%)	NP _{open} (%)	P _{open} (%)	I (Mean ensemble Avg.) [fA]	Unitary current (pA)	Sweeps	n
WT (a)	56.6 ± 6.3	3.6 ± 0.75	3.4 ± 0.69	14.8 ± 3.1	0.89 ± 0.02	2,744	32–35
WT + α -Actinin (b)	76.5 ± 6.2*	9.2 ± 2.0**	7.9 ± 2.0*	31.3 ± 7.5*	0.84 ± 0.02	2,388	23–25
WT + EE847/851KK (c)	32.9 ± 7.5****	1.9 ± 0.7**	1.8 ± 0.7*	7.4 ± 2.8*	0.83 ± 0.03	1,252	13
K1647E + α -Actinin (d)	43 ± 5.0	1.8 ± 0.3	1.7 ± 0.3	8.5 ± 1.5	0.83 ± 0.01	2,601	30
K1647E + EE847/851KK (e)	67.9 ± 6.9**	2.6 ± 0.5	2.5 ± 0.5	11.3 ± 2.7	0.84 ± 0.02	1,376	16
Unpaired t-test	a-b [§]	a-b [§]	a-b [§]	a-b [§]	NS		
	b-c [§]	b-c [§]	b-c [§]	b-c [§]			
	d-e [§]		d-e P = 0.7	d-e P = 0.7			

HEK293 cells were transiently transfected with WT Ca_v1.2 (α_1 1.2, α_2 . δ_1 , and β_{2a}) and, if indicated, with α -actinin-1 WT or E847K/E851K. Single-channel activity was obtained as in Table 5. Statistical significance was determined by pairwise testing of Ca_v1.2 WT alone (a) versus Ca_v1.2 WT + α -actinin WT (b), Ca_v1.2 WT + α -actinin-1 WT versus Ca_v1.2 + α -actinin-1 E847K/E851K (c), and Ca_v1.2 K1647E + α -actinin-1 WT (d) versus Ca_v1.2 K1647E + α -actinin-1 E847K/E851K (e) with an unpaired t-test[§]. Given are mean values ± SEM (*P < 0.05, **P < 0.01, ****P < 0.0001). Values for Ca_v1.2 WT are provided for comparison from Table 5.

observed for apoCaM bound to various target proteins (Houdusse *et al*, 2006; Chagot & Chazin, 2011; Feldkamp *et al*, 2011). However, the semi-open EF-hand conformation of α -actinin-1 binds to the IQ peptide with a polarity opposite to that of apoCaM (see black arrows in Fig EV5A and B). The Ca_v1.2 residue K1647 at the N-terminal end of the IQ helix forms intermolecular salt bridges with α -actinin-1 residues E847 and E851. By stark contrast, the IQ helix is rotated 180 degrees upon binding to apoCaM (see black arrows in Fig EV5). This opposite orientation places Ca_v1.2 residue K1662 at the C-terminal end of the IQ helix in close proximity to CaM residues E85 and E88, which are homologous to α -actinin-1 residues E847 and E851. Similarly, the IQ helices in voltage-gated Na⁺ channels bind to apoCaM and Ca²⁺-saturated CaM with opposite polarity (Hovey *et al*, 2017). Thus, the orientation of the IQ helix bound to the EF-hand motif may be an important structural determinant of binding specificity and may explain why α -actinin-1 and apoCaM have different functional effects.

Voltage-gated Na⁺ channels exhibit Ca²⁺-dependent inactivation (CDI) mediated by Ca²⁺-CaM (Ben-Johny *et al*, 2014; Gabelli *et al*, 2016), similar to Ca_v1.2 (Peterson *et al*, 1999; Zuhlke *et al*, 1999). However, the structure of apoCaM bound to the Ca_v1.2 IQ motif (Fig EV5B) is quite different from previous structures of apoCaM bound to Na_v1.2 (Fig EV5C) or Na_v1.5 (Chagot & Chazin, 2011; Gabelli *et al*, 2014). The Na_v1.2 IQ motif sequence is only 17% identical to that of Ca_v1.2 (Fig EV5D). Na_v1.2 residues A1909, A1915, and Y1919, which are not conserved in Ca_v1.2, each make critical contacts with apoCaM (Fig EV5C). The side-chain methyl groups of A1909 and A1915 are each 2.5 Å away from the side-chain methyl atoms of CaM residues M109 and L85, respectively. The aromatic side chain of Y1919 is in intimate contact with the aromatic side chain of F141 from CaM. Another important difference is that the Ca_v1.2 IQ helix binds to apoCaM with opposite directionality compared to the Na_v1.2 IQ helix (see black arrows in Fig EV5B and C). Hence, the salt bridge that connects Ca_v1.2 (K1662) to apoCaM (E88) is not conserved in Na_v1.2 or Na_v1.5 but the large number of non-conserved intermolecular hydrophobic contacts to Na_v1.2 (Fig EV5C) caused by the opposite binding orientation of the IQ helix should outweigh any stabilization from the salt bridge in Ca_v1.2 and may explain why apoCaM binds to Na_v1.2 and Na_v1.5

with nanomolar affinity (Hovey *et al*, 2017) compared to the much weaker micromolar affinity of apoCaM binding to Ca_v1.2 (Table 4).

The relatively high dissociation constant for apoCaM binding to the α_1 1.2 IQ motif ($K_d = 10 \mu\text{M}$) may be outside the physiological concentration range for apoCaM in neurons. Under basal conditions, the cytosolic apoCaM is kept below 1 μM (Wu & Bers, 2007) by proteins that have a high affinity for apoCaM. For instance, in neurons neurogranin (RC3) (Huang *et al*, 2000, 2004; Ran *et al*, 2003; Zhong *et al*, 2011) and GAP-43 (P-57) (Cimler *et al*, 1985) serve as sinks and reservoirs for apoCaM. In neurons, total concentration of CaM is ~10 μM (Egrie *et al*, 1977; Zhabotinsky *et al*, 2006), of neurogranin is 20 μM (Huang *et al*, 2004; Zhabotinsky *et al*, 2006), and of GAP-43 is 18 μM (Cimler *et al*, 1985; Zhabotinsky *et al*, 2006), and their K_d values for apoCaM are in the range of 1–5 μM (Alexander *et al*, 1987; Huang *et al*, 2000; Zhabotinsky *et al*, 2006), resulting in 0.9 μM free CaM under basal conditions (Zhabotinsky *et al*, 2006). Therefore, on the basis of the relatively low binding affinity of apoCaM ($K_d = 10 \mu\text{M}$), the fractional binding of apoCaM to α_1 1.2 can be estimated to be < 10% ($Y = \frac{[CaM]}{[CaM] + K_d} < 0.1$) under basal physiological conditions in neurons. Recent work suggests that ectopically expressed WT CaM as well as Ca²⁺ binding-deficient CaM₁₂₃₄ is in large excess over endogenous CaM (Iacobucci & Popescu, 2017). As a result, CaM₁₂₃₄ may occupy a much larger fraction of α_1 1.2 than the endogenous WT apoCaM. In this scenario, expression of CaM₁₂₃₄ could impair CDI as seen earlier (Peterson *et al*, 1999) by mechanisms other than displacement of endogenous apoCaM as invoked earlier (Peterson *et al*, 1999).

Alterations of I1609 in α_1 1.3 (equivalent to I1654 in α_1 1.2) impair binding of apoCaM to the closely related Ca_v1.3 channel and Po, which was interpreted to mean that apoCaM binding to this IQ motif augments Po (Adams *et al*, 2014). Here, we show that the homologous I1654 in the highly conserved IQ motif of Ca_v1.2 is not only critical for apoCaM but also α -actinin binding. Accordingly, mutating I1609 could have decreased NPo by impairing α -actinin rather than apoCaM binding. Indeed, cell-attached channel recordings showed an ~90% reduction in Po for all three α -actinin binding-deficient α_1 1.2 IQ mutants. This effect included K1647, which contacts α -actinin (Fig 1C) but not apoCaM. Consistently, the K1647A mutation reduced binding of α -actinin (Table 2) but not apoCaM

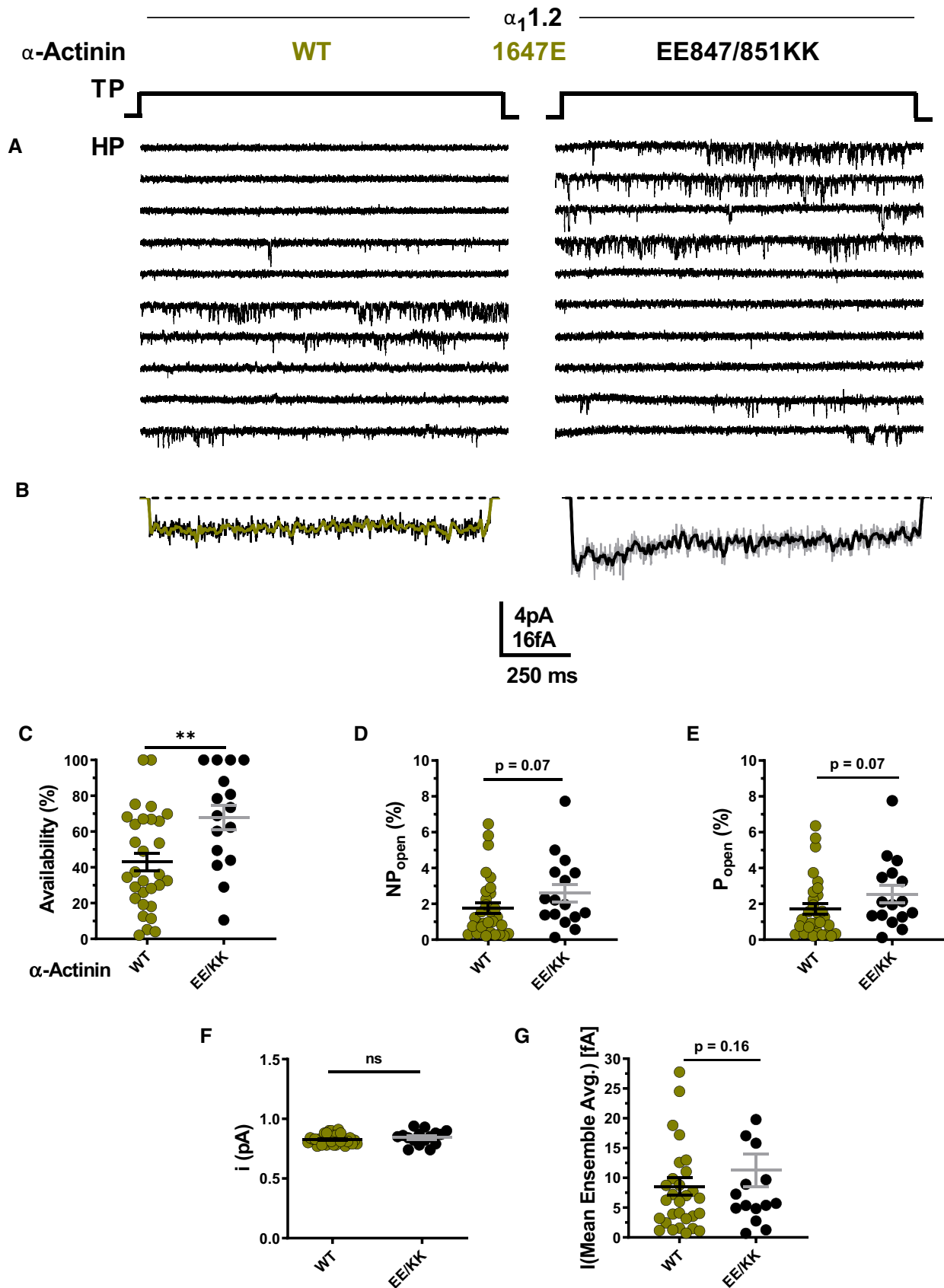


Figure 5.

Figure 5. α -Actinin-1 E847K/E851K partially rescues open probability for $\text{Ca}_v1.2$ K1647E.

HEK293 cells were transfected with $\alpha_1.2$ with the K1647E mutation, $\alpha_2\delta-1$, and β_{2A} plus α -actinin-1 WT or E847K/E851K before cell-attached patch recording.

A Representative single $\text{Ca}_v1.2$ channel recordings of $\text{Ca}_v1.2$ K1647E with WT or E847K/E851K α -actinin-1.

B Mean ensemble averages for all experiments for both combinations.

C–G Dot plots and means \pm SEM for availability (C), NPo (D), Po (E), unitary current amplitude i (F), and mean of the current of a single channel calculated from the ensemble averages of each experiment (G) (** $P < 0.01$; unpaired t -test; $n = 16$ –30; see Table 6 for more details).

(Table 4). The same is true for the Y1649A mutation. Although Y1649 does not form a direct interaction with α -actinin EF3-EF4, the Y1649A mutation does abrogate α -actinin binding in the yeast two-hybrid system (Tseng *et al*, 2017). We suggest that Y1649 is necessary to stabilize the orientation of L1653 and neighboring I1654, which is required for binding to α -actinin (Appendix Fig S4A). Thus, our new data indicate that Po is largely determined by α -actinin and not apoCaM binding. In fact, the F1658A and K1662E mutations, which decreased apoCaM binding (Table 4), did affect neither Po (Fig 3E) nor Q_{on} (Fig 7A, B and D) and minimally if at all α -actinin binding (Table 2). In support of these results, others found no effect of CaM on $\text{Ca}_v1.2$ plasma membrane targeting in HEK293 cells (Bourdin *et al*, 2010). This conclusion is further supported by the charge inversion experiments of K1647E mutant $\alpha_1.2$ and E847K/E851K mutant α -actinin-1 in which impaired functional channel availability and likely impaired Po are partially rescued (Fig 5). These findings support the functional relevance of the interaction of the positively charged K1647 in the IQ motif with the negatively charged E847 and E851 of α -actinin-1. That the rescue of the reduction in Po of K1647E mutant $\alpha_1.2$ by E847K/E851K mutant α -actinin-1 is far from complete can in part be explained by analysis of the E851K rotamers (Appendix Fig S4B–D). Most of the E851K rotamers are predicted to clash with side-chain and backbone atoms within the α -actinin region at the channel– α -actinin interface based on our structure (Fig 1C), which will most likely affect the positioning of the EF-hand region of α -actinin relative to $\alpha_1.2$ and thereby

the α -actinin– $\alpha_1.2$ interaction. As a result, binding of E847K/E851K mutant α -actinin-1 to $\alpha_1.2$ will be decreased as compared to WT α -actinin. In fact, binding affinity is also not fully rescued when the K1647E IQ peptide is titrated with E847K/E851K mutant α -actinin-1 EF3/4 segment (Table 2). A change in the exact structure of the region surrounding the IQ motif in full-length $\alpha_1.2$ could be the reason for further impairment of α -actinin binding furnishing a potential explanation for our finding that functional availability and Po are less effectively rescued by the full charge inversion than the *in vitro* binding affinity.

Further mechanistic insight is provided by the strong reduction in gating charge movement upon loss of α -actinin binding (Fig 7). The most striking and very clear finding for Q_{on} is the observation that gating charges for the three α -actinin binding-deficient $\alpha_1.2$ mutants are so small that they are often barely if at all detectable and amplitudes are difficult to determine. Accordingly, α -actinin binding to the IQ motif promotes the outward movement of the S4 segments, which gives rise to the gating charges, presumably by either lowering energy barriers for this motion or by stabilizing the “outward” conformation of S4 segments. In addition, α -actinin binding to the IQ motif augments also the coupling between this gating movement and channel opening. This finding is reminiscent of the effect of $\text{Ca}_v1.2$ phosphorylation by PKA on S1700, which upregulates this coupling (Fuller *et al*, 2010, 2014). Because of the close proximity of S1700 to the IQ motif, it is tempting to speculate that phosphorylation of S1700 and α -actinin binding to the IQ motif

Table 7. Biophysical properties of $\text{Ca}_v1.2$ macroscopic whole-cell patch currents for WT versus IQ motif mutants.

Analysis Parameter	I-V			G-V			Charge movement Q_{on} (fC/pF)	I_{tail}/Q_{on} Slope
	$V_{1/2act}$ (mV)	k_{act}	E_{rev} (mV)	$V_{1/2act}$ (mV)	k_{low}	k_{high}		
WT (a)	-18.5 ± 0.5	-4.2 ± 0.4 (10)	51.3 ± 1.3	$-6.5.0 \pm 0.4$	7.0 ± 0.3 (16)	-8.5 ± 27.4	3.8 ± 0.9 (18)	3.9 ± 1.5 (16)
K1647A (b)	-19.9 ± 0.9	-5.9 ± 0.6 (11)	55.2 ± 2.0	$-8.5.0 \pm 0.9$	8.5 ± 0.8 (15)	9.0 ± 10.5	$1.3 \pm 0.3^*$ (15)	0.26 ± 1.5 (15)
Y1649A (c)	-19.9 ± 0.6	-4.0 ± 0.5 (10)	49.2 ± 1.5	$-6.3.0 \pm 0.7$	7.5 ± 0.8 (16)	28.7 ± 6.9	$0.98 \pm 0.3^{**}$ (13)	0.19 ± 1.0 (12)
I1654A (d)	$-12.6 \pm 1.0^{****}$	-5.4 ± 0.7 (5)	48.2 ± 2.6	$-2.5 \pm 0.9^{**}$	7.5 ± 0.9 (13)	38.5 ± 11.5	$0.87 \pm 0.3^{**}$ (13)	1.3 ± 0.6 (12)
F1658A (e)	$-26.5 \pm 1.1^{**}$	-4.5 ± 0.9 (6)	58.6 ± 4.1	$-10.6 \pm 1.4^{**}$	5.3 ± 1.6 (11)	20.2 ± 3.9	2.8 ± 0.6 (13)	3.1 ± 1.4 (12)
K1662E (f)	-20.2 ± 0.4	-4.2 ± 0.3 (12)	50.1 ± 1.2	$-6.1.0 \pm 0.7$	7.9 ± 0.8 (21)	49.2 ± 19.4	3.5 ± 1.1 (17)	2.2 ± 1.0 (14)
ANOVA/ t -test	a-d [†]			a-d [†]			a-b [†]	
							a-c [†]	
	a-e [†]	NS	NS	a-e [†]	NS	NS	a-d [†]	

HEK293 cells were transiently transfected with WT $\text{Ca}_v1.2$ ($\alpha_1.2$, $\alpha_2\delta-1$, and β_{2A}). Whole-cell patch recording was performed in 20 mM Ba^{2+} (see Fig 7). To obtain current–voltage relationships (I-V), currents were recorded upon depolarization from a holding potential of -80 mV to increasingly more positive potentials (see Fig 7A for details). The voltage for half maximal activation ($V_{1/2act}$), activation constant (k_{act}), and reversal potential (E_{rev}) was determined. To obtain conductance–voltage relationships (G-V), tail currents (I_{tail}) were recorded upon repolarization to -50 mV following depolarization from a holding potential of -80 mV to increasingly more positive potentials (see Fig 7A for details). The activation kinetics for G-V were best described by double exponential fits, and the rate constants k_{high} and k_{low} were determined accordingly. Total charge movement (Q_{on}) and the ratio of I_{tail}/Q_{on} were determined as in Fig 7. Statistical significance was determined by pairwise multiple testing WT (a) against K1647A (b), Y1649A (c), I1654A (d), F1658A (e), and K1662E (f) by a one-way ANOVA with a Bonferroni[†] post hoc test. Given are mean values \pm SEM (* $P < 0.05$, ** $P < 0.01$, **** $P < 0.0001$).

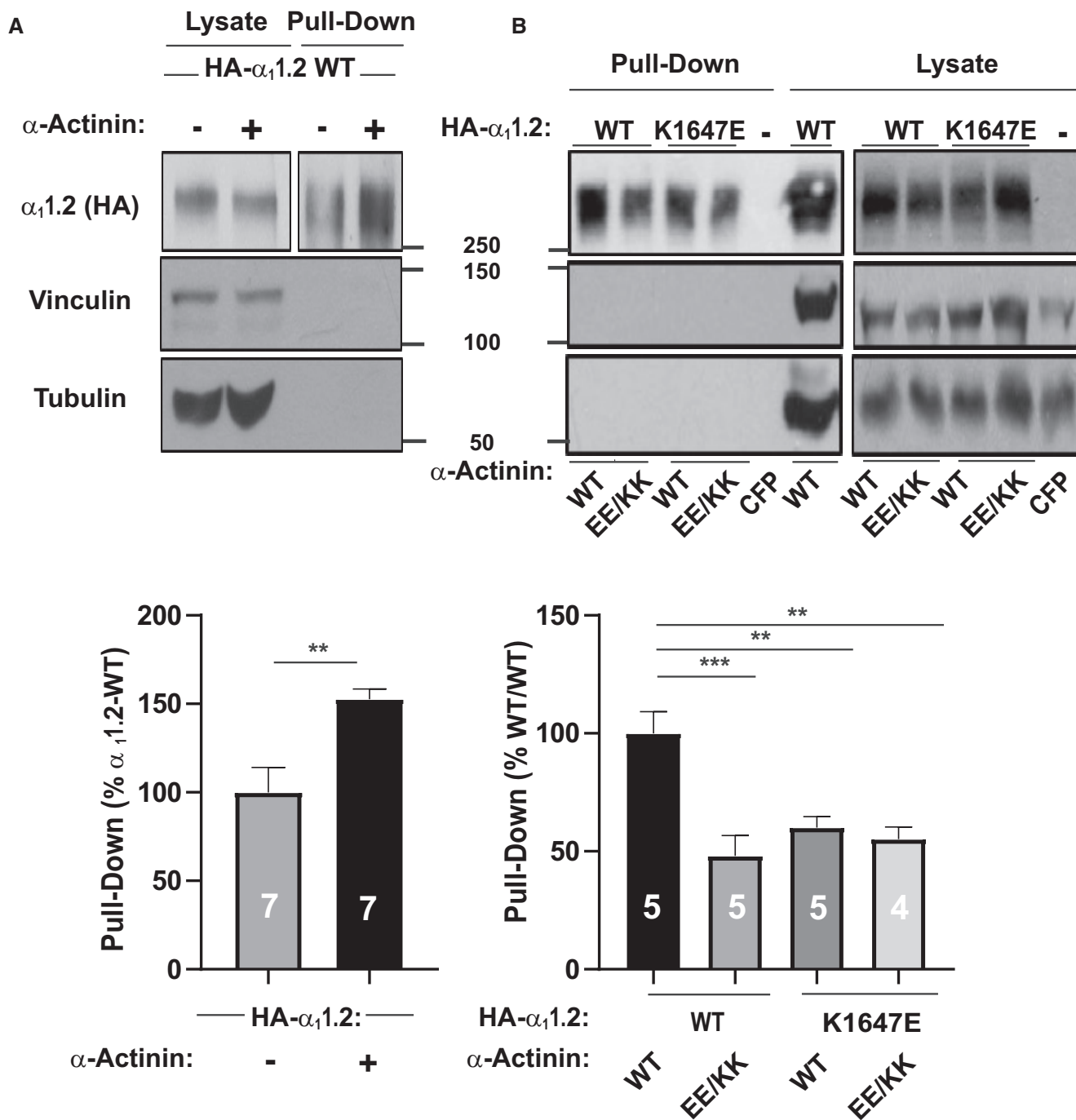


Figure 6. Modulation of $Ca_v1.2$ surface expression via its interaction with α -actinin-1.

A HEK293 cells were transfected with WT $\alpha_1.2$, $\alpha_2\delta-1$, and β_{2A} \pm WT α -actinin-1 and cultured for 22–24 h before surface biotinylation. Shown are representative immunoblots of NeutrAvidin pull-down samples (from lysate containing 600 μ g protein) and total lysate samples containing 20 μ g protein. $\alpha_1.2$ was detected with an antibody against its HA tag (top), which is present in all constructs used throughout this work. Pull-down and lysate samples are from the same blot but different exposures because signals from lysate samples were much stronger than from pull-down samples. Immunoblotting for vinculin (middle) and tubulin (bottom) indicated that comparable amounts of these intracellular control proteins were present in lysate samples. Their absence in pull-down samples as seen on the same blots showed that these prominent intracellular proteins did not undergo biotinylation as control for membrane integrity during surface biotinylation. Bar graph shows means \pm SEM of the pull-down immunosignals in mutants relative to surface labeling of control $\alpha_1.2$ samples lacking α -actinin-1 co-expression (mean set to 100%; see Materials and Methods; ** P < 0.01 two-tailed t -test; n = 7).

B HEK293 cells were transfected with WT or K1647E mutant $\alpha_1.2$, $\alpha_2\delta-1$, and β_{2A} , and WT or E847K/E851K mutant α -actinin-1, or CFP alone as negative control and cultured for 22–24 h before surface biotinylation. Shown are representative immunoblots of pull-down and lysate samples as in (A). Bar graph shows means \pm SEM of the pull-down immunosignals in mutants relative to surface labeling in the WT/WT control (mean set to 100%; see Materials and Methods). ** P < 0.01, *** P < 0.001; one-way ANOVA with Tukey post hoc test; n = 4–5).

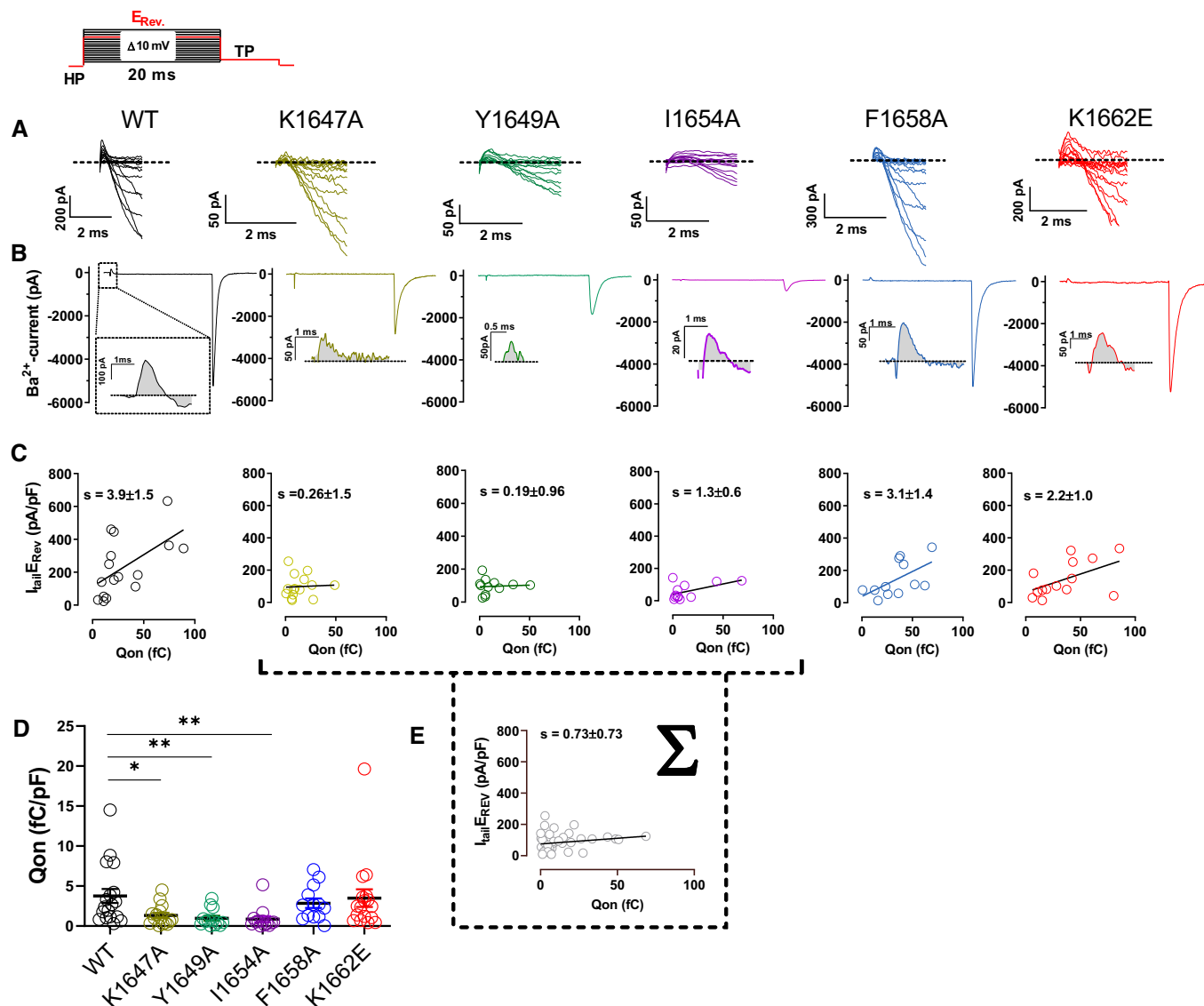


Figure 7. $Ca_v1.2$ mutations that affect α -actinin-1 impair gating charge movement and its coupling to channel opening.

HEK293 cells were transfected with $\alpha_11.2$, $\alpha_2\delta-1$, and β_{2A} before whole-cell patch recording in 20 mM Ba^{2+} .

A Representative current traces of the first 2 ms obtained from recordings upon depolarizations from a holding potential of -80 mV to the indicated potentials (the voltage protocol is schematized in the upper left corner).

B Representative current traces upon step depolarizations to the reversal potential (E_{rev}) for 20 ms to obtain movement of the ON-gating charges (Q_{on}), and subsequent to -50 mV for 10 ms to obtain tail currents (I_{tail}). Insets: magnifications of exemplary Q_{on} for $Ca_v1.2$ WT, K1647A, Y1649A, I1654A, F1658A, and K1662E.

C Plots of I_{tail} (in this panel corrected for variations in cell capacitance) versus total detectable charge transfer for Q_{on} . Slopes of regression curves are strongly reduced for $Ca_v1.2$ K1647A, Y1649A, and I1654A versus WT (see Table 7 for more details).

D Dot plots and means \pm SEM of Q_{on} (in this panel corrected for variations in cell capacitance; * $P < 0.05$; ** $P < 0.01$; one-way ANOVA with Bonferroni post hoc test; $n = 13$ –18; see Table 7 for more details).

E The reduction in slope of the regression curve of combined population data for K1647A, Y1649A, and I1654A versus WT indicates reduced coupling of I_{tail} with Q_{on} when α -actinin binding to the IQ motif is diminished.

intersect to facilitate channel gating, possibly through similar effects on overall conformations of $Ca_v1.2$.

All three α -actinin binding-deficient IQ mutants of $Ca_v1.2$ reduced NPo by $\sim 90\%$ when channel density was reduced by only 35–40% as seen by surface labeling (Tseng *et al*, 2017). To further ascertain that a large portion of the reduction in NPo is due to a reduction in Po and not just N, i.e., not only due to a reduction in

surface expression, we determined the 95% confidence intervals (CIs) for surface biotinylation and surface labeling with antibodies with subsequent analysis by fluorescence-activated cell sorting (Bourdin *et al*, 2010; Yang *et al*, 2010), Po, and Q_{on} (Appendix Tables S1–S3). The CIs for surface biotinylation and surface antibody labeling are remarkably similar (e.g., 52–69% and 51–71%, respectively, for the most relevant mutant K1647A, with

WT being 100%) and overlap not at all with Q_{on} and Po (26–44% and 6–10%, respectively, for K1647A, with WT again being 100%). Thus, the CIs for the 95% CIs for reductions are ~29–49% for surface stainings, 56–74% for Q_{on} , and 90–94% for Po . Accordingly, it appears extremely unlikely that the reductions in surface expression can fully account for the reductions in Q_{on} and Po for α -actinin binding-deficient Cav1.2; rather, loss of surface localization is only responsible for a fraction of the reductions in Q_{on} and Po . Similarly, the reduction in Q_{on} can most likely only partially account for the reduction in Po , supporting the notion that coupling between the movement of the voltage sensor and the channel gate is impaired in addition to the movement of this sensor.

If loss of α -actinin binding to the IQ motif would not affect Po of individual channels, then NPo of all α -actinin binding-deficient IQ mutants should be ~60% of wild-type Cav1.2. A 90% decrease in NPo means that 60% of the Cav1.2 channels that remain on the cell surface upon impairment of α -actinin binding carry only ~10% of the current seen for the wild-type Cav1.2 population. These effects translate into a sixfold reduction in Po of individual Cav1.2 channels upon loss of α -actinin binding.

Together with earlier work that showed that α -actinin increases surface localization and postsynaptic accumulation of Cav1.2 (Hall et al, 2013; Tseng et al, 2017), this new work now demonstrates that α -actinin serves a dual role in regulating Cav1.2 function. It not only promotes Cav1.2 surface expression but, remarkably, also exerts a strong positive effect on Po . This mechanism allows Cav1.2 to be minimally active during secretory trafficking or when it is outside its target regions but to become functionally fully engaged when anchored at proper locations such as postsynaptic sites. Thus, coupling of α -actinin binding to both localization and activity of Cav1.2 is perfectly fine-tuned. This mechanism is so far unique. Whether analogous mechanisms apply to other channels and especially other Ca^{2+} channels, which may require potent mechanisms to prevent inappropriate and potentially harmful Ca^{2+} flux from secretory compartments or at the wrong locations on the cell surface, is now an intriguing premise that will inspire future work.

Materials and Methods

NMR spectroscopy

Xenopus calmodulin was expressed in *E. coli* strain BL21(DE3) grown in LB medium (unlabeled proteins) or M9 media supplemented with $^{15}NH_4Cl$ or $^{15}NH_4Cl/^{13}C$ -glucose for single- or double-labeled proteins, respectively. Recombinant CaM was prepared as described previously (Zhang et al, 2012).

Human α -actinin-1_EF12 (residues 750–812) and α -actinin-1_EF34 (residues 822–893) were each subcloned into pET3b vector and expressed in *E. coli* strain BL21(DE3) grown in LB medium (unlabeled proteins) or M9 media supplemented with $^{15}NH_4Cl$ or $^{15}NH_4Cl/^{13}C$ -glucose for single- or double-labeled proteins, respectively. α -actinin-1_EF12 and α -actinin-1_EF34 were each purified and prepared as described (Turner et al, 2016).

Unlabeled Cav1.2 IQ peptide (residues 1,644–1,664) was purchased from ChinaPeptides. The peptide was dissolved in d6-DMSO to give a peptide concentration of 7.8 mM. An aliquot of

peptide (1.5 equivalents) was added to a dilute solution of α -actinin-1_EF34 or apoCaM (50 μ M protein dissolved in 20 mM 2-amino-2-hydroxymethyl-propane-1,3-diol-d11 (Tris- d_{11}) with 50 mM NaCl, 5 mM dithiothreitol-d10 (DTT- d_{10}), and 95% $H_2O/5\%$ D_2O) and incubated at 15°C for 1 h to ensure complete binding of the peptide. The complex was then concentrated to a final concentration of 500 μ M in a final volume of 500 μ l for NMR experiments.

Production and use of isotope-labeled peptides using pET-31

We expressed ^{15}N - or $^{15}N/^{13}C$ -labeled IQ peptide in *E. coli* as a fusion protein with the ketosteroid isomerase (KSI) using the pET31 plasmid (Kuliopulos et al, 1994) (Novagen/EMD Biosciences). KSI fusion proteins are concentrated in inclusion bodies in *E. coli*, protecting the fused peptide from proteolysis. The fusion protein was purified by affinity chromatography under denaturing conditions via a 6x-His tag at the C-terminus. To release the peptide of interest, the purified fusion is cleaved using cyanogen bromide (CNBr). The CNBr cleaves at methionine residues that were engineered between the KSI and peptide, and between the peptide and 6x-His tag. This cleavage mixture is then rotary evaporated to dryness and resuspended in an appropriate ratio of acetonitrile/water, which solubilizes primarily the peptide and not KSI. Finally, the peptide is purified by reverse-phase HPLC.

Two complementary oligonucleotides that code for Cav1.2 IQ peptide (5'-p-TTT TAT GCG ACC TTT CTG ATT CAG GAA TAT TTT CGC AAA TTT AAA AAA CGC AAA ATG; 5'-p-TTT GCG TTT TTT AAA TTT GCG AAA ATA TTC CTG AAT CAG AAA GGT CGC ATA AAA CAT) were annealed in 40 mM Tris-HCl, pH 8.0, 10 mM $MgCl_2$, and 50 mM NaCl by heating to 95°C and then cooling slowly (> 2 h) to room temperature (RT). The annealed, double-stranded insert was then ligated into AlwNI-digested and dephosphorylated pET31 using T4 DNA ligase. The 5'-phosphorylation augments ligation, and the extra Met codons (underlined) provide compatible sticky ends for the AlwNI-cut plasmid as well as the sites of CNBr cleavage. 2 μ l of the ligation mixture was transformed into DH5 alpha cells and plasmids from individual ampicillin-resistant colonies sequenced. Successful insertions were obtained, including some multiple insertions. We used one of the single-insertion plasmids for expression in M9 minimal media. *E. coli* was lysed by sonication. The insoluble material was collected by ultracentrifugation and resuspended in 6M guanidine, insoluble material removed by ultracentrifugation, and the supernatant loaded onto a Ni-NTA column equilibrated with 6M guanidine buffer. After elution with 300 mM imidazole, the purified fractions were pooled and then dialyzed against ultrapure water, causing the fusion protein to precipitate. Precipitate was collected by centrifugation and resuspended in 80% formic acid, transferred to a round-bottom flask, and injected with N_2 at ~3 psi. For a 2L scale expression, we used 60 ml of formic acid solution and added 2 g of solid CNBr to start the cleavage reaction. After overnight reaction, the flask was roto-evaporated to dryness. The clear peptide film was resuspended in 40% acetonitrile/60% H_2O and mixed for > 1 h. After centrifugation to remove any insoluble material, the supernatant was lyophilized, resuspended in H_2O + 0.1% trifluoroacetic acid, and run over a C18 reverse-phase HPLC column using a gradient of 9–28% acetonitrile. Peak fractions were collected, lyophilized, and analyzed by MALDI-MS to identify

the desired peptide product. Dry fractions of peptide were resolubilized in DMSO-d₆ to a concentration of > 5 mM.

To measure residual dipolar couplings (RDCs) of α -actinin-1_EF34 or apoCaM bound to IQ peptide, the filamentous bacteriophage Pf1 (Asla Biotech Ltd., Latvia) was used as an orienting medium. Pf1 (12 mg/ml) was added to ¹⁵N-labeled α -actinin-1_EF34 or apoCaM bound to unlabeled IQ at pH 7.0, to produce weak alignment of the complex.

Haddock structure determination of α -actinin-1/IQ or apoCaM/IQ

The molecular docking of α -actinin-1 and apoCaM to the Ca_v1.2 IQ motif (residues 1,644–1,664) was performed using the Haddock d-level 2.2 web server as described (van Zundert *et al*, 2016). Residual dipolar couplings, chemical shift perturbation, and mutagenesis data were used as structural restraints. For active restraints or ambiguous interaction restraints (AIRs), chemical shift perturbation was used, selecting residues whose chemical shift perturbation falls above the average perturbation.

The initial docking calculation used NMR-derived structures of α -actinin-1 or apoCaM as determined in this study, which were each docked with the helical structure of Ca_v1.2 IQ peptide (residues 1,644–1,664) (Van Petegem *et al*, 2005) as input structures for Haddock. A total of 69 and 42 AIR restraints were used for α -actinin-1 and apoCaM, respectively, based on chemical shift perturbation data, and 16 active restraints were used for the IQ peptide from chemical shift perturbation. Unambiguous restraints were introduced to define key intermolecular interactions (IQ K1647- α -actinin-1_EF34 E847; IQ K1647- α -actinin-1_EF34 E851; IQ K1662-CaM E88; IQ I1654- α -actinin-1_EF3/4F833; and IQ I1654-apoCaM F90), which were each verified by mutagenesis (Tables 2 and 4).

Initial docking calculations used AIRs based on chemical shift perturbation data, and the top 200 structures were selected for simulated annealing and water refinement. The lowest energy structures were then run again, adding unambiguous restraints based on mutagenesis data. Rigid-body docking, simulated annealing, and water refinement were run using the top 200 structures. RDC restraints assigned to α -actinin-1 and apoCaM were then added using the Sani statement, with tensor values Dr and Da calculated using the program PALES (Zweckstetter, 2008). A total of 74 RDC values were used from residues found in regions of regular secondary structure and as deemed reliable by the PALES calculation.

Fluorescence polarization (FP) assays

Fluorescein-labeled peptides (100 nM; ChinaPeptides, Shanghai, China) were titrated with increasing concentrations of either purified α -actinin-1 or CaM in FP buffer (50 mM HEPES, pH 7.4, 100 mM KCl, 1 mM MgCl₂, 0.05 mM EGTA, 5 mM nitrilotriacetic acid) and FP determined with a Synergy 2 plate reader (BioTek, Winooski, VT) as described (Zhang *et al*, 2014; Patriarchi *et al*, 2016; Tseng *et al*, 2017). FP was calculated as $P = (I_v - g \cdot I_h) / (I_v + g \cdot I_h)$; I_v is vertical and I_h is horizontal fluorescence intensity, respectively, and g is the correction factor for fluorescein. To obtain binding curves and K_d values, data were fitted in GraphPad Prism 5 to the equation $Y = B \cdot X / (K_d + X)$; B is maximal FP value that would

be reached at saturation as determined by extrapolation of the fitted curve.

Isothermal titration calorimetry

ITC experiments were performed using a VP-ITC calorimeter (MicroCal) at 27°C, and data were acquired and processed with MicroCal software as described previously (Wingard *et al*, 2005). Samples of apoCaM (injectant) and IQ (titrant) were prepared by exchanging each into buffer containing 50 mM HEPES, pH 7.4, 100 mM NaCl, 0.05 mM EGTA, and 1 mM MgCl₂. The IQ peptide in the sample cell (10 μ M, 1.5 ml) was titrated with apoCaM (100 μ M) using 35 injections of 10 μ l each.

Expression of Ca_v1.2 and α -actinin-1 in HEK293 cells

HEK293T/17 cells were maintained in DMEM-10 [Dulbecco's modified Eagle's medium (Life Technologies) supplemented with 10% fetal bovine serum (FBS, Atlanta Biologicals)] at 37°C in humidified incubators injected with 5% CO₂ and 95% air (Tseng *et al*, 2017). For expression of Ca_v1.2, HEK293T/17 cells were transfected with rat α_1 1.2 (GenBank ID: M67515.1) cDNA subcloned into pECFP-C1 vector (Tseng *et al*, 2017) encoding an in-frame N-terminally fused eCFP tag and an HA tag in the S5-H5 extracellular loop of domain II (Green *et al*, 2007), which does not affect channel properties (Altier *et al*, 2002). The point mutations in plasmids encoding single-residue K1647A, K1647E, F1648A, Y1649A, I1654A, F1658A, and K1662E exchanges in α_1 1.2 were generated via QuikChange II using the above pECFP-C1 rat α_1 1.2 plasmid DNA as template as described (Tseng *et al*, 2017) and the oligonucleotides described in Appendix Table S4. For full expression of Ca_v1.2, cells were also co-transfected with pGWIH-based plasmids encoding the auxiliary subunits rat β_{2A} (Perez-Reyes *et al*, 1992) and rabbit $\alpha_2\delta$ -1 (Ellis *et al*, 1988). To assess the contributions of α -actinin-1 on Ca_v1.2, cells were transfected with pCMV plasmid DNAs encoding WT (Hall *et al*, 2013) or mutant α -actinin-1. The K847E/K851EE point mutations in α -actinin-1 were produced via QuikChange II mutagenesis as before (Tseng *et al*, 2017). The forward primer for making the K851E mutation, which was performed first, was 5'p-CCA TGG ACA AAT TGC GCA GAA AGC TGC CAC CCG ACC AGG and reverse primer 5'p-CCT GGT CGG GTG GCA GCT TTC TGC GCA ATT TGT CCA TGG. Forward primer for the K847E mutation was 5'p-GAA CTA CAT TAC CAT GAA CAA ATT GCG CCG CGA GCT GCC ACC C and reverse primer 5'p-GGG TGG CAG CTC GCG GCG CAA TTT GTC CAT GGT AAT GTA GTT C. Transfection of HEK293T/17 cells was accomplished using Ca²⁺ phosphate precipitation (Tseng *et al*, 2017) for single-channel recording and surface labeling or Lipofectamine 2000 for the analysis of Q_{on}.

Cell surface biotinylation assays

Seven hours after transfection, cells were washed once with 150 mM NaCl, 10 mM NaHCO₂, pH 7.4 (PBS) and cultured for another 15–17 h in fresh medium. 22–24 h after transfection, cells were either harvested, monodispersed (> 95% viability), and then labeled with EZ-link-sulfo-NHS-LC-biotin (Thermo Fisher Scientific) in solution essentially as described (Tseng *et al*, 2017) or directly labeled while adhered to the petri dish. In the latter case, adherent cells on the dish were washed twice with ice-cold PBS containing

0.5 mM Mg²⁺ and 1 mM Ca²⁺ and incubated on ice with PBS containing 0.4 mg/ml EZ-link-sulfo-NHS-LC-biotin for 15 min. The labeling reaction was quenched by three 5-min washes with 40 mM glycine in PBS containing 0.5 mM Mg²⁺ and 1 mM Ca²⁺ on ice. Cells were harvested by scraping in PBS and collected by centrifugation. Cell pellets were lysed in ice-cold RIPA buffer (50 mM Tris-HCl, pH 7.4, 150 mM NaCl, 5 mM EGTA, 10 mM EDTA, 1% NP-40, 0.05% SDS, 0.4% DOC, and 10% glycerol) supplemented with a cocktail of protease inhibitors (1 µg/ml leupeptin (Merck Millipore), 2 µg/ml aprotinin (Merck Millipore), 1 µg/ml pepstatin A (Merck Millipore), and 34 µg/ml phenylmethanesulfonyl fluoride (PMSF; Sigma)). The solubilized material was cleared of insoluble debris by centrifugation at 200,000× *g* for 30 min at 4°C. Biotinylated constituents in 600 µg of cell protein lysate were affinity purified by incubation with 30 µl of NeutrAvidin-conjugated Sepharose beads (Thermo Fisher Scientific) for 2 h at 4°C. Bead-bound material was collected by centrifugation and washed three times with ice-cold buffer, and immobilized proteins were extracted in SDS sample buffer. Proteins were fractionated by SDS-PAGE in 7.5% acrylamide gels and transferred onto polyvinylidene difluoride (PVDF; Bio-Rad) membranes. PVDF membranes were incubated in blocking buffer (BB) consisting of 150 mM NaCl, 10 mM Tris-HCl, pH 7.4 (TBS) with 0.10% Tween (TBST), and 2% bovine serum albumin (BSA; RPI Corp.) for 1 h at RT before incubation with primary antibodies in BB for 3 h at RT. α₁.2 was detected by antibodies against the HA tag and, for confirmation, the intracellular loop II/III FP1 epitope (Buonarati *et al*, 2017) and the CNC2 epitope near the C-terminus of α₁.2 (Buonarati *et al*, 2017). Probing with antibodies against the cytosolic protein vinculin (Cell Signaling Technologies) and α-tubulin (Santa Cruz Biotechnology) was used to correct for variation in protein content in lysates and as negative control for surface biotinylation. Membranes were washed for 40 min with at least five exchanges of TBST, incubated with horseradish peroxidase-conjugated secondary goat anti-mouse antibodies (HA, α-tubulin; Jackson) or mouse anti-rabbit antibodies (FP1, CNC2, vinculin; Jackson) for 1 h at RT, and washed again with TBST with at least five exchanges for 1.5 h. Immunosignals were detected using the horseradish peroxidase substrates Luminata Classico or Crescendo (Merck Millipore) or Femto (Thermo Fisher Scientific) by X-ray film (Denville Scientific Inc.). Multiple exposures over increasing time periods were taken to ensure that all signals were in the linear range (Davare & Hell, 2003; Hall *et al*, 2006). Films were scanned and assessed via ImageJ to determine signal intensity for each band. Background signals in individual lanes were subtracted from the band signal before further analysis. To correct differences in immunosignal strengths due to potential differences during immunoblotting and film exposures between experiments, the individual immunosignals for each α₁.2 pull-down sample were divided by the sum of all immunosignals from one blot to obtain the relative signal fraction for each band (Degaspero *et al*, 2014). The mean of the WT control signals from all experiments was then calculated and all fractional values from all samples (WT and mutants) divided by this value (the WT mean transforms to 1 with this algorithm) (Degaspero *et al*, 2014). All values were then converted to percent, with the mean of WT control equaling 100%. The data were statistically analyzed applying either a Student's *t*-test (two-sample comparison) or ANOVA with Bonferroni's post hoc test as before (Tseng *et al*, 2017).

Cell-attached Patch-Clamp recording

Cell-attached patch-clamp recordings were performed as before (Davare *et al*, 2001; Patriarchi *et al*, 2016; Qian *et al*, 2017) on an Olympus IX70-inverted microscope at room temperature (22°C). Recordings were obtained with an Axopatch 200B amplifier, and data were sampled at 10 kHz with a low-pass filter at 2 kHz (3 dB, four-pole Bessel) and digitalized with a Digidata 1440 digitizer. Recording electrodes were fabricated from borosilicate capillary glass (0.86 OD) with a Flaming micropipette puller (Model P-97, Sutter Instruments) and polished (polisher from World Precision Instruments; 3.5–6.5 MΩ resistance). The extracellular solution contained (in mM) 145 KCl, 10 NaCl, and 10 HEPES, pH 7.4 (NaOH). The high K⁺ concentration was used for optimal control of the transmembrane potential under the patch during depolarizations to 0 mV. The pipette solution contained (in mM) 20 tetraethylammonium chloride (TEA-Cl), 110 BaCl₂ (as charge carrier), and 10 HEPES, pH 7.3 (TEA-OH). Cells were depolarized from a holding potential of –80 mV to 0 mV every 5 s. Event lists were translated from raw Ba²⁺ currents after leak, and capacity transients were digitally subtracted. Data were analyzed based on the half-height criterion (Sachs *et al*, 1982) with the single-channel software provided by pClamp 10. The number of channels (*k*) in the patch was estimated based on the observed simultaneous and stacked openings over several minutes at the depolarizing test potential (Herzig *et al*, 2007; Bartels *et al*, 2018). The *k*-value is then determined by the observed maximum current amplitude divided by the unitary current amplitude. Data with more than > 3 channels (*k* > 3) in the patch were not considered for statistical analysis in order to prevent overinterpretation of channel open probability. For statistical analysis, single-channel parameters were corrected by the channel number as previously (Schroder *et al*, 1998; Bartels *et al*, 2009). For a sufficient statistical analysis, 50–100 Ba²⁺ current traces were recorded on average for each cell for each experimental condition.

Whole-cell patch-clamp recordings

Whole-cell patch-clamp recordings were performed as before (Bartels *et al*, 2018) on an Olympus IX70-inverted microscope at room temperature (22°C). Macroscopic Ba²⁺ currents (I_{Ba}) of Ca_v1.2 were recorded in external solution containing (in mM) 75 CsCl, 40 TEA-Cl, 20 BaCl₂, 1 MgCl₂, 10 HEPES, and 10 glucose with a pH adjusted to 7.2 (TEA-OH) and an osmolarity of 300–310 (sucrose). The internal pipette solution contained (in mM) 110 CsCl, 30 TEA-Cl, 1 MgCl₂, 4 Mg-ATP, and 10 HEPES, pH 7.2 (CsOH), mOsm 290–300 (sucrose). Pipette resistance was usually between 1.7 and 2.5 MΩ. The series resistance and the cell capacitance were taken from an Axopatch 200B amplifier (Molecular Devices) and compensated not more than < 40% in order to prevent current oscillation. On-gating currents (Q_{on}) were sampled at 50 kHz and low-pass-filtered at 5 kHz and further quantified through current integration over the first 2–3 ms of the beginning of the test pulse. Cells were clamped at a holding potential of –80 mV and depolarized by a 20 ms test pulse of a series of activating potentials starting from –60 mV to +80 mV to determine the reversal potential (E_{rev}). Tail currents (I_{tail}) were then measured after repolarization to –50 mV for 10 ms. Recorded data were leak and capacity corrected with an online *P/4*

protocol. The liquid junction potential was not considered for correction in the experiment. Data acquisition and analysis were obtained with pClamp 10. Curve fitting was performed by using GraphPad Prism VIII software (San Diego).

Data availability

The NMR assignments have been deposited in the BMRB (accession number 25902; <http://www.bmrwisc.edu/>). The atomic coordinates have been deposited into the Protein Databank (6COA and 6CTB).

Expanded View for this article is available online.

Acknowledgements

We thank Dr. Elza Kuzmenkina (University of Cologne, Germany) for providing the coding of the algorithm for calculating assembly averages. This work was supported by NIH grants T32 GM113770 (AMC), T32 GM099608 (PBH), R01 HL098200 (MFN), R01 HL121059 (MFN), R01 EY012347 (JBA), R01MH097887 (JWH), R01 AG017502 (JWH), R01 NS078792 (JWH), and the American Heart Association (AHA) Predoctoral Fellowship AHA 14PRE19900021 (PBH).

Author contributions

MT, DEA, MN-C, PB, KNMM, P-YT, MFN, MCH, JBA, and JWH designed experiments; MT, DEA, MN-C, PB, AMC, KNMM, PBH, P-YT, MFN, and MCH performed experiments; MT, DEA, MN-C, PB, AMC, PBH, VY-Y, DMB, MFN, MCH, JBA, and JWH analyzed data; and MT, DEA, MN-C, PB, VY-Y, DMB, MFN, MCH, JBA, and JWH wrote the manuscript.

Conflict of interest

The authors declare that they have no conflict of interest.

References

- Adams PJ, Ben-Johny M, Dick IE, Inoue T, Yue DT (2014) Apocalmodulin itself promotes ion channel opening and Ca(2+) regulation. *Cell* 159: 608–622
- Alexander KA, Cimler BM, Meier KE, Storm DR (1987) Regulation of calmodulin binding to P-57. A neurospecific calmodulin binding protein. *J Biol Chem* 262: 6108–6113
- Altier C, Dubel SJ, Barrere C, Jarvis SE, Stotz SC, Spaetgens RL, Scott JD, Cornet V, De Waard M, Zamponi GW et al (2002) Trafficking of L-type calcium channels mediated by the postsynaptic scaffolding protein AKAP79. *J Biol Chem* 277: 33598–33603
- Atkinson RA, Joseph C, Kelly G, Muskett FW, Frenkiel TA, Nietlispach D, Pastore A (2001) Ca²⁺-independent binding of an EF-hand domain to a novel motif in the alpha-actinin-titin complex. *Nat Struct Biol* 8: 853–857
- Backman L (2015) Calcium affinity of human alpha-actinin 1. *PeerJ* 3: e944
- Bartels P, Behnke K, Michels G, Groner F, Schneider T, Henry M, Barrett PQ, Kang HW, Lee JH, Wiesen MH et al (2009) Structural and biophysical determinants of single Ca(V)3.1 and Ca(V)3.2 T-type calcium channel inhibition by N(2)O. *Cell Calcium* 46: 293–302
- Bartels P, Yu D, Huang H, Hu Z, Herzig S, Soong TW (2018) Alternative splicing at N terminus and domain I modulates Cav1.2 inactivation and surface expression. *Biophys J* 114: 2095–2106
- Ben Johny M, Yang PS, Bazzazi H, Yue DT (2013) Dynamic switching of calmodulin interactions underlies Ca²⁺ regulation of Cav1.3 channels. *Nat Commun* 4: 1717
- Ben-Johny M, Yang PS, Niu J, Yang W, Joshi-Mukherjee R, Yue DT (2014) Conservation of Ca(2+)/calmodulin regulation across Na and Ca(2+) channels. *Cell* 157: 1657–1670
- Berkefeld H, Sailer CA, Bildl W, Rohde V, Thumfart JO, Eble S, Klugbauer N, Reisinger E, Bischofberger J, Oliver D et al (2006) BKCa-Cav channel complexes mediate rapid and localized Ca²⁺-activated K⁺ signaling. *Science* 314: 615–620
- Berman DE, Dudai Y (2001) Memory extinction, learning anew, and learning the new: dissociations in the molecular machinery of learning in cortex. *Science* 291: 2417–2419
- Bourdin B, Marger F, Wall-Lacelle S, Schneider T, Klein H, Sauve R, Parent L (2010) Molecular determinants of the Cavbeta-induced plasma membrane targeting of the Cav1.2 channel. *J Biol Chem* 285: 22853–22863
- Buonarati OR, Henderson PB, Murphy GG, Horne MC, Hell JW (2017) Proteolytic processing of the L-type Ca²⁺ channel alpha 1.2 subunit in neurons. *FL000 Res* 6: 1166
- Cahill L, Prins B, Weber M, McGaugh JL (1994) Beta-adrenergic activation and memory for emotional events. *Nature* 371: 702–704
- Carter ME, Yizhar O, Chikahisa S, Nguyen H, Adamantidis A, Nishino S, Deisseroth K, de Lecea L (2010) Tuning arousal with optogenetic modulation of locus coeruleus neurons. *Nature Neurosci* 13: 1526–1533
- Chagot B, Chazin WJ (2011) Solution NMR structure of Apo-calmodulin in complex with the IQ motif of human cardiac sodium channel Nav1.5. *J Mol Biol* 406: 106–119
- Cimler BM, Andreassen TJ, Andreassen KI, Storm DR (1985) P-57 is a neural specific calmodulin-binding protein. *J Biol Chem* 260: 10784–10788
- Cohen SM, Suutari B, He X, Wang Y, Sanchez S, Tirko NN, Mandelberg NJ, Mullins C, Zhou G, Wang S et al (2018) Calmodulin shuttling mediates cytonuclear signaling to trigger experience-dependent transcription and memory. *Nat Commun* 9: 2451
- Dai S, Hall DD, Hell JW (2009) Supramolecular assemblies and localized regulation of voltage-gated ion channels. *Physiological Rev* 89: 411–452
- Davare MA, Avdonin V, Hall DD, Peden EM, Burette A, Weinberg RJ, Horne MC, Hoshi T, Hell JW (2001) A beta2 adrenergic receptor signaling complex assembled with the Ca²⁺ channel Cav1.2. *Science* 293: 98–101
- Davare MA, Hell JW (2003) Increased phosphorylation of the neuronal L-type Ca(2+) channel Ca(v)1.2 during aging. *Proc Natl Acad Sci USA* 100: 16018–16023
- Degasperi A, Birtwistle MR, Volinsky N, Rauch J, Kolch W, Kholodenko BN (2014) Evaluating strategies to normalise biological replicates of Western blot data. *PLoS ONE* 9: e87293
- Dolmetsch RE, Pajvani U, Fife K, Spotts JM, Greenberg ME (2001) Signaling to the nucleus by an L-type calcium channel-calmodulin complex through the MAP kinase pathway. *Science* 294: 333–339
- Dolphin AC (2012) Calcium channel auxiliary alpha(2)delta and beta subunits: trafficking and one step beyond. *Nature Rev Neurosci* 13: 542–555
- Dolphin AC (2016) Voltage-gated calcium channels and their auxiliary subunits: physiology and pathophysiology and pharmacology. *J Physiol* 594: 5369–5390
- Egrie JC, Campbell JA, Flangas AL, Siegel FL (1977) Regional, cellular and subcellular distribution of calcium-activated cyclic nucleotide phosphodiesterase and calcium-dependent regulator in porcine brain. *J Neurochem* 28: 1207–1213
- Ellis SB, Williams ME, Ways NR, Brenner R, Sharp AH, Leung AT, Campbell KP, McKenna E, Koch WJ, Hui A et al (1988) Sequence and expression of mRNAs encoding the alpha₁ and alpha₂ subunits of the DHP-sensitive calcium channel. *Science* 241: 1661–1664

- Evans TI, Hell JW, Shea MA (2011) Thermodynamic linkage between calmodulin domains binding calcium and contiguous sites in the C-terminal tail of Ca(V)1.2. *Biophys Chem* 159: 172–187
- Feldkamp MD, Yu L, Shea MA (2011) Structural and energetic determinants of apo calmodulin binding to the IQ motif of the Na(V)1.2 voltage-dependent sodium channel. *Structure* 19: 733–747
- Findeisen F, Rumpf CH, Minor DL Jr (2013) Apo states of calmodulin and CaBP1 control Cav1 voltage-gated calcium channel function through direct competition for the IQ domain. *J Mol Biol* 425: 3217–3234
- Fuller MD, Emrick MA, Sadilek M, Scheuer T, Catterall WA (2010) Molecular mechanism of calcium channel regulation in the fight-or-flight response. *Sci Signal* 3: ra70
- Fuller MD, Fu Y, Scheuer T, Catterall WA (2014) Differential regulation of Cav1.2 channels by cAMP-dependent protein kinase bound to A-kinase anchoring proteins 15 and 79/150. *J Gen Physiol* 143: 315–324
- Gabelli SB, Boto A, Kuhns VH, Bianchet MA, Farinelli F, Aripirala S, Yoder J, Jakoncic J, Tomaselli GF, Amzel LM (2014) Regulation of the NaV1.5 cytoplasmic domain by calmodulin. *Nat Commun* 5: 5126
- Gabelli SB, Yoder JB, Tomaselli GF, Amzel LM (2016) Calmodulin and Ca(2+) control of voltage gated Na(+) channels. *Channels* 10: 45–54
- Ghosh D, Syed AU, Prada MP, Nystoriak MA, Santana LF, Nieves-Cintrón M, Navedo MF (2017) Calcium channels in vascular smooth muscle. *Adv Pharmacol* 78: 49–87
- Ghosh D, Nieves-Cintrón M, Tajada S, Brust-Mascher I, Horne MC, Hell JW, Dixon RE, Santana LF, Navedo MF (2018) Dynamic L-type Cav1.2 channel trafficking facilitates Cav1.2 clustering and cooperative gating. *Biochim Biophys Acta Mol Cell Res* 1865: 1341–1355
- Green EM, Barrett CF, Bultynck G, Shamah SM, Dolmetsch RE (2007) The tumor suppressor e1F3e mediates calcium-dependent internalization of the L-type calcium channel Cav1.2. *Neuron* 55: 615–632
- Grover LM, Teyler TJ (1990) Two components of long-term potentiation induced by different patterns of afferent activation. *Nature* 347: 477–479
- Hall DD, Feekes JA, Arachchige Don AS, Shi M, Hamid J, Chen L, Strack S, Zamponi GW, Horne MC, Hell JW (2006) Binding of protein phosphatase 2A to the L-type calcium channel Cav1.2 next to Ser 1928, its main PKA site, is critical for Ser1928 dephosphorylation. *Biochemistry* 45: 3448–3459
- Hall DD, Dai S, Tseng P-Y, Malik ZA, Nguyen M, Matt L, Schnitzler K, Shephard A, Mohapatra D, Tsuruta F et al (2013) Competition between α -Actinin and Ca²⁺-calmodulin controls surface retention of the L-type Ca²⁺ channel Cav1.2. *Neuron* 78: 483–497
- Hell JW, Yokoyama CT, Wong ST, Warner C, Snutch TP, Catterall WA (1993) Differential phosphorylation of two size forms of the neuronal class C L-type calcium channel α 1 subunit. *J Biol Chem* 268: 19451–19457
- Hell JW (2014) CaMKII: claiming center stage in postsynaptic function and organization. *Neuron* 81: 249–265
- Herzig S, Khan IF, Grundemann D, Matthes J, Ludwig A, Michels G, Hoppe UC, Chaudhuri D, Schwartz A, Yue DT et al (2007) Mechanism of Ca(v)1.2 channel modulation by the amino terminus of cardiac beta2-subunits. *FASEB J* 21: 1527–1538
- Houdusse A, Gaucher JF, Kremontsova E, Mui S, Trybus KM, Cohen C (2006) Crystal structure of apo-calmodulin bound to the first two IQ motifs of myosin V reveals essential recognition features. *Proc Natl Acad Sci USA* 103: 19326–19331
- Hovey L, Fowler CA, Mahling R, Lin Z, Miller MS, Marx DC, Yoder JB, Kim EH, Tefft KM, Waite BC et al (2017) Calcium triggers reversal of calmodulin on nested anti-parallel sites in the IQ motif of the neuronal voltage-dependent sodium channel NaV1.2. *Biophys Chem* 224: 1–19
- Hu H, Real E, Takamiya K, Kang MG, Ledoux J, Huganir RL, Malinow R (2007) Emotion enhances learning via norepinephrine regulation of AMPA-receptor trafficking. *Cell* 131: 160–173
- Huang KP, Huang FL, Li J, Schuck P, McPhee P (2000) Calcium-sensitive interaction between calmodulin and modified forms of rat brain neurogranin/RC3. *Biochemistry* 39: 7291–7299
- Huang KP, Huang FL, Jager T, Li J, Reymann KG, Balschun D (2004) Neurogranin/RC3 enhances long-term potentiation and learning by promoting calcium-mediated signaling. *J Neurosci* 24: 10660–10669
- Iacobucci GJ, Popescu GK (2017) Resident calmodulin primes NMDA receptors for Ca(2+)-Dependent inactivation. *Biophys J* 113: 2236–2248
- Kuliopulos A, Nelson NP, Yamada M, Walsh CT, Furie B, Furie BC, Roth DA (1994) Localization of the affinity peptide-substrate inactivator site on recombinant vitamin K-dependent carboxylase. *J Biol Chem* 269: 21364–21370
- Li H, Pink MD, Murphy JG, Stein A, Dell'Acqua ML, Hogan PG (2012) Balanced interactions of calcineurin with AKAP79 regulate Ca²⁺-calcineurin-NFAT signaling. *Nat Struct Mol Biol* 19: 337–345
- Lian LY, Myatt D, Kitmitto A (2007) Apo calmodulin binding to the L-type voltage-gated calcium channel Cav1.2 IQ peptide. *Biochem Biophys Res Commun* 353: 565–570
- Ma H, Groth RD, Cohen SM, Emery JF, Li B, Hoedt E, Zhang G, Neubert TA, Tsien RW (2014) gammaCaMKII shuttles Ca(2+)/CaM to the nucleus to trigger CREB phosphorylation and gene expression. *Cell* 159: 281–294
- Man KNM, Navedo MF, Horne MC, Hell JW (2020) β ₂ adrenergic receptor complexes with the L-type Ca²⁺ channel Cav1.2 and AMPA-type glutamate receptors: paradigms for pharmacological targeting of protein interactions. *Annu Rev in Pharmacol and Toxicol* 60: 29.1–29.20
- Marrion NV, Tavalin ST (1998) Selective activation of Ca²⁺-activated K⁺ channels by co-localized Ca²⁺ channels in hippocampal neurons. *Nature* 395: 900–905
- Matt L, Kim K, Hergarden AC, Patriarchi T, Malik ZA, Park DK, Chowdhury D, Buonarati OR, Henderson PB, Gokcek Sarac C et al (2018) alpha-actinin anchors PSD-95 at postsynaptic sites. *Neuron* 97: 1094–1109 e9
- Minzenberg MJ, Watrous AJ, Yoon JH, Ursu S, Carter CS (2008) Modafinil shifts human locus coeruleus to low-tonic, high-phasic activity during functional MRI. *Science* 322: 1700–1702
- Patriarchi T, Qian H, Di Biase V, Malik ZA, Chowdhury D, Price JL, Hammes EA, Buonarati OR, Westenbroek RE, Catterall WA et al (2016) Phosphorylation of Cav1.2 on S1928 uncouples the L-type Ca²⁺ channel from the β ₂ adrenergic receptor. *EMBO J* 35: 1330–1345
- Perez-Reyes E, Castellano A, Kim HS, Bertrand P, Bagstrom E, Lacerda AE, Wei XY, Birnbaumer L (1992) Cloning and expression of a cardiac/brain beta subunit of the L-type calcium channel. *J Biol Chem* 267: 1792–1797
- Peterson BZ, DeMaria CD, Adelman JP, Yue DT (1999) Calmodulin is the Ca²⁺ sensor for Ca²⁺-dependent inactivation of L-type calcium channels. *Neuron* 22: 549–558
- Qian H, Patriarchi T, Price JL, Matt L, Lee B, Nieves-Cintrón M, Buonarati OR, Chowdhury D, Nanou E, Nystoriak MA et al (2017) Phosphorylation of Ser1928 mediates the enhanced activity of the L-type Ca²⁺ channel Cav1.2 by the beta2-adrenergic receptor in neurons. *Sci Signal* 10: eaaf9659
- Ran X, Miao HH, Sheu FS, Yang D (2003) Structural and dynamic characterization of a neuron-specific protein kinase C substrate, neurogranin. *Biochemistry* 42: 5143–5150
- Ribeiro Ede A Jr, Pinotsis N, Ghisleni A, Salmazo A, Konarev PV, Kostan J, Sjöblom B, Schreiner C, Polyansky AA, Gkougkoulia EA et al (2014) The structure and regulation of human muscle alpha-actinin. *Cell* 159: 1447–1460
- Sachs F, Neil J, Barkakati N (1982) The automated analysis of data from single ionic channels. *Pflugers Arch* 395: 331–340

- Schroder F, Handrock R, Beuckelmann DJ, Hirt S, Hullin R, Priebe L, Schwinger RH, Weil J, Herzig S (1998) Increased availability and open probability of single L-type calcium channels from failing compared with nonfailing human ventricle. *Circulation* 98: 969–976
- Schwieters CD, Kuszewski JJ, Tjandra N, Clore GM (2003) The Xplor-NIH NMR molecular structure determination package. *J Magn Reson* 160: 65–73
- Seisenberger C, Specht V, Welling A, Platzer J, Pfeifer A, Kuhbandner S, Striessnig J, Klugbauer N, Feil R, Hofmann F (2000) Functional embryonic cardiomyocytes after disruption of the L-type $\alpha 1C$ (Cav1.2) calcium channel gene in the mouse. *J Biol Chem* 275: 39193–39199
- Sinnegger-Brauns MJ, Hetzenauer A, Huber IG, Renstrom E, Wietzorrek G, Berjukov S, Cavalli M, Walter D, Koschak A, Waldschutz R et al (2004) Isoform-specific regulation of mood behavior and pancreatic beta cell and cardiovascular function by L-type Ca^{2+} channels. *J Clin Invest* 113: 1430–1439
- Splawski I, Timothy KW, Sharpe LM, Decher N, Kumar P, Bloise R, Napolitano C, Schwartz PJ, Joseph RM, Condouris K et al (2004) $Ca(V)1.2$ calcium channel dysfunction causes a multisystem disorder including arrhythmia and autism. *Cell* 119: 19–31
- Tjandra N, Bax A (1997) Direct measurement of distances and angles in biomolecules by NMR in a dilute liquid crystalline medium. *Science* 278: 1111–1114
- Tseng PY, Henderson PB, Hergarden AC, Patriarchi T, Coleman AM, Lillya MW, Montagut-Bordas C, Lee B, Hell JW, Horne MC (2017) α -Actinin promotes surface localization and current density of the Ca^{2+} channel $CaV1.2$ by binding to the IQ region of the $\alpha 1$ subunit. *Biochemistry* 56: 3669–3681
- Tuluc P, Molenda N, Schlick B, Obermair GJ, Flucher BE, Jurkat-Rott K (2009) A $CaV1.1$ Ca^{2+} channel splice variant with high conductance and voltage-sensitivity alters EC coupling in developing skeletal muscle. *Biophys J* 96: 35–44
- Turner M, Anderson DE, Rajan S, Hell JW, Ames JB (2016) Chemical shift assignments of the C-terminal EF-hand domain of α -actinin-1. *Biomol NMR Assign* 10: 219–222
- Van Petegem F, Chatelain FC, Minor DL Jr (2005) Insights into voltage-gated calcium channel regulation from the structure of the $CaV1.2$ IQ domain- Ca^{2+} /calmodulin complex. *Nat Struct Mol Biol* 12: 1108–1115
- Wingard JN, Chan J, Bosanac I, Haeseleer F, Palczewski K, Ikura M, Ames JB (2005) Structural analysis of Mg^{2+} and Ca^{2+} binding to CaBP1, a neuron-specific regulator of calcium channels. *J Biol Chem* 280: 37461–37470
- Wu X, Bers DM (2007) Free and bound intracellular calmodulin measurements in cardiac myocytes. *Cell Calcium* 41: 353–364
- Wyszynski M, Lin J, Rao A, Nigh E, Beggs AH, Craig AM, Sheng M (1997) Competitive binding of α -actinin and calmodulin to the NMDA receptor. *Nature* 385: 439–442
- Yang T, Xu X, Kernan T, Wu V, Colecraft HM (2010) Rem, a member of the RGC GTPases, inhibits recombinant $CaV1.2$ channels using multiple mechanisms that require distinct conformations of the GTPase. *J Physiol* 588: 1665–1681
- Zamponi GW, Striessnig J, Koschak A, Dolphin AC (2015) The physiology, pathology, and pharmacology of voltage-gated calcium channels and their future therapeutic potential. *Pharmacol Rev* 67: 821–870
- Zhabotinsky AM, Camp RN, Epstein IR, Lisman JE (2006) Role of the neurogranin concentrated in spines in the induction of long-term potentiation. *J Neurosci* 26: 7337–7347
- Zhang Y, Li Z, Sacks DB, Ames JB (2012) Structural basis for Ca^{2+} -induced activation and dimerization of estrogen receptor α by calmodulin. *J Biol Chem* 287: 9336–9344
- Zhang Y, Matt L, Patriarchi T, Malik ZA, Chowdhury D, Park DK, Renieri A, Ames JB, Hell JW (2014) Capping of the N-terminus of PSD-95 by calmodulin triggers its postsynaptic release. *EMBO J* 33: 1341–1353
- Zhong L, Kaleka KS, Gerges NZ (2011) Neurogranin phosphorylation fine-tunes long-term potentiation. *Eur J Neurosci* 33: 244–250
- Zuhlke RD, Pitt GS, Deisseroth K, Tsien RW, Reuter H (1999) Calmodulin supports both inactivation and facilitation of L-type calcium channels. *Nature* 399: 159–162
- van Zundert GC, Rodrigues JP, Trellet M, Schmitz C, Kastiris PL, Karaca E, Melquiond AS, van Dijk M, de Vries SJ, Bonvin AM (2016) The HADDOCK2.2 web server: user-friendly integrative modeling of biomolecular complexes. *J Mol Biol* 428: 720–725
- Zweckstetter M (2008) NMR: prediction of molecular alignment from structure using the PALES software. *Nat Protoc* 3: 679–690

Expanded View Figures

Figure EV1. Mapping the Ca_v1.2 IQ binding site in α -actinin and apoCaM.

- A Overlay of ^{15}N - ^1H HSQC spectra of ^{15}N -labeled α -actinin-1 CH1/CH2 domain (residues 19–192) by itself (black peaks) and after addition of saturating, unlabeled IQ peptide (red peaks).
- B Overlay of ^{15}N - ^1H HSQC spectra of ^{15}N -labeled α -actinin-1 EF-hand domain (residues 750–892) by itself (black peaks) and after addition of saturating, unlabeled IQ peptide (red peaks).
- C Overlay of ^{15}N - ^1H HSQC spectra of ^{15}N -labeled α -actinin-1 C-lobe (α -actinin-1 EF34; residues 822–892) by itself (black peaks) and after addition of saturating, unlabeled IQ peptide (red peaks).
- D Overlay of ^{15}N - ^1H HSQC spectra of ^{15}N -labeled apoCaM by itself (black peaks) and after addition of saturating, unlabeled IQ peptide (red peaks).

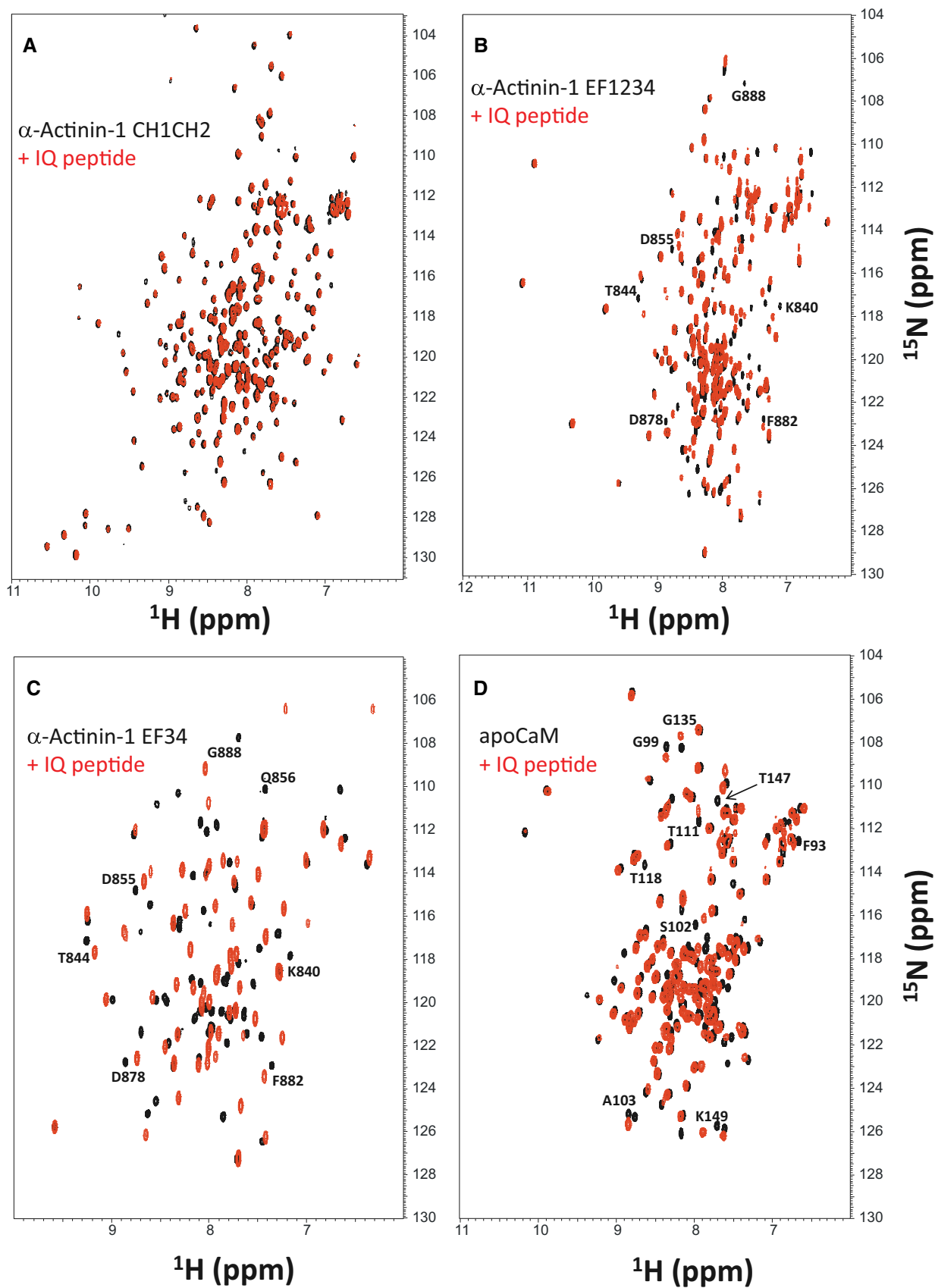


Figure EV1.

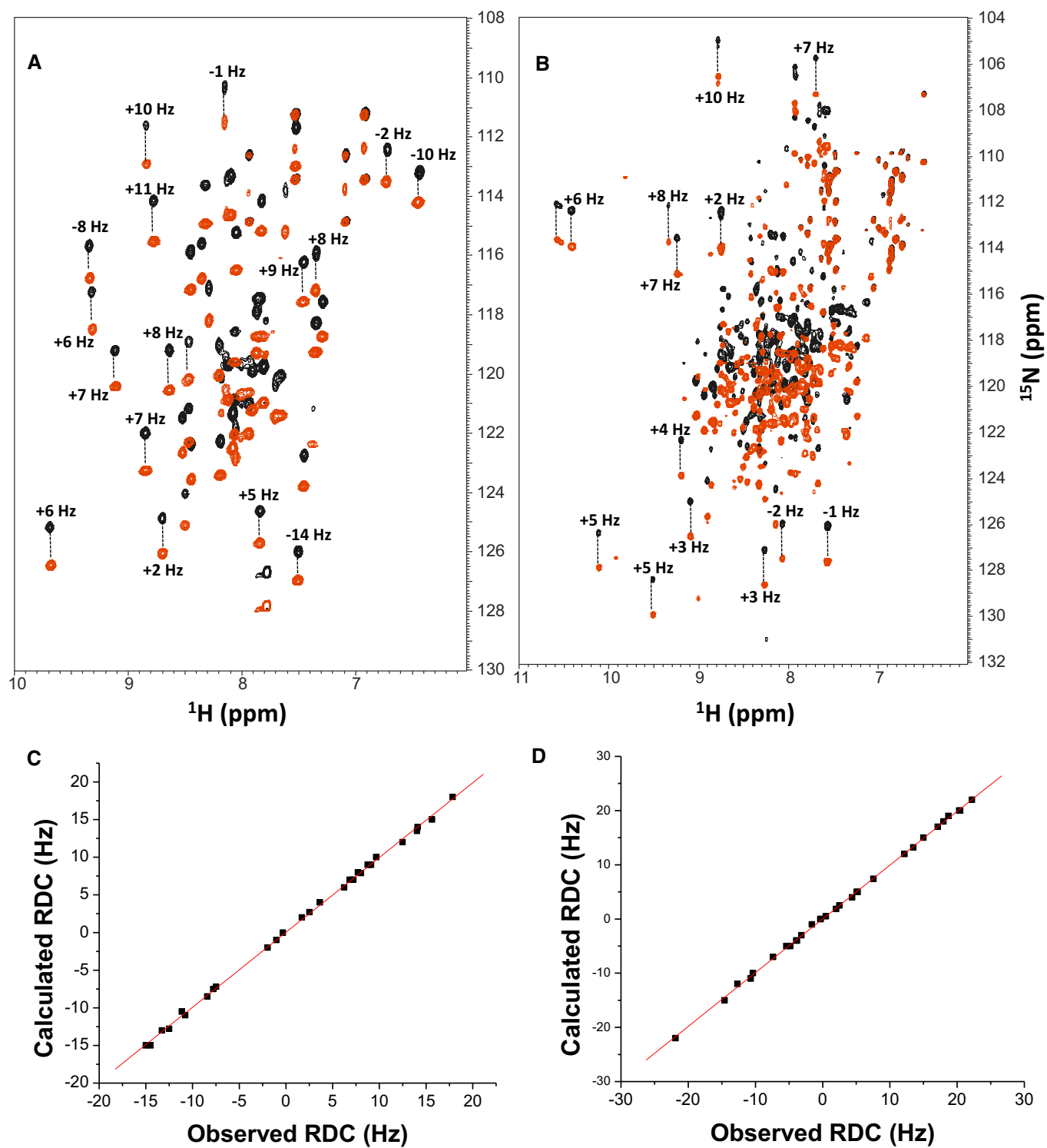


Figure EV2.

Figure EV2. NMR structural analysis using residual dipolar couplings (RDCs).

- A, B ^{15}N - ^1H HSQC-IPAP spectra (Tjandra & Bax, 1997) of ^{15}N -labeled α -actinin-1_EF34 (A) or apoCaM (B) in the presence of saturating unlabeled IQ peptide. Representative and measured RDC values are marked above-selected peaks. Samples used in HSQC-IPAP experiments were prepared by adding 5 mg of ^{15}N -labeled protein to 0.5 ml of NMR buffer containing 12 mg/ml of filamentous bacteriophage Pf1. HSQC-IPAP spectra were recorded in the presence of Pf1 (A, B) and absence of Pf1 (not shown). Residual dipolar couplings (RDCs) were measured (in Hz) as the difference in splitting for the ^{15}N - ^1H doublet components relative to the isotropic $^1\text{J}_{\text{NH}}$ coupling. RDCs measured for 34 residues (α -actinin-1_EF34/IQ) and 36 residues (apoCaM/IQ) served as orientational structural restraints applied during the refinement phase of the structure calculation (Schwieters *et al*, 2003).
- C, D Plots showing the correlation between observed versus calculated backbone RDCs predicted from the final NMR-derived structures for α -actinin-1_EF34/IQ and apoCaM/IQ, respectively. The correlation coefficient (r^2) equals 0.99, and Q is 0.095 and 0.089 for α -actinin-1_EF34/IQ and apoCaM/IQ, respectively.

Figure EV3. α -actinin-1 and apoCaM do not form a ternary complex with IQ.

- A Overlay of ^{15}N - ^1H HSQC spectra of ^{15}N -labeled α -actinin-1 EF-hand domain (residues 750–892) by itself (black peaks), after adding an equivalent amount of unlabeled IQ peptide (red peaks), and after adding fivefold excess of unlabeled apoCaM combined with the 1 equivalent of unlabeled IQ peptide (green peaks).
- B Overlay of ^{15}N - ^1H HSQC spectra of ^{15}N -labeled apoCaM by itself (black peaks), after adding an equivalent amount of unlabeled IQ peptide (red peaks), and after adding fivefold excess of unlabeled α -actinin-1 combined with the 1 equivalent of unlabeled IQ peptide (green peaks).

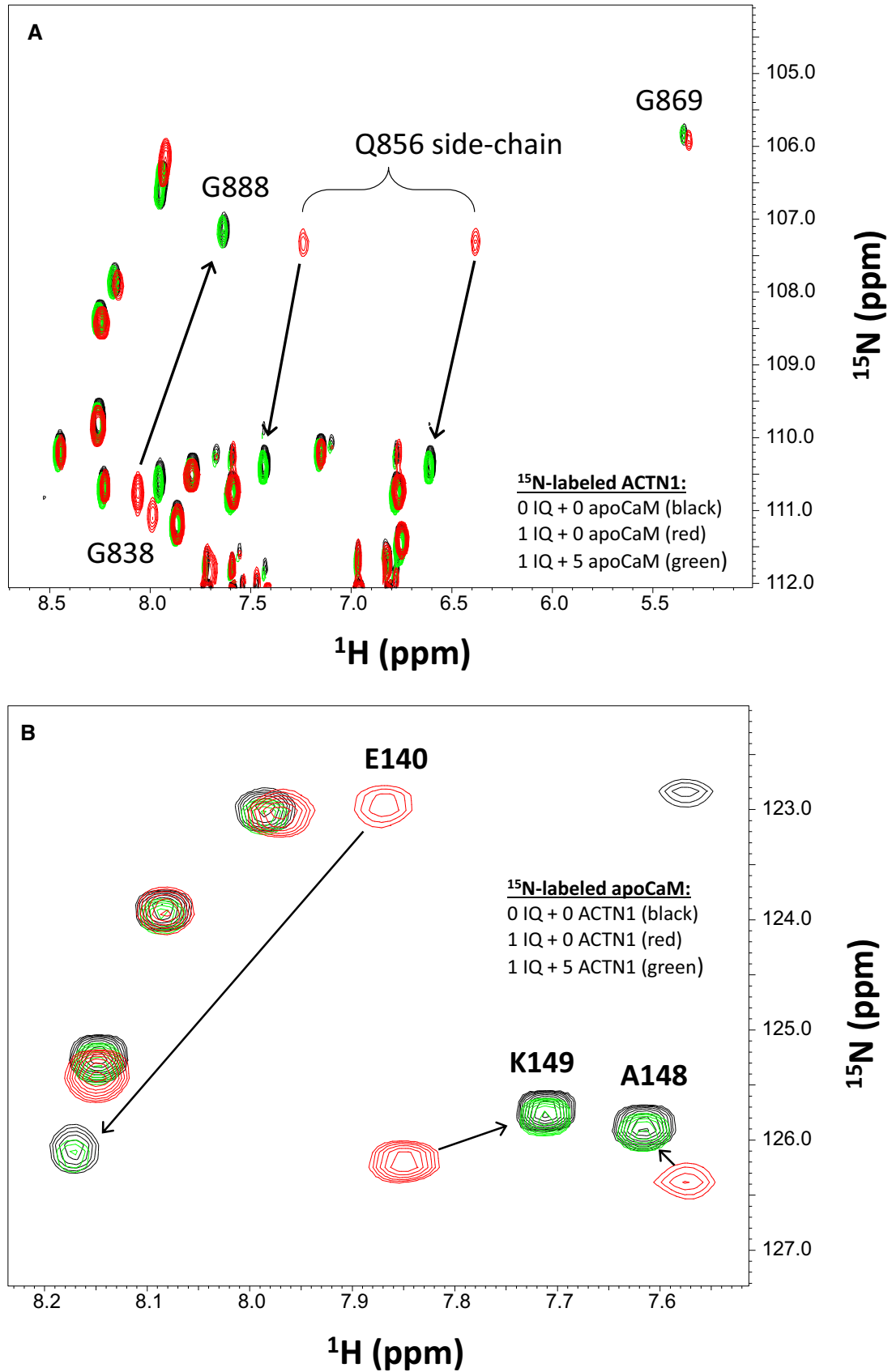


Figure EV3.

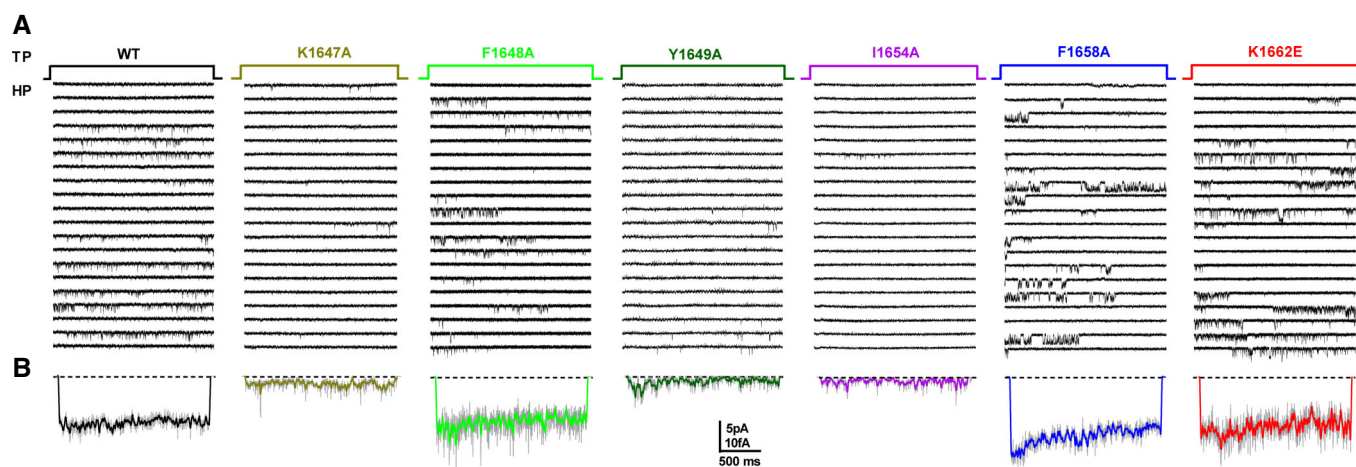


Figure EV4. Representative single-channel traces for $Ca_v1.2$ WT, K1647A, F1648A, Y1649A, I1654A, F1658A, and K1662E. HEK293 cells were transfected with $\alpha_1.2$, $\alpha_2\delta-1$, and β_{2A} before cell-attached patch recording.

A, B Holding potential (HP) was -80 mV and test potential (TP) 0 mV. Shown are 20 consecutive sweeps from representative experiments (A) and mean assemble average currents (B) for all experiments for $Ca_v1.2$ WT and each mutant.

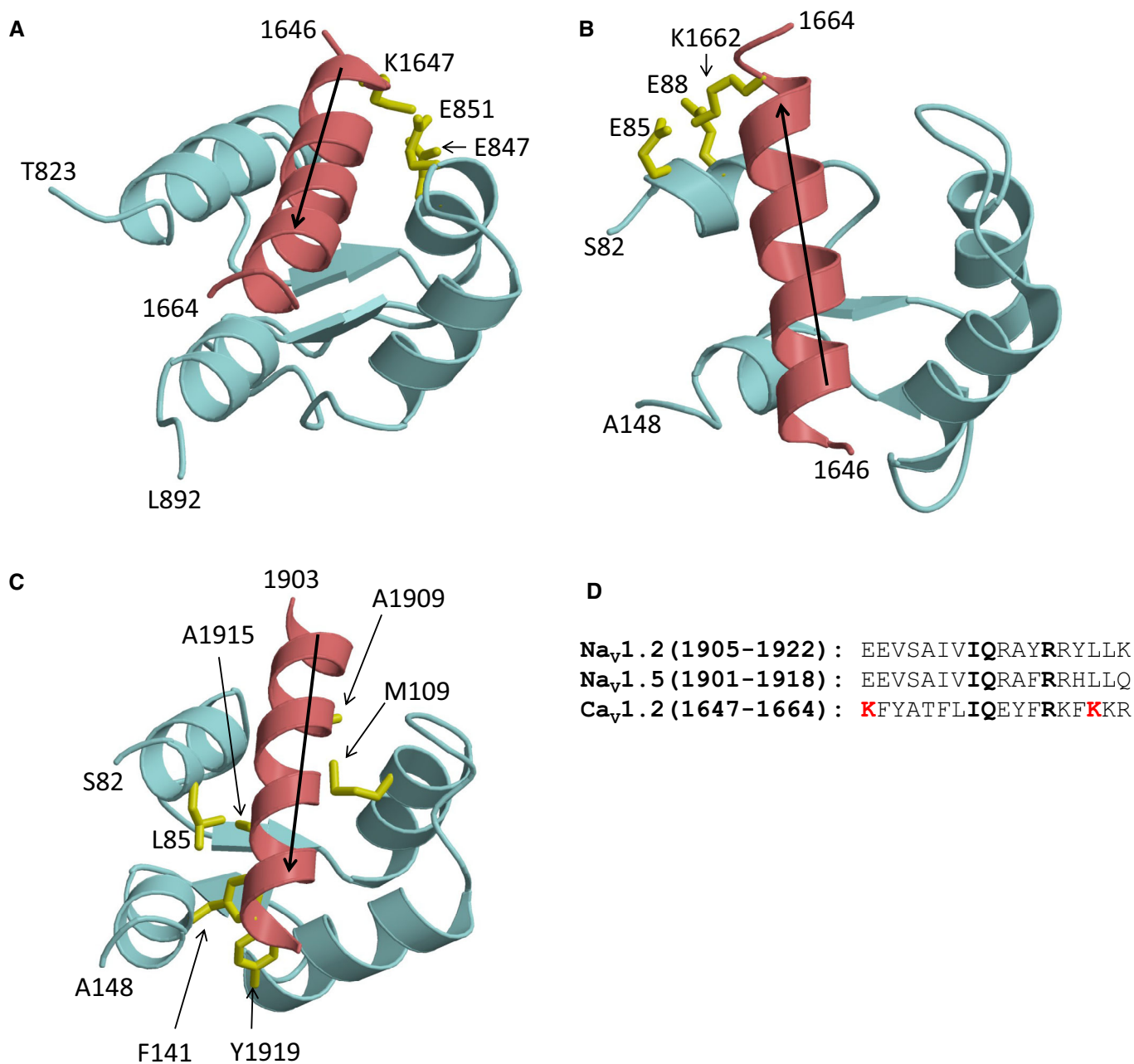


Figure EV5. IQ peptide binds with opposite polarity to α -actinin-1 versus apoCaM.

A NMR structure of α -actinin-1 (cyan) bound to Ca_v1.2 IQ motif (red).

B NMR structure of apoCaM (cyan) bound to Ca_v1.2 IQ motif (red).

C NMR structure apoCaM (cyan) bound to the Na_v1.2 IQ motif (red). PDB accession number is 2KXW (Feldkamp *et al.*, 2011). Non-conserved intermolecular contacts between hydrophobic side-chain atoms are colored yellow. The β -methyl side-chain atoms of Na_v1.2 residues A1909 and A1915 are 2.5 Å away from side-chain methyl atoms of apoCaM residues M109 and L85, respectively. The aromatic side-chain atoms of Na_v1.2 residue Y1919 are 3.3 Å away from aromatic side-chain atoms of apoCaM residue F141.

D Amino acid sequence alignment of IQ motifs from Na_v1.2, Na_v1.5, and Ca_v1.2. Residues that are conserved between Na_v and Ca_v are shown in boldface font. Lysine residues in Ca_v1.2 that form intermolecular salt bridges in the Ca_v1.2 IQ peptide complexes with α -actinin-1_EF3/4 and apoCaM and are not conserved between the Ca²⁺ and Na²⁺ channels are colored red.

Data information: (A–C), Black arrows depict directionality of the IQ helix.

α -Actinin-1 promotes activity of the L-type Ca^{2+} Channel Cav1.2

Matthew Turner¹§, David E. Anderson¹§, Peter Bartels²§, Madeline Nieves-Cintrón²§, Andrea M. Coleman^{1,2}, Peter B. Henderson², Kwun Nok Mimi Man², Pang-Yen Tseng², Vladimir Yarov-Yarovoy³, Donald M. Bers², Manuel F. Navedo², Mary C. Horne²#, James B. Ames¹#, and Johannes W. Hell²#

¹Department of Chemistry, ²Department of Pharmacology, and ³Department of Physiology and Membrane Biology, University of California, Davis, CA 95616, USA.

§ These authors are equal first authors.

Co-corresponding Authors

Contact information : mhorne@ucdavis.edu ; jbames@ucdavis.edu ; jwhell@ucdavis.edu

Table of Content :

- Appendix Figure S1. Amino acid sequence alignment of Cav1.2.
- Appendix Figure S2. Isothermal titration.
- Appendix Figure S3. Cav1.2 mutations that affect α -actinin-1 binding.
- Appendix Figure S4. Structural modeling of the IQ domain of Cav1.2.
- Appendix Table S1. 95% Confidence intervals (CI).
- Appendix Table S2. 95% Confidence intervals (CI).
- Appendix Table S3. 95% Confidence intervals (CI).
- Appendix Table S4. Oligonucleotides used for QuikChange II mutagenesis.

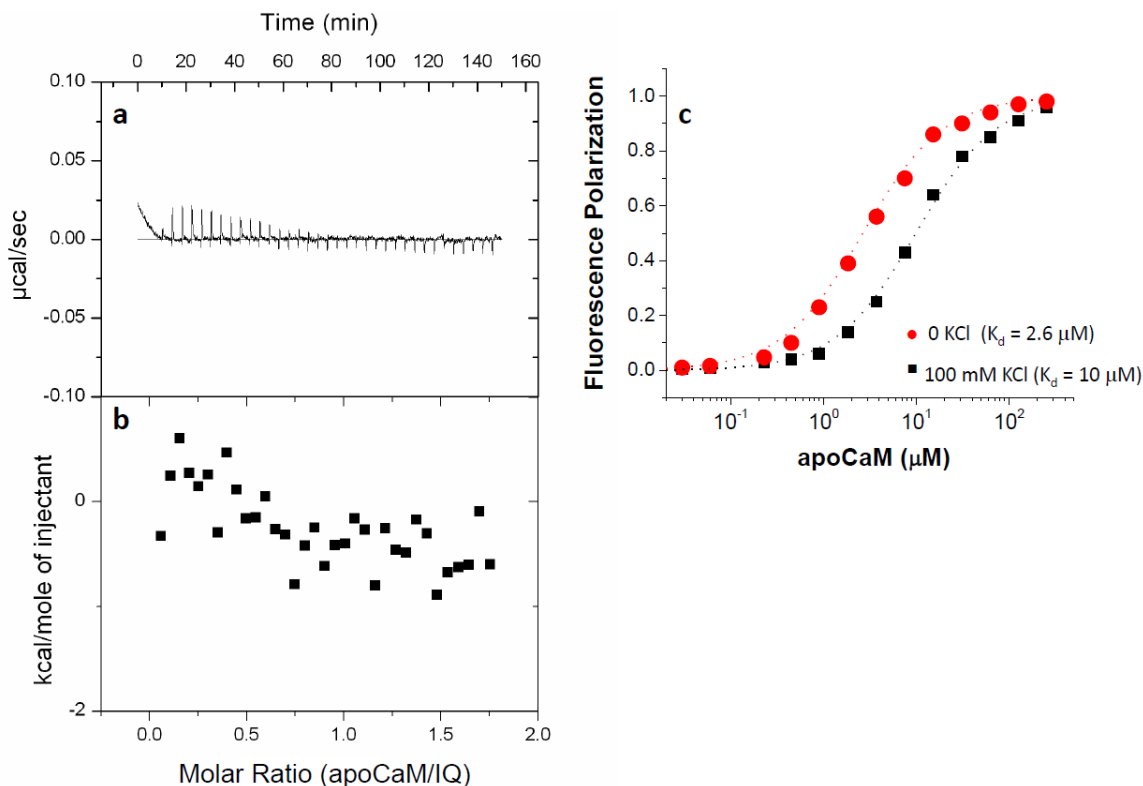
Appendix Figure S1



Appendix Figure S1. Amino acid sequence alignment of the membrane proximal portion of the C-terminal tail of L-type Ca²⁺ channels.

Bold refers to reference sequence (rat $\alpha_11.2$), turquoise to divergency in amino acid sequence, red to residues K1647 and Y1649, which are important for α -actinin binding only, green to I1654, which is important for both, α -actinin and apoCaM binding, and yellow to F1658 and K1662, which are important for apoCaM binding only. Amino acid sequences were derived from species according to the numerical labeling¹⁻¹³. Data were extracted and compiled from uswest.ensembl.org.

Appendix Figure S2

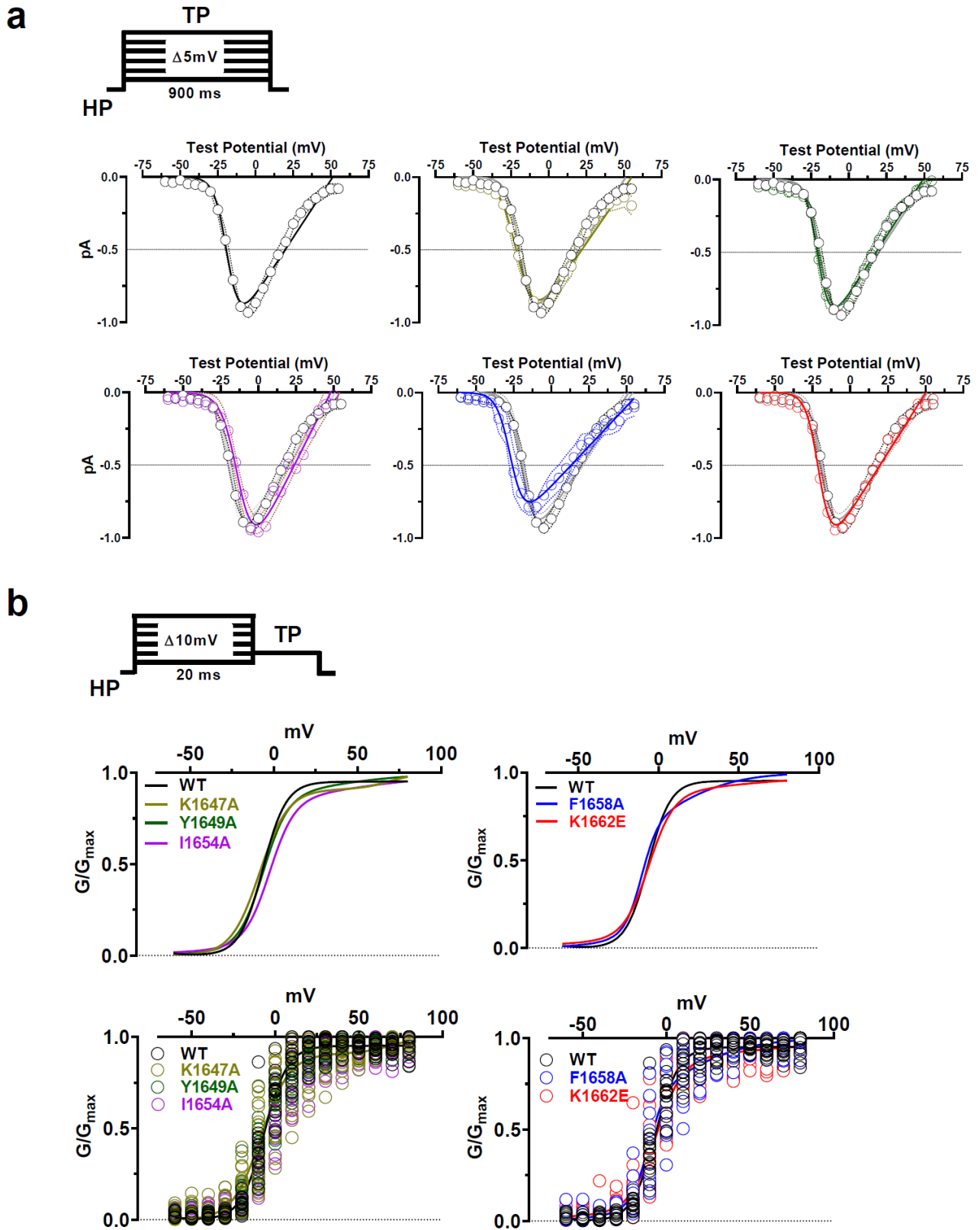
**Appendix Figure S2. Isothermal titration calorimetry of apoCaM added to IQ peptide.**

a, Change of heat resulting from incremental addition of apoCaM (100 μM stock solution) into IQ peptide (10 μM) during ITC titration at 27°C in 50 mM HEPES (pH 7.4), 100 mM KCl, 0.05 mM EGTA and 1 mM MgCl₂.

b, A binding isotherm of apoCaM binding to IQ peptide was derived from the integrated heat at each injection after subtracting a blank titration (to remove heat of dilution). The binding isotherm for apoCaM binding to IQ exhibited no detectable heat signal above the noise level, consistent with low fractional binding under ITC conditions and/or low enthalpy caused by the relatively weak binding affinity ($K_d = 10 \mu\text{M}$, see Fig. 2e and Table 4).

c, Fluorescence polarization for binding of apoCaM (0.015 to 256 μM) to fluorescein-labeled WT IQ peptide (1.0 μM) in the presence of 100 mM KCl (black squares) versus zero KCl (red dots) at room temperature. The buffer was the same as in (a) except that KCl was excluded in the zero KCl sample. The data were fit to a one-site model (dotted lines) with $K_d = 10 \mu\text{M}$ in the presence of 100 mM KCl and $K_d = 2.6 \mu\text{M}$ in the absence of KCl.

Appendix Figure S3



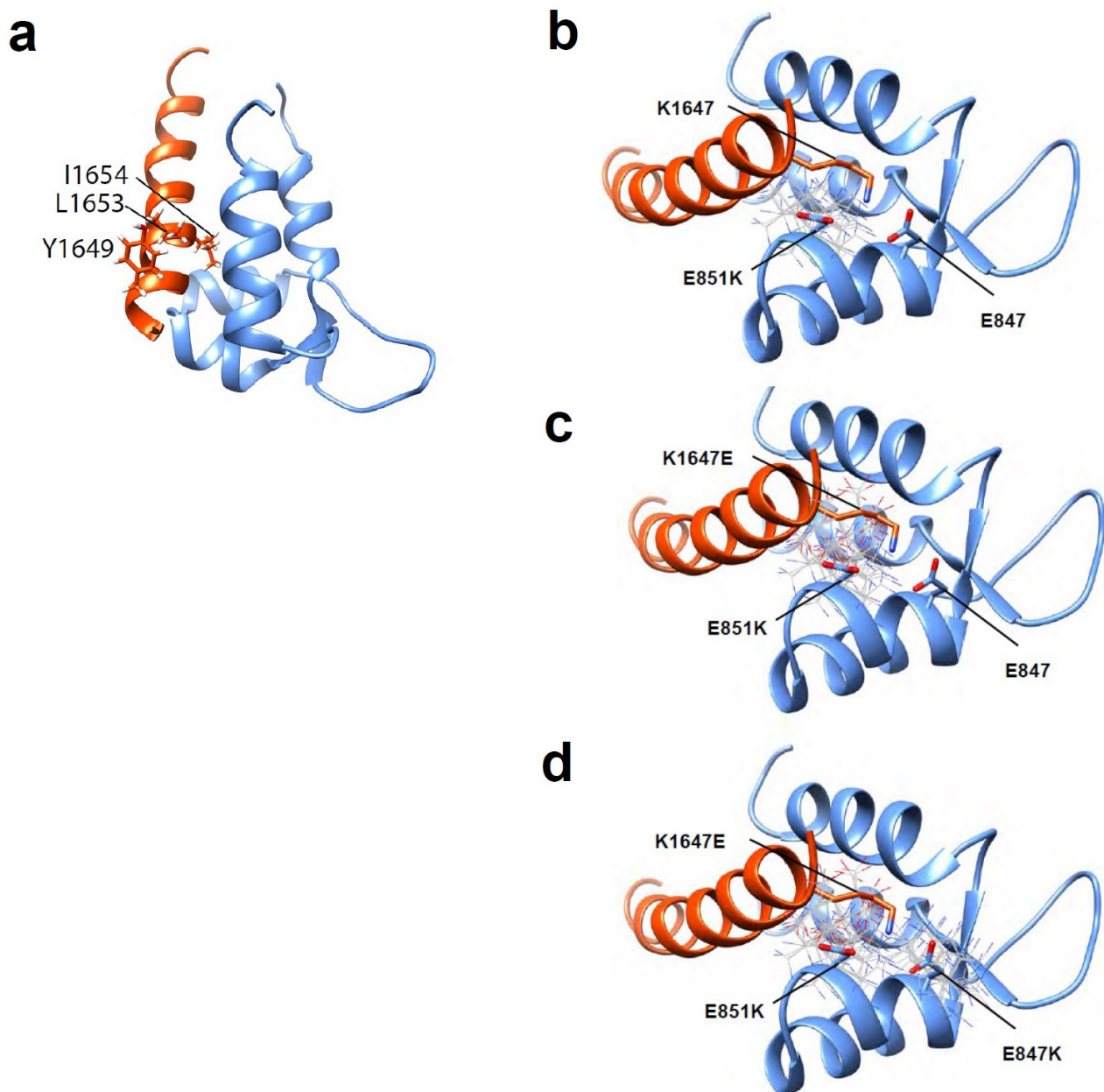
Appendix Figure S3. Cav1.2 mutations that affect α -actinin-1 binding do not impair voltage sensitivity of channel activation.

HEK293 cells were transfected with $\alpha_11.2$, $\alpha_2\delta-1$, and β_{2A} before whole cell patch recording in 20 mM Ba^{2+} .

a, I-V curves. Currents were recorded upon depolarization from a holding potential of -80 mV to increasingly more positive potentials (insert on left). Shown are peak currents. Dashed lines indicate SEM. The WT Cav1.2 curve is reproduced in all graphs for the Cav1.2 mutants.

b, G-V curves. Tail currents (I_{Tail}) were recorded upon repolarization to -50 mV following depolarization from a holding potential of -80 mV to increasingly more positive potentials. Shown are fitted curves in top panels and dot blots in bottom panels.

Appendix Figure S4



Appendix Figure S4. Structural modeling addressing the function of Y1649 in the α_1 1.2 IQ motif and how the E851K mutation of α -actinin affects its binding to the IQ motif.

a, Y1649 stabilizes the α -helical conformation of the α_1 1.2 IQ motif and thereby α -actinin binding. Shown is a cartoon representation of α_1 1.2 IQ motif α -helix (orange) and α -actinin-1 EF3-EF4 (blue). Sidechains of key residues are depicted as stick representation and labeled. Y1649 is in close proximity to L1653, which is about one α -helical turn downstream of Y1649. Stabilization of this α helix ensures correct positioning of I1654, which is critical for binding to α -actinin. This figure was created using UCSF Chimera (Pettersen et al., 2004).

b-d, The lysine residue in the E851K mutation of α -actinin destabilizes the canonical EF hand structure. Conformers of the lysine residues when used to substitute E851 by itself or together with E847 in α -Actinin-1 and of the glutamate residue when used to substitute K1647 in the IQ motif were calculated for the structure of the complex between the IQ motif of α_1 1.2 and EF3_EF4 of α -Actinin-1 using the UCSF Chimera rotamer tool (Pettersen et al., 2004). The α_1 1.2 IQ α -helix is shown in orange and the α -actinin-1 EF3-EF4 in blue. Sidechains of key residues are depicted as stick representation and labeled. The lysine rotamers (thin sticks) are overlaid on top of the original E851 and E847 residues and the glutamate rotamers on top of the original K1647 residue.

b, Simulation of rotamers for the E851K mutation in α -actinin-1 to show possible conformations of the lysine sidechain.

c, Simulation of rotamers for the E851K mutation in α -actinin-1 and the K1647E mutation in α_1 1.2 to show possible conformations of the lysine and glutamate sidechains.

d, Simulation of rotamers for the E847K and E851K mutations in α -actinin-1 and the K1647E mutation in α_1 1.2 to show possible conformations of the lysine and glutamate sidechains.

Appendix Table S1. 95% Confidence intervals (CI) for surface labelling, Qon, and Po for WT and IQ mutant Cav1.2

Given are means±SEM and 95% CIs for experimental values. The number of experiments is shown in parenthesis. *The biotinylation and flow cytometry data are based on data originally published by Tseng et al (2017).

Parameter	*Biotinylation (% of WT)	95% CI	*Flow Cytometry (% of WT)	95% CI	Gating Current Qon (% of WT)	95% CI	P _{open} (% of WT)	95% CI
α 1.2 WT	100±0 (16)	0-0	100±0 (7)	0-0	100±24 (18)	78-122	100±20 (35)	87-113
K1647A	61±5 (11)	52-69	61±7 (7)	51-71	35±9 (15)	26-44	8±2 (12)	6-10
F1648A	94±7 (8)	85-104	ND		ND		93±20 (14)	73-114
Y1649A	66±5 (12)	61-72	63±7 (6)	52-74	26±8 (13)	18-35	15±5 (8)	8-22
I1654A	68±4 (10)	63-73	61±8 (6)	49-74	23±10 (13)	1-34	10±5 (7)	3-17
Q1655A	85±5 (7)	78-92	104±6 (4)	93-116	ND		ND	
F1658A	ND		ND		76±16 (13)	59-93	139±64 (12)	45-121
K1662E	ND		ND		93±29 (17)	52-134	120±32 (13)	86-154

Appendix Table S2. 95% Confidence intervals (CI) for surface biotinylation for Cav1.2 / α -actinin-1 charge inversion experiments

Given are means \pm SEM and 95% CIs (based on original data from this manuscript). The number of experiments is shown in parenthesis.

Parameter	Biotinylation (%)	95% CI
α 1.2 WT	100 \pm 6 (7)	86-114
α 1.2 WT + α -Actinin WT	153 \pm 6 (7)	139-167
α 1.2WT+ α -Actinin WT	100 \pm 9 (5)	74-126
α 1.2 WT + α -Actinin EE/KK	48 \pm 9 (5)	24-72
α 1.2 K1647E + α -Actinin WT	60 \pm 5 (5)	47-73
α 1.2 K1647E + α -Actinin EE/KK	55 \pm 5 (4)	39-71

Appendix Table S3. 95% Confidence intervals (CI) for P_o for Cav1.2 / α -actinin-1 charge inversion experiments

Given are means \pm SEM and 95% CIs (based on original data from this manuscript). The number of experiments is shown in parenthesis.

Parameter	P_{open} (%)	95% CI
$\alpha_11.2$ WT	100 \pm 20 (35)	87- 113
$\alpha_11.2$ WT + α-Actinin WT	233 \pm 59 (23)	186 - 280
$\alpha_11.2$ WT+ α-Actinin EE/KK	55 \pm 22 (13)	32- 78
$\alpha_11.2$ K1647E + α-Actinin WT	100 \pm 18 (30)	87- 113
$\alpha_11.2$K1647E + α-Actinin EE/KK	147 \pm 28 (16)	120- 174

Appendix Table S4. Oligonucleotides used for QuikChange II mutagenesis.

Cav1.2/ α-Actinin-1	Used primers
	Primer (Forward/Reverse; Bold type indicates mutated nucleotide)
RtBr-Cav1.2-a1c-K1647E-Forw	5' – CGA GGT CAC AGT GGG CGA ATT CTA TGC CAC CTT C – 3'
RtBr-Cav1.2-a1c-K1647E-Rev	5' – GAA GGT GGC ATA GAA TTC GCC CAC TGT GAC CTC G – 3'
RtBr-Cav1.2-a1c-K1662-Forw	5' – CAA GAG TAC TTC AGG AAA TTC GAA AAG CGA AAA GAG CAG GGG CTG – 3'
RtBr-Cav1.2-a1c-K1662-Rev	5' – CAG CCC CTG CTC TTT TCG CTT TTC GAA TTT CCT GAA GTA CTC TTG – 3'
Hum-ACTN-1-E847K-Forw	5' – GAA CTA CAT TAC CAT GGA CAA ATT GCG CCG CGA GCT GCC ACC C – 3'
Hum-ACTN-1-E847K-Rev	5' – GGG TGG CAG CTC GCG GCG CAA TTT GTC CAT GGT AAT GTA GTT C – 3'
Hum-ACTN-1-E847KE851K-Forw	5' – CCA TGG ACA AAT TGC GCA GAA AGC TGC CAC CCG ACC AGG – 3'
Hum-ACTN-1-E847KE851K-Rev	5' – CCT GGT CGG GTG GCA GCT TTC TGC GCA ATT TGT CCA TGG – 3'

α -Actinin-1 promotes activity of the L-type Ca²⁺ Channel Cav1.2

Matthew Turner^{1§}, David E. Anderson^{1§}, Peter Bartels^{2§}, Madeline Nieves-Cintrón^{2§}, Andrea M. Coleman^{1,2}, Peter B. Henderson², Kwun Nok Mimi Man², Pang-Yen Tseng², Vladimir Yarov-Yarovoy³, Donald M. Bers², Manuel F. Navedo², Mary C. Horne^{2#}, James B. Ames^{1#}, and Johannes W. Hell^{2#}

Review timeline:

Submission date:	5th Jun 2019
Editorial Decision:	5th Jul 2019
Revision received:	13th Nov 2019
Editorial Decision:	26th Nov 2019
Revision received:	4th Dec 2019
Accepted:	6th Dec 2019

Editor: Daniel Klimmeck

Transaction Report:

(Note: With the exception of the correction of typographical or spelling errors that could be a source of ambiguity, letters and reports are not edited. The original formatting of letters and referee reports may not be reflected in this compilation.)

1st Editorial Decision

5th Jul 2019

Thank you for the submission of your manuscript (EMBOJ-2019-102622) to The EMBO Journal. Your manuscript has been sent to three reviewers, and we have received reports from all of them, which I enclose below.

As you will see, the referees acknowledge the potential interest and novelty of your results, although they also express a number of issues that will have to be addressed before they can support publication of your manuscript in The EMBO Journal. In more detail, referee #3 states a number of conceptual concerns about your proposed model and conclusions and asks you to complement the study with additional experiments to consolidate physiological relevance of your findings with additional experiments in neuronal cells (ref#3, pt.2), explore potential synergistic interplay between Cav1.2 IQ domain with ApoCaM and alpha-actinin in a trimeric complex (ref#3, pt.1, see also ref#1's point on binding mutants), and test the cation type-dependence of the results (ref#3, pt.3). In addition, the reviewers raise a number of issues related to methods annotation, statistics, appropriate discussion of the results as well as wording that would need to be conclusively addressed to achieve the level of robustness and clarity needed for The EMBO Journal.

I judge the comments of the referees to be generally reasonable and given their overall interest, we are in principle happy to invite you to revise your manuscript experimentally to address the referees' comments. We do concur with the reviewers that in light of the findings contrasting earlier work in the field, excluding potential ambiguities and providing results of high robustness will be essential.

REFeree REPORTS:

Referee #1:

L-type voltage-gated Ca²⁺ channels are key regulators of cardiovascular, endocrine, and neuronal function. This manuscript by Turner et al. reports several important new findings that significantly modify and extend our understanding regarding how L-type voltage-gated Ca²⁺ channels are regulated by molecular interactions with the apo-form of the EF-hand Ca²⁺ binding protein calmodulin (CaM) and the EF-hand domains of the actin cytoskeleton-associated scaffold protein alpha-actinin. The authors employ a powerful combination of NMR-spectroscopy structure determination, biochemical assays of protein binding, and single-channel electrophysiological recordings to reach the conclusion that competitive binding of alpha-actinin to the Cav1.2 IQ CaM binding domain not only regulates L-channel targeting to the cell surface, as previously appreciated, but also directly increases channel open probability (P_o) by promoting coupling of gating charge movement to channel opening. Additional data presented also indicates that the affinity of the Cav1.2 IQ domain for apo-CaM is much lower under physiological salt concentrations conditions than previously thought, suggesting that apo-CaM does not likely basally interact with Cav1.2 under physiological conditions in cells such as neurons. Accordingly, the authors go on to show that apo-CaM binding to the Cav1.2 IQ domain is not required for maintaining basal channel open probability, which is in contrast to the conclusions of previous high-impact published work from David Yue's group (Adams et al., 2014 Cell) that relied on an I to A mutant in the IQ domain to disrupt apo-CaM binding. Importantly, the authors here show that this IA mutant not only disrupts apo-CaM binding to the Cav1.2 IQ domain but also disrupts alpha-actinin binding. These new findings regarding how alpha-actinin, but not apo-CaM, binding controls L-channel P_o indicate that current mechanistic models for how CaM regulates L-channel function during Ca²⁺-dependent dependent inactivation (CDI), which acts as an important negative feedback mechanism to limit Ca²⁺ entry through these channels, should be re-evaluated.

Key findings reported by this study are: 1) two novel NMR solution structures of apo-CaM and the alpha-actinin EF3,4 domain bound to the Cav1.2 IQ motif; 3) structural identification and functional validation by mutagenesis and binding assays of key residues in the Cav1.2 IQ domain that either regulate both apo-CaM and alpha-actinin binding (I1654A) or only alpha-actinin (K1647E, Y1649A) or apo-CaM (F1658A, K1662E) binding specifically; 4) IQ domain mutations in residues that specifically impair alpha-actinin binding decrease channel P_o in single channel recordings, while mutations that specifically impair apo-CaM binding have no impact; 5) alpha-actinin binding to the Cav1.2 IQ domain increases P_o by increasing coupling of gating charge movement to channel opening. Importantly, the conclusions of these biochemical and electrophysiological experiments are all reinforced by additional mutagenesis of key corresponding binding residues in alpha-actinin or CaM, including an elegant "charge reversal" rescue.

Overall this study is very comprehensive and carefully executed. The data are of high quality and the findings are important. I have no major concerns, but do have one minor concern that should be addressed regarding how the new findings may change how we should think about CDI. At minimum, the authors should at least further discuss how alpha-actinin regulation of P_o and CDI may be connected. In particular, CDI requires Ca²⁺-CaM binding to the IQ motif, which also displaces alpha-actinin binding as previously shown by the authors in Tseng et al 2017. In addition, the authors mention in the Discussion that alpha-actinin binding increases P_o by promoting coupling of gating charge movement to channel opening like previously shown for PKA regulation (Fuller et al, 2010). A requirement for alpha-actinin binding to increase P_o as a prerequisite for subsequent CDI would further parallel PKA regulation of current density and P_o that is intertwined with priming channels to under subsequent CDI mediated by Ca²⁺-CaM binding and reversal of PKA actions via dephosphorylation by the phosphatase PP2B. (See Chad and Eckert, 1986; Armstrong and Eckert, 1987; Oliveria et al., 2007,2012; Dittmer et al. 2012).

In this regard, the authors should also seriously consider adding a few additional experiments determining the impacts of mutants that inhibit both apo-CaM and alpha-actinin binding (classic I1654A mutant that disrupts CDI as a positive control) versus only alpha-actinin (K1647E or Y1649A) or apo-CaM (F1658A or K1662E) binding on CDI in macroscopic whole-cell recordings in Ca²⁺ compared to Ba²⁺. As mentioned above, these new findings regarding how alpha-actinin, but not apo-CaM, binding controls L-channel P_o indicate that current mechanistic models for how CaM regulates L-channel function during CDI should be re-evaluated and doing so here through inclusion of the above suggested experiments would even further increase the impact of this excellent study on the field.

Referee #2:

Using NMR to solve structures of CaV1.2 $\alpha 1$ subunit bound to either α -actinin-1 and to apo-calmodulin in combination with patch clamp electrophysiology and surface biotinylation assays in 293 cells, Turner et al studied how CaV1.2 activity is regulated by these by these interactions and builds upon their previous study Tseng et al 2017 PMID:28613835 that identified that the α -actinin-1 was important for membrane localization. In this study the solved NMR solutions structures give insight to the how the EF hand region of α -actinin-1 and apo-calmodulin interact with CaV1.2 IQ motif. Subsequent, characterization demonstrate that the α -actinin-1 not only impact CaV1.2 surface localization as previous reported, by Tseng et al 2017, but they find that the α -actinin-1 interactions are positive regulators CaV1.2 channel open probability and gating. Importantly they show that apo-calmodulin interaction does not regulate CaV1.2 channel open probability and gating. These findings demonstrate that while α -actinin-1 and apo-calmodulin both interact with the IQ motif the respective interactions differentially regulate CaV1.2 channels and that apo-calmodulin regulation of CaV 1.2 is distinct from CaV 1.3. Based on these findings their main conclusion is that the α -actinin-1 regulation of CaV1.2 channel activity ensures that CaV1.2 channel activity is minimal while trafficking to its proper location at the cell surface.

Overall the experiments in this study are very well designed and executed, analyses are quite thorough. The electrophysiological data elegantly integrates the findings of the NMR solution structures and offers potential mechanistic insights into understanding how Cav1.2 channel activity is regulated outside of its proper location. The findings in this study are important for many cell types that utilize CaV1.2 channels and therefore of general significance for understanding the mechanisms of CaV1.2 channel regulation.

Major comments.

1) Eleven supplemental figures are excessive, and some supplemental figures appear to just be different graphs of the same data found in the main figures. To give a better representation of the data and make it easier on the reader the authors should present data either as box mean plots, or scatter plots in the main text and get rid of the duplicative supplemental data. Also, figure 4 And 5 could be consolidated.

2) Figure 5. For the experiments analyzing of EE/KK the control there is 2 fold more control than mutant. The scatter plots in the supplemental data give the appearance of a different distribution between the two data sets although the means appear to be similar. I am not arguing for P hunting but having 2X more data collected for the WT compared to the EE/KK data will affect the robustness of the statistical test. I highly recommend that the authors increase the sample numbers for this experiment. This will allow them to draw a firm conclusion.

3) The discussion highlights the Nav1.2 structure compared their findings. Since this is a major point of their discussion they should move this supplemental figure into the main text. This makes it easier on the reader if this figure is in the main text.

Referee #3:

In this manuscript Turner and his colleagues examine the molecular mechanism underlying upregulation of Cav1.2 activity by alpha-actinin-1. In previous work the same group had shown that alpha-actinin-1 binds to the IQ motif of Cav1.2. Furthermore, they had identified three key residues in the sequence of the IQ motif that were crucial for this interaction. In the present study, NMR is employed to determine the 3D structure of the Cav1.2 IQ bound to the two distal EF hands (EF3/4) of alpha-actinin-1. The authors identify three charged amino acid residues (K1647 in IQ and E847/E851 in alpha-actinin-1) that form salt bridges between the IQ and EF3/4, and a hydrophobic interaction (I1654 in IQ, F833 in alpha-actinin-1) as crucial determinants for the interaction. Mutation of the charged residues abolished interaction while binding could be rescued by charge inversion mutagenesis. In a series of cell-attached single channel patch-clamp experiments the

authors show that alpha-actinin-1 increases the open probability (P_o) of Cav1.2. In agreement with their NMR studies and binding assays effects on P_o were strongly dependent on the identified charged amino acid residues. Charge movement measurements suggest that the stimulatory effect on P_o is caused by an augmentation of gating charge movement including downstream coupling of charge movement to pore opening. Finally, the authors have also determined a NMR structure of the apocalmodulin (apoCaM) / Cav1.2-IQ complex. They show that the apoCaM binding site is distinct from that of alpha-actinin-1. Surprisingly, apoCaM did not affect P_o of Cav1.2. This finding contrasts with previous work of the Yue group on the related Cav1.3 channel (Adams et al. Cell 2014) that proposed an increase of P_o induced by apoCaM.

In conclusion this is an interesting study that extends our knowledge on the regulation of L-type calcium channels. While the study is technically sound I have a few conceptual concerns that reduce my general enthusiasm for this manuscript.

1. In native cells (e.g. neurons) Cav1.2 is coassembled with both alpha-actinin-1 and apoCaM. Since both proteins can bind to the IQ they may exert complex (e.g. synergistic) functional effects on Cav1.2 that are not seen when the channel is only characterized in the presence of alpha-actinin-1 or apoCaM alone. For example, the authors discuss that the conclusion of the Yue group that apoCaM enhances P_o could reflect the fact that I1655 in the IQ not only contributes to apoCaM but also to alpha-actinin-1 binding. Given this complexity, I feel that it is necessary to examine interactions between all three components in a trimeric complex (IQ + apoCaM + alpha-actinin-1) in binding assays, NMR and patch-clamp.

2. All patch-clamp experiments are performed in HEK293 cells. In neurons and cardiac cell the amount and compartmentalization of Cav1.2 / alpha-actinin-1 and apoCaM might be quite different compared to a heterologous expression system. The authors should make a serious attempt to substantiate their conclusions with data from a more physiological system.

3. It is obvious that Cav1.2 currents are much easier to characterize using Ba^{2+} instead of Ca^{2+} as charge carrier. Nevertheless, physiologically the channels conduct Ca^{2+} . Since the IQ motif is involved in calcium-dependent inactivation which may profoundly interfere with effects reported in this study the authors should complement their analysis with electrophysiological data using Ca^{2+} as charge carrier. These experiments are crucial to demonstrate that proposed alpha-actinin-1 effects are independent of the cation passing the channel.

1st Revision - authors' response

13th Nov 2019

Referee #1:

L-type voltage-gated Ca^{2+} channels are key regulators of cardiovascular, endocrine, and neuronal function. This manuscript by Turner et al. reports several important new findings that significantly modify and extend our understanding regarding how L-type voltage-gated Ca^{2+} channels are regulated by molecular interactions with the apo-form of the EF-hand Ca^{2+} binding protein calmodulin (CaM) and the EF-hand domains of the actin cytoskeleton-associated scaffold protein alpha-actinin. The authors employ a powerful combination of NMR-spectroscopy structure determination, biochemical assays of protein binding, and single-channel electrophysiological recordings to reach the conclusion that competitive binding of alpha-actinin to the Cav1.2 IQ CaM binding domain not only regulates L-channel targeting to the cell surface, as previously appreciated, but also directly increases channel open probability (P_o) by promoting coupling of gating charge movement to channel opening. Additional data presented also indicates that the affinity of the Cav1.2 IQ domain for apo-CaM is much lower under physiological salt concentrations conditions than previously thought,

suggesting that apo-CaM does not likely basally interact with Cav1.2 under physiological conditions in cells such as neurons. Accordingly, the authors go on to show that apo-CaM binding to the Cav1.2 IQ domain is not required for maintaining basal channel open probability, which is in contrast to the conclusions of previous high-impact published work from David Yue's group (Adams et al., 2014 Cell) that relied on an I to A mutant in the IQ domain to disrupt apo-CaM binding. Importantly, the authors here show that this IA mutant not only disrupts apo-CaM binding to the Cav1.2 IQ domain but also disrupts alpha-actinin binding. These new findings regarding how alpha-actinin, but not apo-CaM, binding controls L-channel P_o indicate that current mechanistic models for how CaM regulates L-channel function during Ca^{2+} -dependent inactivation (CDI), which acts as an important negative feedback mechanism to limit Ca^{2+} entry through these channels, should be re-evaluated.

Key findings reported by this study are: 1) two novel NMR solution structures of apo-CaM and the alpha-actinin EF3,4 domain bound to the Cav1.2 IQ motif; 2) structural identification and functional validation by mutagenesis and binding assays of key residues in the Cav1.2 IQ domain that either regulate both apo-CaM and alpha-actinin binding (I1654A) or only alpha-actinin (K1647E, Y1649A) or apo-CaM (F1658A, K1662E) binding specifically; 3) IQ domain mutations in residues that specifically impair alpha-actinin binding decrease channel P_o in single channel recordings, while mutations that specifically impair apo-CaM binding have no impact; 4) alpha-actinin binding to the Cav1.2 IQ domain increases P_o by increasing coupling of gating charge movement to channel opening. Importantly, the conclusions of these biochemical and electrophysiological experiments are all reinforced by additional mutagenesis of key corresponding binding residues in alpha-actinin or CaM, including an elegant "charge reversal" rescue.

Overall this study is very comprehensive and carefully executed. The data are of high quality and the findings are important. I have no major concerns, but do have one minor concern that should be addressed regarding how the new findings may change how we should think about CDI. At minimum, the authors should at least further discuss how alpha-actinin regulation of P_o and CDI may be connected. In particular, CDI requires Ca^{2+} -CaM binding to the IQ motif, which also displaces alpha-actinin binding as previously shown by the authors in Tseng et al 2017. In addition, the authors mention in the Discussion that alpha-actinin binding increases P_o by promoting coupling of gating charge movement to channel opening like previously shown for PKA regulation (Fuller et al, 2010). A requirement for alpha-actinin binding to increase P_o as a prerequisite for subsequent CDI would further parallel PKA regulation of current density and P_o that is intertwined with priming channels to under subsequent CDI mediated by Ca^{2+} -CaM binding and reversal of PKA actions via dephosphorylation by the phosphatase PP2B. (See Chad and Eckert, 1986; Armstrong and Eckert, 1987; Oliveria et al., 2007,2012; Dittmer et al. 2012).

In this regard, the authors should also seriously consider adding a few additional experiments determining the impacts of mutants that inhibit both apo-CaM and alpha-actinin binding (classic I1654A mutant that disrupts CDI as a positive control) versus only alpha-actinin (K1647E or Y1649A) or apo-CaM (F1658A or K1662E) binding on CDI in macroscopic whole-cell recordings in Ca^{2+} compared

to Ba²⁺. As mentioned above, these new findings regarding how alpha-actinin, but not apo-CaM, binding controls L-channel Po indicate that current mechanistic models for how CaM regulates L-channel function during CDI should be re-evaluated and doing so here through inclusion of the above suggested experiments would even further increase the impact of this excellent study on the field.

The notion that alpha-actinin binding to increase Po might be a prerequisite for subsequent CDI, with CDI possibly being at least in part accomplished by displacement of alpha-actinin by Ca/CaM, is definitely highly intriguing. It would be analogous to the antagonistic roles PKA and the Ca/CaM-activated phosphatase calcineurin/PP2B play, with PKA augmenting Po and thereby priming Cav1.2 for CDI, and Ca/CaM activating calcineurin to dephosphorylate Cav1.2 at its PKA site(s). We spent a substantial amount of time and effort to evaluate this possibility over the last few months (Fig. A). However, our data suggest that CDI is actually normal for Y1649A mutant Cav1.2 in which alpha-actinin and not CaM binding is affected (Fig. A). As a positive control CDI is impaired for the ‘classic’ I1654A mutation (Fig. A) as shown earlier (Zühlke et al., 1999: Nature 399, 159-162; Zühlke et al., 2000: J Biol Chem 275, 21121-21129). This loss of CDI is likely

because I1654 is central to binding of Ca/CaM (Van Petegem, Chatelain, and Minor, 2005: Nature Struct Mol Biol 12, 1108-1115; Fallon et al., 2005: Structure 13, 1881-1886), which is required for CDI (Peterson et al., 1999: Neuron 22, 549-558). Thus, against the initial captivating hypothesis here,

we do **not** believe that CDI is due to a reduction of Po as a result of an immediate (within ms) displacement of alpha-actinin even though binding of Ca/CaM is required for CDI. The lack of CDI for the I1654A mutant is thus most likely due to loss of CaM binding but not alpha-actinin binding.

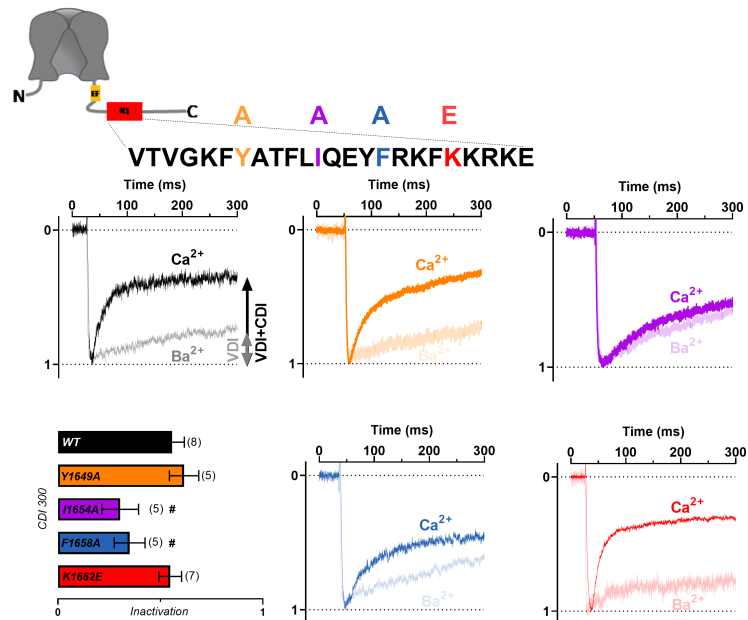


Fig. A: CDI analysis. HEK293 cells were transfected with α_1 1.2, $\alpha_2\delta$ -1, and β_{2A} before whole cell patch recording in 20 mM Ba²⁺ (light traces) or 10 mM Ca²⁺ (dark traces) for WT (gray/black), Y1649A (orange), I1654A (purple), F1658A (blue) and K1662E (red). Shown are representative current traces of the first 300 ms obtained from recordings upon depolarizations from a holding potential of -80 mV to +20 mV. Bar diagram shows **CDI** as the fractional difference between the residual current at 300 ms (R₃₀₀) in 10 mM Ca²⁺ versus R₃₀₀ in 20 mM Ba²⁺ (50-60% for WT, Y1649A, K1662E and ~35% for I1654A and F1658A; n=5-8; # <0.05, unpaired T-test).

We also analyzed the effects of our mutants that impair apoCaM binding on CDI. We find that **CDI of Cav1.2 K1662E is actually not different from CDI for WT** (Fig. A). This finding is consistent with earlier results by the late David Yue and

co-workers in which the equivalent mutation in Cav1.3 did not affect CDI (Ben-Johny et al., 2013: Nat Commun 4, 1717, Fig. 3; Bazzazi et al., 2013: Cell Reports 5, 367-377, Fig. 2). This result actually suggests that pre-association of apoCaM with the Cav1.2 IQ motif is **not** required for CDI because K1662 forms a strong salt bridge with apoCaM (Fig. 2 in our manuscript) and the Kd value is increased by 6-fold (i.e., affinity is decreased) for the K1662E IQ peptide versus WT IQ peptide (Table 4). At the same time K1662 makes minimal contact with Ca/CaM in the crystal structure (Van Petegem, Chatelain, and Minor, 2005: Nature Struct Mol Biol 12, 1108-1115; Fallon et al., 2005: Structure 13, 1881-1886). These findings are consistent with the model we propose in the Discussion that the main species of CaM associated with Cav1.2 under resting conditions is CaM with Ca²⁺ bound to EF3 and EF4 in the C lobe (please see Discussion for more details). In further support of this model, F1658 forms several interactions with residues of Ca/CaM and thus should impair CDI. In fact, such an impairment was reported for the equivalent mutation in Cav1.3 (Ben-Johny et al., 2013: Nat Commun 4, 1717, Fig. 3; Bazzazi et al., 2013: Cell Reports 5, 367-377, Fig. 2). Accordingly, we find that the **F1658A** mutant Cav1.2 has **decreased CDI vs. WT** (Fig. A). However, we are performing further structural and functional analyses to thoroughly address the question of whether pre-association of Ca/CaM with the IQ motif is required for CDI before we feel we can publish in detail and with greater depth on this issue. These experiments, which include new structural analyses, will take much more time than can be accomplished in the next few months and thus have to remain beyond the scope of our already very extensive work on how alpha-actinin affects Cav1.2 function under basal conditions.

Referee #2:

Using NMR to solve structures of CaV1.2 $\alpha 1$ subunit bound to either α -actinin-1 and to apo-calmodulin in combination with patch clamp electrophysiology and surface biotinylation assays in 293 cells, Turner et al studied how CaV1.2 activity is regulated by these by these interactions and builds upon their previous study Tseng et al 2017 PMID:28613835 that identified that the α -actinin-1 was important for membrane localization. In this study the solved NMR solution structures give insight to the how the EF hand region of α -actinin-1 and apo-calmodulin interact with CaV1.2 IQ motif. Subsequent, characterization demonstrate that the α -actinin-1 not only impact CaV1.2 surface localization as previous reported, by Tseng et al 2017, but they find that the α -actinin-1 interactions are positive regulators CaV1.2 channel open probability and gating. Importantly they show that apo-calmodulin interaction does not regulate CaV1.2 channel open probability and gating. These findings demonstrate that while α -actinin-1 and apo-calmodulin both interact with the IQ motif the respective interactions differentially regulate CaV1.2 channels and that apo-calmodulin regulation of CaV 1.2 is distinct from CaV 1.3. Based on these findings their main conclusion is that the α -actinin-1 regulation of CaV1.2 channel activity ensures that CaV1.2 channel activity is minimal while trafficking to its proper location at the cell surface.

Overall the experiments in this study are very well designed and executed, analyses are quite thorough. The electrophysiological data elegantly integrates the findings of the NMR solution structures and offers potential mechanistic insights into understanding how Cav1.2 channel activity is regulated outside of its proper location. The findings in this study are important for many cell types that utilize CaV1.2 channels and therefore of general significance for understanding the mechanisms of CaV1.2 channel regulation.

Major comments.

1) Eleven supplemental figures are excessive, and some supplemental figures appear to just be different graphs of the same data found in the main figures. To give a better representation of the data and make it easier on the reader the authors should present data either as box mean plots, or scatter plots in the main text and get rid of the duplicative supplemental data. Also, figure 4 And 5 could be consolidated.

We moved the dot plot diagrams to the main text to eliminate those from the Supplemental Data section. We reduced the number of sample sweeps we show in Fig 3, 4, and 5 but show all original sample sweeps as Expanded View figures.

2) Figure 5. For the experiments analyzing of EE/KK the control there is 2 fold more control than mutant. The scatter plots in the supplemental data give the appearance of a different distribution between the two data sets although the means appear to be similar. I am not arguing for P hunting but having 2X more data collected for the WT compared to the EE/KK data will affect the robustness of the statistical test. I highly recommend that the authors increase the sample numbers for this experiment. This will allow them to draw a firm conclusion.

We completely agree that it would have been reassuring if we could have performed more of these recordings and obtain p values that would perfectly match the criterion for rejecting the null hypothesis (i.e., $p < 0.05$). However, we had to make a choice in how to allocate our efforts and especially the time the electrophysiologist in my lab would spend on the different requests by all Reviewers. We spent a lot of time on testing whether binding of alpha-actinin to the IQ motif is a prerequisite for CDI and whether displacement of alpha-actinin by Ca/CaM could drive CDI, as suggested by Reviewer 1. We also extensively tried to get recordings from neurons, which, unfortunately, did not pan out (see Reviewer 3 #2).

3) The discussion highlights the Nav1.2 structure compared their findings. Since this is a major point of their discussion they should move this supplemental figure into the main text. This makes it easier on the reader if this figure is in the main text.

We moved this Figure to Expanded View, which is immediately accessible through the EMBO J portal.

Referee #3:

In this manuscript Turner and his colleagues examine the molecular mechanism underlying upregulation of Cav1.2 activity by alpha-actinin-1. In previous work the same group had shown that alpha-actinin-1 binds to the IQ motif of Cav1.2. Furthermore, they had identified three key residues in the sequence of the IQ motif that were crucial for this interaction. In the present study, NMR is employed to determine the 3D structure of the Cav1.2 IQ bound to the two distal EF hands (EF3/4) of alpha-actinin-1. The authors identify three charged amino acid residues (K1647 in IQ and E847/E851 in alpha-actinin-1) that form salt bridges between the

IQ and EF3/4, and a hydrophobic interaction (I1654 in IQ, F833 in alpha-actinin-1) as crucial determinants for the interaction. Mutation of the charged residues abolished interaction while binding could be rescued by charge inversion mutagenesis. In a series of cell-attached single channel patch-clamp experiments the authors show that alpha-actinin-1 increases the open probability (P_o) of Cav1.2. In agreement with their NMR studies and binding assays effects on P_o were strongly dependent on the identified charged amino acid residues. Charge movement measurements suggest that the stimulatory effect on P_o is caused by an augmentation of gating charge movement including downstream coupling of charge movement to pore opening. Finally, the authors have also determined a NMR structure of the apocalmodulin (apoCaM) / Cav1.2-IQ complex. They show that the apoCaM binding site is distinct from that of alpha-actinin-1. Surprisingly, apoCaM did not affect P_o of Cav1.2. This finding contrasts with previous work of the Yue group on the related Cav1.3 channel (Adams et al. Cell 2014) that proposed an increase of P_o induced by apoCaM.

In conclusion this is an interesting study that extends our knowledge on the regulation of L-type calcium channels. While the study is technically sound I have a few conceptual concerns that reduce my general enthusiasm for this manuscript.

1. In native cells (e.g. neurons) Cav1.2 is co-assembled with both alpha-actinin-1 and apoCaM. Since both proteins can bind to the IQ they may exert complex (e.g. synergistic) functional effects on Cav1.2 that are not seen when the channel is only characterized in the presence of alpha-actinin-1 or apoCaM alone. For example, the authors discuss that the conclusion of the Yue group that apoCaM enhances P_o could reflect the fact that I1655 in the IQ not only contributes to apoCaM but also to alpha-actinin-1 binding. Given this complexity, I feel that it is necessary to examine interactions between all three components in a trimeric complex (IQ + apoCaM + alpha-actinin-1) in binding assays, NMR and patch-clamp.

We conducted multiple NMR titrations to probe structural aspects of the hypothesized ternary complex (Expanded View Fig. 3). However, all results were negative and we conclude that the IQ peptide, apoCaM, and alpha-actinin-1 cannot form a ternary complex. We provide the NMR spectra in Expanded View Fig. 3 and describe these spectra in a new section in the Results on page 10 (lines 212-227). The lack of a ternary complex is consistent with our finding that Ile1654 forms multiple contacts with both, alpha-actinin-1 EF hand region and apoCaM and that Ile1654 is required for both alpha-actinin-1 binding and apoCaM binding. Thus, binding of apoCaM and alpha-actinin-1 to the IQ motif at least as far as it involves the eponymous Ile should be competitive and occlude binding of the other partner. Our new NMR data (Suppl Fig. 12) now demonstrate that apoCaM and alpha-actinin bind competitively to the IQ motif and the IQ peptide does not bind simultaneously to both apoCaM and alpha-actinin.

2. All patch-clamp experiments are performed in HEK293 cells. In neurons and cardiac cell the amount and compartmentalization of Cav1.2 / alpha-actinin-1 and apoCaM might be quite different compared to a heterologous expression system. The authors should make a serious attempt to substantiate their conclusions with data from a more physiological system.

The question how Cav1.2 interacts with alpha-actinin and CaM in a native system is definitely an important one. We mutated T1066 of Cav1.2 to Tyr, which makes Cav1.2 dihydropyridine-insensitive. We express T1066Y Cav1.2 in our high quality cultured hippocampal neurons. Application of the dihydropyridine isradipine does block all endogenous L-type currents in the absence of ectopically expressed T1066Y Cav1.2. However, and against expectation, even with ectopic expression of Cav1.2 T1066Y isradipine abrogated nearly all activity in our single channel recordings. We re-sequenced Cav1.2 to make sure that the mutation was present. Despite extensive trouble shooting and multiple attempts we were not able to get this strategy to work.

3. It is obvious that Cav1.2 currents are much easier to characterize using Ba²⁺ instead of Ca²⁺ as charge carrier. Nevertheless, physiologically the channels conduct Ca²⁺. Since the IQ motif is involved in calcium-dependent inactivation which may profoundly interfere with effects reported in this study the authors should complement their analysis with electrophysiological data using Ca²⁺ as charge carrier. These experiments are crucial to demonstrate that proposed alpha-actinin-1 effects are independent of the cation passing the channel.

We tried very hard to record single channel activity in HEK293 cells with Ca rather than Ba as charge carrier. However, Ca provides much smaller currents and we were not able to discern those from the noise. Our initial attempts with 1.8 mM and 10 mM Ca under our standard cell attached recording conditions did not yield any discernable currents above our noise level, which is roughly 0.4 pA. We then performed experiments using borosilicate glass with an outer diameter of 1.5 mm and inner diameter of 0.86 mm and heavy elastomer coating (Levis and Rae 1993: Biophys J 65, 1666-1677). For that, Sylgard was applied close to the tip of the recording pipette to improve the seal and thereby reduce noise. However, this strategy still did not improve the noise level sufficiently enough for detection of unitary Ca currents.

Thus, finally, we resorted to whole cell patch recordings with Ca to confirm the effect we saw with Ba. We found an ~80% reduction in whole cell current for the key K1647A mutation, the only mutation we tested due to time restraints, versus WT Cav1.2.

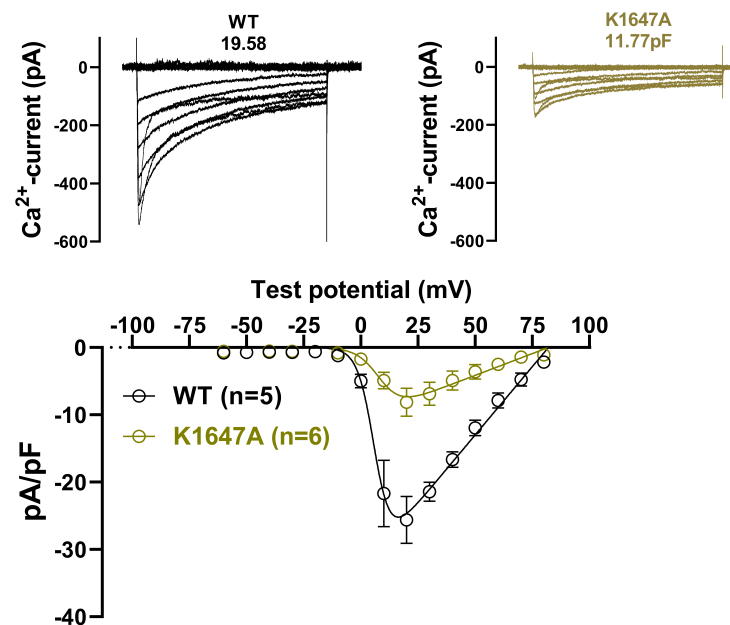


Fig. B: Analysis of whole cell currents with Ca as charge carrier. HEK293 cells were transfected with α_1 1.2, $\alpha_2\delta$ -1, and β_{2A} before whole cell patch recording in 10 mM Ca²⁺ from a holding potential of -70 mV to the indicated potentials. **Top** shows sample recordings to the various test potentials for WT Cav1.2 (left) and K1647A mutant Cav1.2 (right). **Bottom** shows I/V curves from 5-6 experiments.

2nd Editorial Decision

26th Nov 2019

Thank you for submitting your revised manuscript for consideration by The EMBO Journal. Your amended study was sent back to two of the referees for re-evaluation, and we have received comments from both of them, which I enclose below.

As you will see the referees find that their concerns have been sufficiently addressed and they are now broadly in favour of publication.

Thus, we are pleased to inform you that your manuscript has been accepted in principle for publication in The EMBO Journal, pending some minor issues related to formatting and data representation as listed below, which need to be adjusted at re-submission.

REFeree REPORTS:

Referee #2:

The authors have adequately addressed my previous comments. Congrats to the authors on a great study.

Referee
#3:

The authors have addressed all three points raised in my previous review. Importantly, their new NMR data convincingly demonstrate that apoCaM and alpha-actinin bind competitively to the IQ motif of Cav1.2 rather than forming a ternary complex. The authors also show macroscopic Ca²⁺ currents of the K1647A mutant that support the basic conclusions of this study. Unfortunately, due to technical problems, the author failed to characterize Cav1.2 in hippocampal neurons. Although it would be nice to have such data I don't think that they are absolutely crucial. In summary, the revision has profoundly improved this manuscript. I have no further objections.

2nd Revision - authors' response

4th Dec 2019

The authors have performed the requested editorial changes.

3rd Editorial Decision

6th Dec 2019

Thank you for submitting the revised version of your manuscript. I have now evaluated your amended manuscript and concluded that the remaining minor concerns have been sufficiently addressed.

Thus, I am pleased to inform you that your manuscript has been accepted for publication in the EMBO Journal.

YOU MUST COMPLETE ALL CELLS WITH A PINK BACKGROUND ↓

PLEASE NOTE THAT THIS CHECKLIST WILL BE PUBLISHED ALONGSIDE YOUR PAPER

Corresponding Author Name: Johannes W. Hell

Journal Submitted to: EMBO

Manuscript Number: EMBOJ-2019-102622R

Reporting Checklist For Life Sciences Articles (Rev. June 2017)

This checklist is used to ensure good reporting standards and to improve the reproducibility of published results. These guidelines are consistent with the Principles and Guidelines for Reporting Preclinical Research issued by the NIH in 2014. Please follow the journal's authorship guidelines in preparing your manuscript.

A- Figures**1. Data****The data shown in figures should satisfy the following conditions:**

- the data were obtained and processed according to the field's best practice and are presented to reflect the results of the experiments in an accurate and unbiased manner.
- figure panels include only data points, measurements or observations that can be compared to each other in a scientifically meaningful way.
- graphs include clearly labeled error bars for independent experiments and sample sizes. Unless justified, error bars should not be shown for technical replicates.
- if $n < 5$, the individual data points from each experiment should be plotted and any statistical test employed should be justified
- Source Data should be included to report the data underlying graphs. Please follow the guidelines set out in the author ship guidelines on Data Presentation.

2. Captions**Each figure caption should contain the following information, for each panel where they are relevant:**

- a specification of the experimental system investigated (eg cell line, species name).
- the assay(s) and method(s) used to carry out the reported observations and measurements
- an explicit mention of the biological and chemical entity(ies) that are being measured.
- an explicit mention of the biological and chemical entity(ies) that are altered/ varied/ perturbed in a controlled manner.
- the exact sample size (n) for each experimental group/condition, given as a number, not a range;
- a description of the sample collection allowing the reader to understand whether the samples represent technical or biological replicates (including how many animals, litters, cultures, etc.).
- a statement of how many times the experiment shown was independently replicated in the laboratory.
- definitions of statistical methods and measures:
 - common tests, such as t-test (please specify whether paired vs. unpaired), simple χ^2 tests, Wilcoxon and Mann-Whitney tests, can be unambiguously identified by name only, but more complex techniques should be described in the methods section;
 - are tests one-sided or two-sided?
 - are there adjustments for multiple comparisons?
 - exact statistical test results, e.g., P values = x but not P values < x;
 - definition of 'center values' as median or average;
 - definition of error bars as s.d. or s.e.m.

Any descriptions too long for the figure legend should be included in the methods section and/or with the source data.

In the pink boxes below, please ensure that the answers to the following questions are reported in the manuscript itself. Every question should be answered. If the question is not relevant to your research, please write NA (non applicable). We encourage you to include a specific subsection in the methods section for statistics, reagents, animal models and human subjects.

B- Statistics and general methods

Please fill out these boxes ↓ (Do not worry if you cannot see all your text once you press return)

1.a. How was the sample size chosen to ensure adequate power to detect a pre-specified effect size?	The sample sizes for our biochemical, electrophysiological and immunofluorescence analyses was chosen based on extensive previously published work indicating that sample sizes were adequate.
1.b. For animal studies, include a statement about sample size estimate even if no statistical methods were used.	NA
2. Describe inclusion/exclusion criteria if samples or animals were excluded from the analysis. Were the criteria pre-established?	NA
3. Were any steps taken to minimize the effects of subjective bias when allocating animals/samples to treatment (e.g. randomization procedure)? If yes, please describe.	Single channel data were only analyzed for $n < 3$ channels in the patch to not overstate channel open probability. See also Herzig et al., 2007 and Bartels et al., 2018
For animal studies, include a statement about randomization even if no randomization was used.	NA
4.a. Were any steps taken to minimize the effects of subjective bias during group allocation or/and when assessing results (e.g. blinding of the investigator)? If yes please describe.	Single channel recordings and Popen analysis were performed based on a single blinded approach. In brief, transfected cells were handed over to the patcher only with a code which was only revealed after data analysis (Popen).
4.b. For animal studies, include a statement about blinding even if no blinding was done	NA
5. For every figure, are statistical tests justified as appropriate?	Yes
Do the data meet the assumptions of the tests (e.g., normal distribution)? Describe any methods used to assess it.	The data population distribution was tested by a D'agostino & Pearson Test. The data showed a normal or log-normal distribution and were further tested for significance with an ANOVA with Bonferroni correction. See also Material and Methods.

USEFUL LINKS FOR COMPLETING THIS FORM<http://www.antibodypedia.com><http://1degreebio.org><http://www.equator-network.org/reporting-guidelines/improving-bioscience-research-repo><http://grants.nih.gov/grants/olaw/olaw.htm><http://www.mrc.ac.uk/Ourresearch/Ethicsresearchguidance/Useofanimals/index.htm><http://ClinicalTrials.gov><http://www.consort-statement.org><http://www.consort-statement.org/checklists/view/32-consort/66-title><http://www.equator-network.org/reporting-guidelines/reporting-recommendations-for-tur><http://datadryad.org><http://figshare.com><http://www.ncbi.nlm.nih.gov/gap><http://www.ebi.ac.uk/ega><http://biomodels.net/><http://biomodels.net/miriam/><http://jij.biochem.sun.ac.za>http://oba.od.nih.gov/biosecurity/biosecurity_documents.html<http://www.selectagents.gov/>

Is there an estimate of variation within each group of data?	Standard error of mean (SEM) is depicted for all data.
Is the variance similar between the groups that are being statistically compared?	The variance between the groups is similar due to similar sample size between groups

C- Reagents

6. To show that antibodies were profiled for use in the system under study (assay and species), provide a citation, catalog number and/or clone number, supplementary information or reference to an antibody validation profile. e.g., Antibodypedia (see link list at top right), IDegreeBio (see link list at top right).	See "Materials and Methods"
7. Identify the source of cell lines and report if they were recently authenticated (e.g., by STR profiling) and tested for mycoplasma contamination.	HEK from cells a standard source were used in our studies which were in the past tested negative for mycoplasma contamination.

* for all hyperlinks, please see the table at the top right of the document

D- Animal Models

8. Report species, strain, gender, age of animals and genetic modification status where applicable. Please detail housing and husbandry conditions and the source of animals.	NA
9. For experiments involving live vertebrates, include a statement of compliance with ethical regulations and identify the committee(s) approving the experiments.	NA
10. We recommend consulting the ARRIVE guidelines (see link list at top right) (PLoS Biol. 8(6), e1000412, 2010) to ensure that other relevant aspects of animal studies are adequately reported. See author guidelines, under 'Reporting Guidelines'. See also: NIH (see link list at top right) and MRC (see link list at top right) recommendations. Please confirm compliance.	NA

E- Human Subjects

11. Identify the committee(s) approving the study protocol.	NA
12. Include a statement confirming that informed consent was obtained from all subjects and that the experiments conformed to the principles set out in the WMA Declaration of Helsinki and the Department of Health and Human Services Belmont Report.	NA
13. For publication of patient photos, include a statement confirming that consent to publish was obtained.	NA
14. Report any restrictions on the availability (and/or on the use) of human data or samples.	NA
15. Report the clinical trial registration number (at ClinicalTrials.gov or equivalent), where applicable.	NA
16. For phase II and III randomized controlled trials, please refer to the CONSORT flow diagram (see link list at top right) and submit the CONSORT checklist (see link list at top right) with your submission. See author guidelines, under 'Reporting Guidelines'. Please confirm you have submitted this list.	NA
17. For tumor marker prognostic studies, we recommend that you follow the REMARK reporting guidelines (see link list at top right). See author guidelines, under 'Reporting Guidelines'. Please confirm you have followed these guidelines.	NA

F- Data Accessibility

18. Provide a "Data Availability" section at the end of the Materials & Methods, listing the accession codes for data generated in this study and deposited in a public database (e.g. RNA-Seq data: Gene Expression Omnibus GSE39462, Proteomics data: PRIDE PXD000208 etc.) Please refer to our author guidelines for 'Data Deposition'. Data deposition in a public repository is mandatory for: a. Protein, DNA and RNA sequences b. Macromolecular structures c. Crystallographic data for small molecules d. Functional genomics data e. Proteomics and molecular interactions	The NMR assignments have been deposited in the BMRB (accession number 25902). The atomic coordinates have been deposited into the Protein Databank (6COA and 6CTB).
19. Deposition is strongly recommended for any datasets that are central and integral to the study; please consider the journal's data policy. If no structured public repository exists for a given data type, we encourage the provision of datasets in the manuscript as a Supplementary Document (see author guidelines under 'Expanded View' or in unstructured repositories such as Dryad (see link list at top right) or Figshare (see link list at top right).	
20. Access to human clinical and genomic datasets should be provided with as few restrictions as possible while respecting ethical obligations to the patients and relevant medical and legal issues. If practically possible and compatible with the individual consent agreement used in the study, such data should be deposited in one of the major public access-controlled repositories such as dbGAP (see link list at top right) or EGA (see link list at top right).	
21. Computational models that are central and integral to a study should be shared without restrictions and provided in a machine-readable form. The relevant accession numbers or links should be provided. When possible, standardized format (SBML, CellML) should be used instead of scripts (e.g. MATLAB). Authors are strongly encouraged to follow the MIRIAM guidelines (see link list at top right) and deposit their model in a public database such as BiomedRxiv (see link list at top right) or JWS Online (see link list at top right). If computer source code is provided with the paper, it should be deposited in a public repository or included in supplementary information.	

G- Dual use research of concern

22. Could your study fall under dual use research restrictions? Please check biosecurity documents (see link list at top right) and list of select agents and toxins (APHIS/CDC) (see link list at top right). According to our biosecurity guidelines, provide a statement only if it could.	NA
---	----